Advances in the Contour Method for Residual Stress Measurement

Thesis

Faculty of Science, Technology, Engineering and Mathematics

School of Engineering and Innovation

Advances in the contour method for residual stress measurement

by

Anas Achouri

September 2018

This dissertation is submitted for the degree of

Doctor of Philosophy

Abstract

The aim of this PhD thesis is to extend the capability of the contour method for residual stress measurement in metallic components by resolving two of its main limitations. The contour method involves sectioning a body into two equal parts that have mirror-symmetric geometry, stiffness and residual stress field. The deformations of the cut surfaces introduced by sectioning are then measured. These raw measured data are processed using filtering and smoothing techniques. The last step involves back calculating the residual stress distribution acting out of the cut plane that has been relaxed. This is equal to the original residual stress present at the cut plane before the body was cut. A major limitation of the contour technique is that it is strictly only applicable to flat cuts along a symmetry plane of a body.

Another fundamental assumption in the contour method is that residual stresses re-distribute elastically during the sectioning cut. However, this assumption can be violated if the residual stress magnitude is close to the material yield strength value and lead to plasticity cutting induced errors in the contour method results. Thus another major limitation of the technique is the risk of cutting induced plasticity that can introduce significant stress measurement errors.

This PhD thesis contributes to knowledge in the field through first presenting a novel contour data analysis approach for the more general case of sectioning at an arbitrary plane where the cut parts do not possess mirror-symmetry. This greatly extends the types of structure, and the volume of material within structures, where residual stresses can be measured using the contour method. The second contribution to knowledge is the invention of an incremental contour measurement method involving multiple cuts. This new approach can be applied to sequentially reduce residual stresses in the structure of interest and thereby lower or eliminate the risk of inducing plasticity during cutting and reduce consequent measurement errors. Both new approaches proposed in this PhD thesis are successfully demonstrated through numerical simulation using the finite element method and experimentally on benchmark steel specimens and against neutron diffraction measurements.

Acknowledgements

My deepest gratitude to Dr. Foroogh Hosseinzadeh and Professor John Bouchard for their supervision, advice, support and crucial contributions throughout this project.

This PhD project has been financially supported by Rolls-Royce and The Open University.

Neutron beam allocation for the Engin-X instrument at Rutherford Appleton Laboratory is gratefully acknowledged.

I am grateful to Dr Jan Kowal and Dr Amir Shirzadi for their critical feed-back during my probation examination. Dr Shahram Taherzadeh and Dr Roger James Dennis are acknowledged for their examination and interesting discussions during my PhD Viva.

I am grateful to the following people for their assistance with my work:

- Dr Supriyo Ganguly at Cranfield University for assistance with laser welding.
- Mr. Stan Hiller, Mr. Pete Ledgard, Mr. Damian Flack and Mr. Gordon Imlach for their workshop support and assistance with many of the experiments.
- All my colleagues in the Materials Engineering group for invaluable discussions and support.

I convey my special acknowledgements to my friends Sanjoo, Yéli, Olivia, Donna, Ho Kyeom, Jeferson, Rahul, Yadu, Abdullah, Jose, Safaa, Loua, Sophie, Gerardo, Hema, Julia, Johannes, Jino, Mushfiq, Sakiba, and Beverly for their continuous support and encouragement.

I leave my final word of thanks to my family Mina, Mohammed, Hachim and Ali for their continuous support, encouragement and love. This thesis is dedicated to them.

Preface

This thesis is submitted for the degree of Doctor of Philosophy of The Open University, United Kingdom. The work in this thesis was carried out in the School of Engineering and Innovation, of the Faculty of Mathematics, Computing and Technology, between October 2014 and September 2018 under the supervision of Dr Foroogh Hosseinzadeh and Professor Peter John Bouchard.

Except where clearly referenced, the work is entirely the author's own work. None of this work has been submitted for a degree or qualification at this or another university. Some of the results of this work have been published in an academic journal, conference proceedings and as oral or poster presentations as listed below:

- Abburi Venkata, K., Khayatzadeh, S., **Achouri, A.**, de Oliveira, J., Forsey, A., Gungor, S., Bouchard, P. J., and Truman, C., "Examining Stress Relaxation in a Dissimilar Metal Weld Subjected to Postweld Heat Treatment," *Materials Performance and Characterization*, https://doi.org/10.1520/MPC20180018. ISSN 2379-1365.

- **Achouri, A.**; Bouchard, P. J.; Kabra, S. and Hosseinzadeh, F. Asymmetric Cuts In The Contour Method For Residual Stress Measurement. In: 7th International Conference on Mechanics and Materials in Design,, 11-15 Jun 2017, Albufeira/Portugal.

- **Achouri, A.**; Bouchard, P. J. and Hosseinzadeh, F. Advances in the contour method for residual stress measurements. In: Universities Nuclear Technology Forum, 31st March-2nd April 2015, Milton Keynes, UK.

- **Achouri, A.**; Bouchard, P. J. and Hosseinzadeh, F. Advances in the contour method for residual stress measurements. In: Engineering and Innovation Seminar, 20th November 2014, Milton Keynes, UK.

Table of Contents

Chapter 1: Introduction

Engineering structures are becoming more and more complex nowadays. Any viable engineering project must match the cost optimization and the environmental friendly requirements. To tackle these 21st century challenges, the design of engineering structures must be optimized, especially in relation to structural integrity and safety. Engineers are required to make trade-off decisions about key factors including cost, environmental impact and performance of their products. Although often overlooked, knowledge about residual stresses retained in materials is key information that can be exploited for optimizing the design of engineering structures [1,2,3]. Residual stresses are defined as 'locked in' stresses that remain within the material even when the body is not subject to any external load. They are introduced by most manufacturing processes as often evidenced by associated distortion. Residual stresses interact with in-service stresses and can have detrimental or beneficial effects on the performance of engineering components. Compressive residual stresses tend to mitigate the risk of crack propagation. However, often tensile residual stresses play a key role in premature failures of engineering structures [3]. Accurate knowledge of residual stresses introduced into components and structures is increasingly required in order to improve engineering manufacturing and repair processes as well as validating numerical models [4]. Knowledge of the residual stress field locked into structures is also an essential input for lifetime prediction and structural integrity assessments, in particular for safety critical applications [4].

Residual stresses can be introduced within materials by virtually any manufacturing process such as welding [5], casting [6], forging [7], or additive manufacturing [8], and may well change during the life cycle of engineering structures. All residual stresses arise from displacement misfits [1]. These misfits can be at different locations within the material like for example between different phases. Furthermore, these misfits can have different origins such as differential contraction or thermo-mechanical plasticity. Sometimes, residual stresses can be predicted using analytical or numerical models. However, many manufacturing processes are complex for which models predicting residual stress can be inaccurate and prone to uncertainties. Moreover, residual stresses generated during the life cycle of an engineering structure, introduced for example during a weld reparation, can be complex to predict as they can also be influenced by the service history of the engineering structure.

Residual stress measurement tools are becoming increasingly indispensable for manufacturing and demanding applications, for example in the nuclear, aerospace and offshore industries.

Nowadays there is a wide variety of techniques for residual stress measurement [9]. The contour method is one of the youngest but most promising methods for measuring residual stresses. It is based on mechanical strain relief and elastic relaxation of residual stresses upon material removal. The method involves carefully sectioning a body into two halves over a flat mirror-symmetric plane using wire electro discharge machining. The created cut surfaces deform owing to the relaxation of residual stresses. These deformations are measured typically using a coordinate measurement machine and used to back calculate the original residual stresses acting normal to the cut plane using finite element modelling. The contour method has a unique advantage of generating a 2D cross-sectional map of residual stresses over the plane of interest within the component at a relatively cheap cost with equipment available in most workshops [10]. In theory, the contour method is not limited by the size of the component. Moreover, unlike diffraction techniques, the contour method is not sensitive to microstructural variation of materials.

However, the contour method is still young and needs further development to improve its reliability and extend its capability. In particular, application of the contour method in its current form is limited to a planar cut that sections the component into two symmetric halves. A further limitation is that contour method results are not reliable when measuring residual stresses close to the yield strength of the material due to risk of introducing plasticity during cutting that violates the elastic stress relaxation assumption of the contour method. This PhD thesis aims to address these two limitations.

The research explores approaches for analysing displacement data generated by introducing a contour cut at an arbitrary cross-section in a body producing asymmetric cut parts. Asymmetry of the stress, geometry and stiffness of the cut parts is considered. Secondly, an incremental contour measurement method involving multiple cuts is proposed where residual stresses in the structure of interest are sequentially reduced by successive cuts. This novel approach has the potential to lower or eliminate the risk of inducing plasticity during cutting and thereby reduce consequent measurement errors. Both new approaches proposed in this PhD thesis are successfully demonstrated through numerical simulation using the finite element method and experimentally on benchmark steel specimens and against neutron diffraction measurements.

1.2 Thesis layout

A literature review related to the research studies is presented in chapter 2, which concludes by outlining the methodology used in the thesis. Chapter 3 deals with the first limitation of the contour residual stress measurement method relating to the use of symmetric planar cuts. A new data analysis approach is developed and validated to extend the application of the contour method to cuts made at any location in a component. The proposed data analysis approach for asymmetric contour cuts is further explored in Chapter 4 and its limitations and scope of application discussed. Chapter 5 deals with the second limitation of the contour method; that is when plasticity occurs during cutting owing to the presence of residual stresses of high magnitude. A new approach called the incremental Contour Method (iCM) is proposed and applied to a case example with detailed discussion of the results arising. Chapter 6 draws together and discusses the main contributions to knowledge of this thesis, drawing together overall conclusions and providing some suggestions for future work. A bibliography is provided at the end of this thesis.

Chapter 2: Literature review

2.1 Introduction to residual stress and measurement techniques

2.1.1 Residual stress

Residual stresses are defined as self-balanced internal stresses that remain within a body in the absence of external loading [3]. Residual stress investigation has applications in various fields including biological [11] [12] [13] [14] and engineering structures, but this thesis is concerned only with the latter one. Residual stresses are generated from displacement misfits within the material or body [3]. Any engineering process can potentially introduce residual stress in a body [15] either during the initial manufacturing stage or during the service life. For example overloaded engineering structures [9] may retain residual stress even at rest [16].

Residual stresses can be categorized in three main types according to the length scale at which the stresses self-equilibrate. Macro residual and micro residual stresses are schematically illustrated in Figure 2-1.

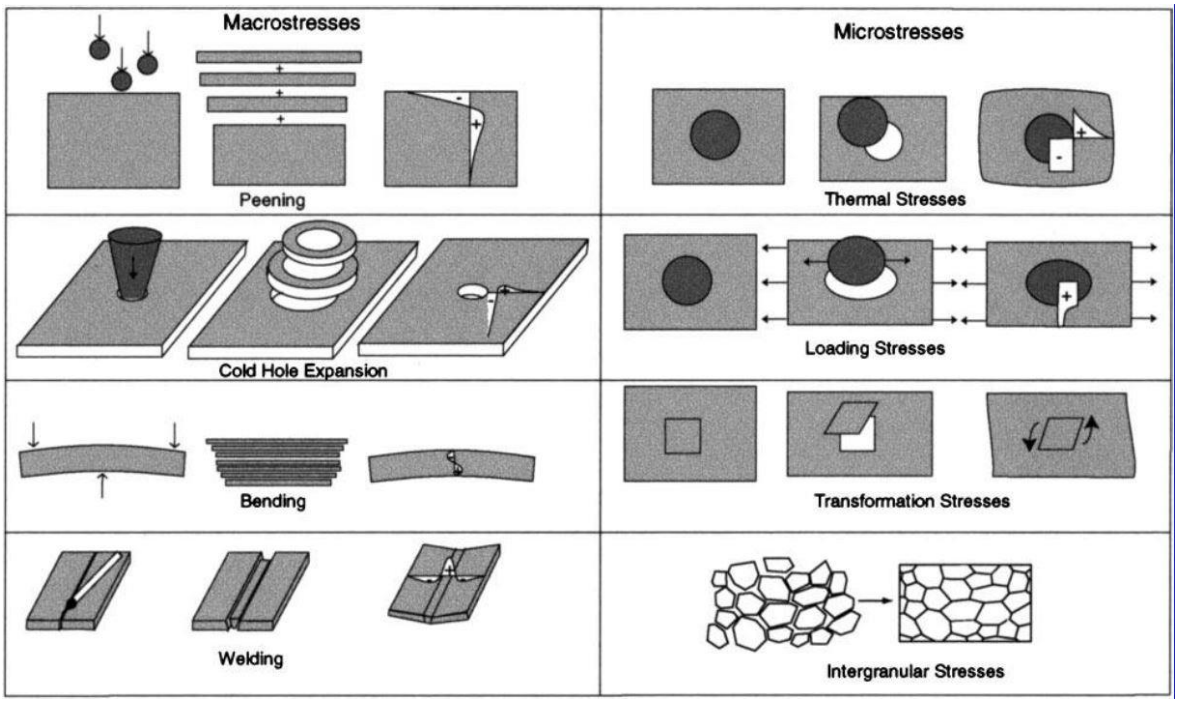

Figure 2-1 Different examples of process originating misfits which generate macro residual and micro residual stresses. In each case the left side illustrates the process, the misfit is indicated in the middle and the generated residual stress distribution is illustrated on the right [3].

The first type is macro stress and equilibrates within the body over a length-scale range much larger than the grain size. There are at least four main ways to generate macro residual stresses [1]. Through the interaction between mis-fitting parts within an assembly, for example riveted plates (if one considers a complete riveted plate as an assembly), chemically introduced (for example arising from the nitriding process), thermally generated (for example via welding components), and plastically induced (for example by the shot-peening process) misfits between different regions within one part. The second type of stress (termed micro stress or intergranular stress) balances over a length-scale comparable to the size of the grain structure, and can be generated by different means such as thermal loading and plasticity. Multiphase materials often 'host' this second type of stress. The third type of stress balances over a length-scale smaller than the characteristic length-scale of the microstructure. The third type of stress can be generated by dislocations for example. This thesis is concerned with macro residual stress, as it is the most important type of stress for engineering applications. For example, it controls distortion during manufacture, affects fatigue life, influences susceptibility to stress corrosion cracking, creep crack growth, hydrogen embrittlement and fracture [15].

Detailed knowledge of the residual stress distribution within a component is required to undertake structural integrity assessments for safety critical plant. For example in the R6 defect assessment procedure [4], which is widely used in nuclear industry for structural integrity assessment, requires the contribution of residual stress to be taken into account.

Numerical methods are increasingly being used to simulate manufacturing processes and predict residual stresses [17][18]. However, reliable prediction of the residual stress distribution within the material is a difficult task when engineering processes used in manufacturing components are complex [19] [20]. For example, welding computational mechanics [21] [22] can give widely varying results [23][24][25][26][27]. Where results from such analyses need to be used in safety assessments the R6 procedure insists that simulations must be validated by measurements ([4] section III-15). There are several techniques available for measuring residual stresses.

2.1.2 Measurement techniques

Residual stress measurement techniques can be classified into three main categories: non-destructive, semi-destructive and destructive techniques [9] as shown in Figure 2-2.

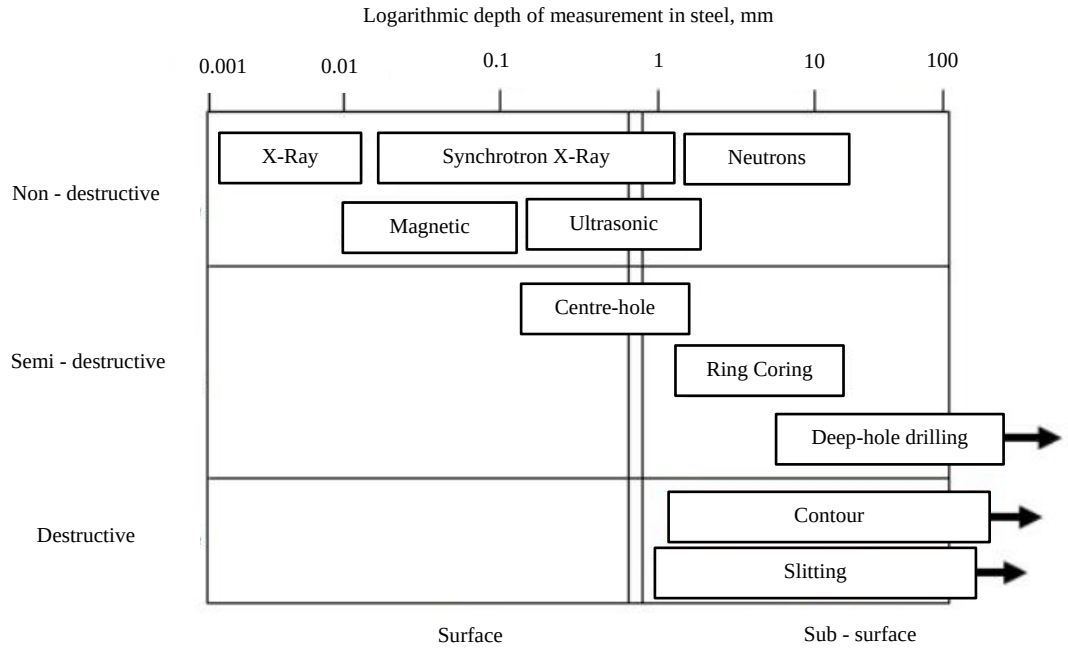

Figure 2-2 Residual stress measurement methods in steel [28]. Courtesy of Foroogh Hosseinzadeh, The Open University, UK.

Non-destructive techniques allow the measured component to be used after the measurement. The most widely used methods in engineering applications are diffraction techniques. Among diffraction methods, X-ray diffraction [29] is feasible in laboratories and is portable for in-situ measurements, whereas neutron diffraction (ND) and synchrotron X-ray diffraction are only available at Central Facilities such as the ISIS Neutron and Muon Source, a world-leading centre for research in the physical and life sciences at the STFC Rutherford Appleton Laboratory near Oxford in the United Kingdom [30].

The main advantage of the ND method is its capability of measuring the full residual stress tensor including stress gradient within the body of a component. In fact, it is possible to measure high stress gradients by reducing the size of the ND gauge volume to around 1 mm by adjusting the irradiated area on the sample and the field of views of the detectors using slits or collimators. However, the technique is sensitive to microstructural variations and is not suitable for near to surface measurements. In fact, when the gauge volume is only partially immersed in the material this generates pseudo strain errors [31]. Other disadvantages are that the ND

method is only applicable to crystalline materials, components have to be taken to large specialist facilities as mentioned above, and the penetration depth is limited [2]. More details about the ND method are presented in the next section as this technique is used for validating the novel contour method approaches developed during this PhD project.

Mechanical relaxation (strain relaxation) methods are categorised as either semi-destructive or destructive residual stress measurement methods. All the mechanical strain relief techniques involve machining part of the material away, measuring the strain or deformation associated with material removal and assuming strict elastic relaxation of residual stresses [32]. However, when the magnitude of residual stresses is high relative to the yield strength of the material, some stress relaxation by plasticity may occur as material is removed which violates the elastic relaxation assumption. This introduces a so-called 'plasticity error' in the measured value of residual stress determined by the mechanical strain relief method. Understanding and controlling plasticity errors has been a longstanding concern for many residual stress measurement practitioners.

Semi-destructive mechanical strain relief techniques allow the component to be used after a residual stress measurement has been done if effective reparation can be achieved. The principal semi-destructive techniques [9] are surface centre hole drilling, and deep hole drilling (DHD) methods. The incremental centre hole drilling (ICHD) measures near surface residual stresses within 1-2 mm below the surface [33]. It involves drilling a small hole and measuring the relaxed strains using specially designed strain gauges. It only measures in-plane stresses along a line profile. The method is cost effective and the equipment is portable so the measurement can be done *in-situ*.

The principal destructive techniques [9] are slitting and the contour method. The main advantages of the slitting method are its high repeatability and insensitivity to material microstructure. However, the main limitation of the slitting method is that it measures one stress component averaged across the thickness of the sample.

This thesis focuses on the contour method which is a promising technique, still under development, for residual stress measurement [10]. The minimum penetration of the contour method is about 0.5 mm below the surface of the body because near surface measurements are error prone as detailed later (Figure 2-2). The maximum penetration depth for the technique is 600 mm as this is currently the maximum section size for wire electrical discharge machining. One unique advantage of this method is its ability to generate 2D cross-sectional maps of

residual stress over the plane of interest at a relatively cheap cost [9]. Unlike diffraction methods, the contour method is not sensitive to microstructure of materials [34]. Nonetheless the main limitations of the contour method are that it is a destructive method, its uncertainty increases near the specimen's surfaces [9], only one component of the stress tensor can be measured [35], and the body must be cut across a mirror-symmetry plane. Moreover, like all mechanical relaxation methods, the contour method can be susceptible to plasticity induced residual stress measurement errors.

2.2 Neutron diffraction method

Neutron diffraction is a well-established technique for measuring residual stress [36] which has been used as an independent method to validate the contour method research measurement results presented later in this thesis. Hence a more detailed overview of the technique is given here. Neutrons can penetrate deep into engineering materials (a few centimetres), when the neutron wavelength is of the same order as the lattice spacing of the material being measured [37], and achieve a spatial resolution better than one millimetre for some steels [2].

Generating neutrons

Neutrons are generated in nuclear reactors or by spallation sources. In nuclear reactors, Uranium atoms are split which leads to a continuous radiation of neutrons. A monochromator is then used to obtain a continuous monochromatic neutron beam. In spallation sources neutrons are generated by bombarding high energy accelerated protons into a target made from elements having a heavy nucleus such as Tungsten, Uranium and Tantalum. This generates a pulsed beam of neutrons having different wavelengths. Spallation sources, also referred to as pulsed sources, use time-of-flight diffractometers to measure lattice spacings [33]. When a monochromatic neutron beam is used for residual stress measurement a single lattice reflection is obtained while a polychromatic beam from a pulsed source gives a full or partial diffraction spectrum [38]. Hence pulsed sources are more attractive than reactor ones in that multiple diffraction peaks can be simultaneously analysed. In fact, the complete or partial diffraction pattern from a pulsed source can be analysed using a multi-peak fitting such as Rietveld [39] or Pawley [40] refinements. The most effective and attractive way to generate neutrons is fusion but this technique is still under development.

Bragg's law

The theory of neutron diffraction measurement is based on Bragg's law given by Equation 2-1 and illustrated in Figure 2-3.

$$\lambda_{hkl} = 2\, d_{hkl} \sin\theta \qquad \text{Equation 2-1}$$

Where λ is the neutron wavelength, d is the lattice spacing, θ is the Bragg scattering angle and *hkl* are Miller's indices.

The incident beams (see "1", "2" and "3" in Figure 2-3) of wavelength λ are diffracted if they pass through a crystal with lattice plane hkl of spacing d similar to the wavelength of the incident neutrons. The diffracted beams (see " 1' ", " 2' " and " 3' " in Figure 2-3) create an angle equal to 2θ with the incident beams.

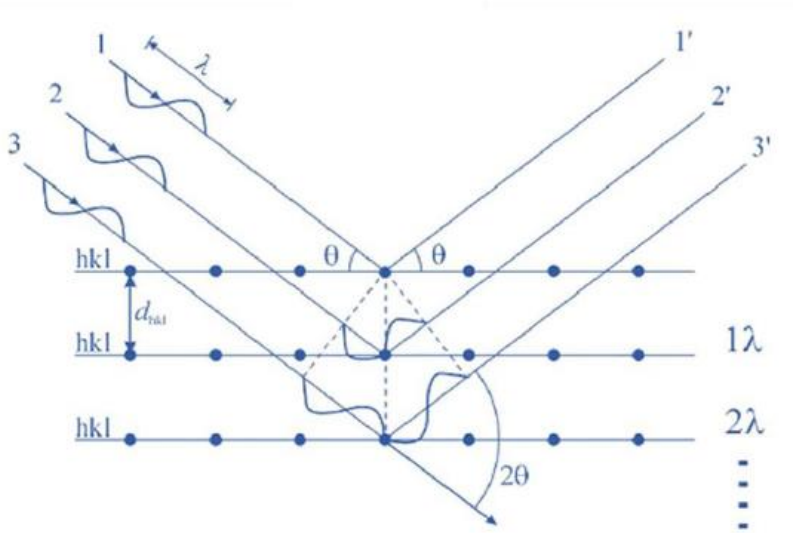

Figure 2-3 Illustration of Bragg's law for diffraction techniques [28]

The lattice spacing d_{hkl} is sensitive to the stress state in the material. A change of lattice spacing d_{hkl} results in a shift in the diffracted peaks during neutron diffraction measurement. Hence any change of stress state within the sample can be detected by comparing the lattice spacing of its material before and after the change.

Stress free lattice parameter

In the neutron diffraction technique, the measured lattice spacing in a material is compared to a reference value where the material is assumed to be stress-free. The difference between the

two states is used as an input to calculate the residual stress retained in the material. Hence measuring this reference value, called the stress free lattice parameter (*d0*), is of paramount importance in the neutron diffraction stress measurement technique [41]. In fact, the final results are very sensitive to the values of *d0* used in the calculations [42]. Measurements of the *d0* value [43] can be done at a remote position (far field assumption) known to contain negligible stress, on a stress-free powder or filings that are representative of the material being measured and on stress-free reference cubes or combs extracted from the specimen. Alternative approaches to the direct measurement of *d0* [38] can be to apply force/moment balance or impose a zero stress condition perpendicular to a free surface to calculate the value of *d0*. Assessing the value of *d0* in weldments can be challenging [44] as there may be a variation of the *d0* value at different locations within a weld and the area around it due to the variation of the material microstructure. Once a value of lattice spacing and a relevant stress free lattice parameter are obtained, strain and stress can be calculated.

Strain and stress calculation

The strain calculation is given by Equation 2-2.

$$\varepsilon_i = \frac{d_i - d_{i0}}{d_{i0}} \qquad \text{Equation 2-2}$$

Where ε is the strain acting in direction *i*, d_i is the stressed lattice spacing along direction *i*, and d_{i0} is the stress-free lattice parameter along direction *i*.

Then stress is calculated from strain using Hooke's law [45] given by Equation 2-3.

$$\sigma_{xx} = \frac{E}{(1+\nu)(1-2\upsilon)}\left[(1-\nu)\varepsilon_{xx} + \nu(\varepsilon_{yy} + \varepsilon_{zz})\right]$$

$$\sigma_{yy} = \frac{E}{(1+\nu)(1-2\upsilon)}\left[(1-\nu)\varepsilon_{yy} + \nu(\varepsilon_{xx} + \varepsilon_{zz})\right]$$

$$\sigma_{zz} = \frac{E}{(1+\nu)(1-2\upsilon)}\left[(1-\nu)\varepsilon_{zz} + \nu(\varepsilon_{yy} + \varepsilon_{xx})\right] \qquad \text{Equation 2-3}$$

Where σ_{xx}, σ_{yy} and σ_{zz} are the stresses acting in directions *x*, *y* and *z*, respectively. E is the crystallographic Young's modulus. ν is Poisson's ratio of the material. ε_{xx}, ε_{yy} and ε_{zz} are the strains acting in directions *x*, *y* and *z*, respectively.

Neutron diffraction facilities

Various international neutron diffraction facilities are currently used for residual stress measurement including the Institut Laue at Langevin (ILL) in France and ANSTO [46] in Australia which are reactor sources. Examples of spallation sources are the Paul Scherrer Institut (PSI) in Switzerland and the ISIS Neutron and Muon Source in the UK. Neutron beam time was awarded for the Engin-X instrument [47] at the ISIS Facility for validating the novel contour method developed during this PhD project (see later chapters).

2.3 The contour method

The contour method involves carefully cutting a body into two mirror symmetric parts. Then the deformations on the cut surfaces, assumed to be due to the relaxation of residual stress acting on the cut plane, are measured, analysed, and used to back calculate the original residual stress distribution prior to the cut [35].

2.3.1 Theory of the contour method

The contour method theory is based on a variation of Bueckner's elastic superposition principle [48]. Bueckner states that the residual stress along a plane of interest in a body (see 'Step A' in Figure 2-4) is equal to the superposition of the stress fields when the part is cut (see 'Step B' in Figure 2-4) and when the opposite of the original stress along the plane is applied on the cut faces (see 'Step C' in Figure 2-4). This principle was illustrated by Paris [49] and Barenblatt [50].

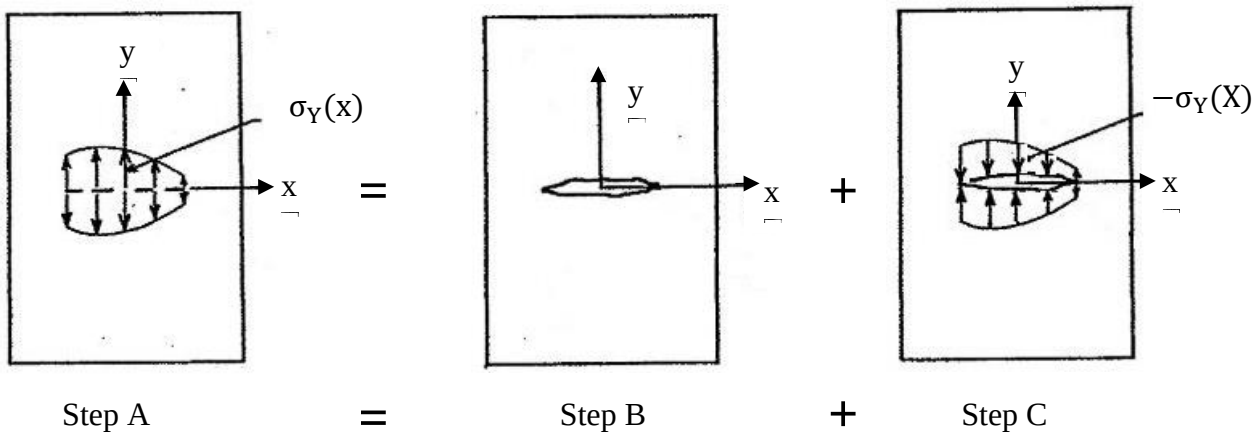

Figure 2-4 Illustration of Bueckner's superposition principle. Adapted from [49].

Prime [35] proposed a variation of that principle where the displacements on the cut faces are measured in Step B (see Figure 2-4). Then the negative of the measured displacement "contour" is applied as a boundary condition in Step C (see Figure 2-4). The main difference between the original Bueckner's principle and Prime's approach is that Prime proposes to apply displacements instead of stress boundary conditions in Step C.

The principle of the contour method [35] is illustrated in Figure 2-5 [51].

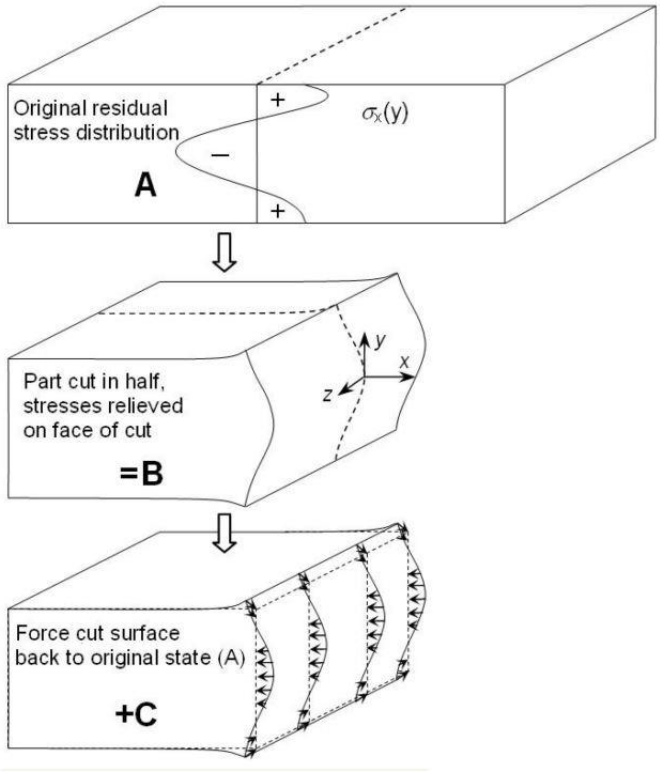

Figure 2-5 Schematic drawing illustrating the principle of the contour method for residual stress measurement [51].

As mentioned above the original stress field within the body (Step A in Figure 2-5) is perturbed through introducing a symmetrical planar cut. As a result, the cut surfaces distort releasing the macro residual stresses acting normal to the cut plane (Step B in Figure 2-5). Then the deformed cut surface is forced back to its original flat shape (Step C in Figure 2-5). Step C involves calculating the resulting change in stress due to the cut.

The original residual stress distribution within the specimen in A (in Figure 2-5) is equal to the sum of the remaining residual stress after the symmetrical cut of the body in B (in Figure 2-5) and the released stress on the cut surface in C (Figure 2-5). Therefore the stress field resulting from the superposition of the stress distribution after the cut was processed in B (in Figure 2-5) with the change in stress field from C (Figure 2-5) is equivalent to the original residual stresses distribution prior to the cut in A (Figure 2-5) [52]:

$$\sigma^A\,(x,y,z) = \sigma^B\,(x,y,z) + \sigma^C\,(x,y,z), \qquad \text{Equation 2-4}$$

Where σ refers to the entire stress tensor and the super-scripts refer to the steps illustrated in Figure 2-5.

The remaining stresses (Step B in Figure 2-5) through the entire cut part are not known. As such one cannot obtain the entire stress tensor throughout the body. However the normal (σ) and shear (τ) stresses acting on the cut surface: σ_x^B, τ_{xy}^B and τ_{xz}^B must be zero due to the free surface boundary condition. Therefore:

$$\sigma_x^B(0,y,z) = \tau_{xy}^B(0,y,z) = \tau_{xz}^B(0,y,z) = 0, \qquad \text{Equation 2-5}$$

Where $\sigma_x, \tau_{xy}, \tau_{xz}$ refers to components of the stress tensor and the super-scripts refers to the steps illustrated in Figure 2-5.

Hence, from Equation 2-4 and Equation 2-5:

$$\sigma_x^A(0,y,z) = \sigma_x^C(0,y,z) \qquad \text{Equation 2-6}$$

$$\tau_{xy}^A(0,y,z) = \tau_{xy}^C(0,y,z),$$

$$\tau_{xz}^A(0,y,z) = \tau_{xz}^C(0,y,z)$$

Where $\sigma_x, \tau_{xy}, \tau_{xz}$ refer to components of the stress tensor and the super-scripts refer to the steps illustrated in Figure 2-5.

However, in practice, one can only measure displacements normal to the cut surface. The in-plane displacements associated with the release of shear stresses are not measured. Therefore, the contour method can measure normal stress to the cut surface only. If shear stresses on the cut plane are zero then Step C (Figure 2-5) correctly calculates the normal stresses. In the general case, where there are shear stresses on the cut surface, one only needs to average the

surface deformations or the two mating cut surfaces to cancel out the effect of shear stress. The shear stresses acting on the cut surfaces are illustrated in Figure 2-6.

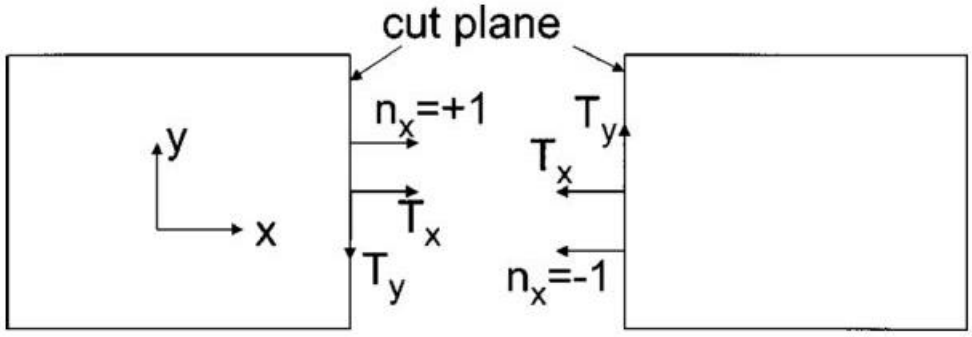

Figure 2-6 Schematic view of the surface tractions acting on the cut surfaces (normal to the direction n_x). The normal tractions T_x are symmetric whereas the shear tractions T_y are asymmetric [35].

T_x is the surface traction equivalent to releasing the normal stress and T_y is the surface traction equivalent to releasing the shear stress. As can be observed, the normal traction T_x is symmetric about the cut plane while the transverse traction T_y is asymmetric. As such, the released shear residual stress generates asymmetric displacements on the cut surfaces [52] as illustrated in Figure 2-6. Averaging the displacements from the opposing cut surfaces cancels out the shear stress effect [35] whilst giving a more accurate contour method measurement of stresses acting normal to the cut plane.

There are three main assumptions inherent to the contour method for residual stress measurement [35]:

a. The stress relaxation process is strictly elastic.
b. The cutting process doesn't introduce significant additional stress to affect the measured displacement.
c. The cut removes a constant width of material from the original specimen without any re-cutting of the previous cut faces.

The first two assumptions (a and b) must be satisfied for the superposition principle described above to apply. These two assumptions are common to most mechanical relaxation methods for residual stress measurement [9] and have been studied extensively [53] (although the cutting method for other techniques is not the same). The third assumption c is specific to the contour method [52]. Any violation of the three assumptions listed above generates errors in the contour method results [51] and will be explored later in the thesis.

2.3.2 Experimental procedure for the contour method

Step 1: Cutting the sample

The cut step is crucial for the contour method as it has considerable impact on the quality and accuracy of the results. The ideal cut has zero width and does not introduce additional stress in the material [54].

The technology that matches best those two assumptions is wire electrical discharge machining (EDM) [55]. In fact, wire EDM is a non-contact cutting technique [56] that vaporizes the material being cut through electrical arc discharges [57] [58]. The specimen being cut is submerged in dielectric liquid, usually de-ionized water. Thus a thin layer of dielectric liquid is separating the EDM wire from the specimen which avoids short circuiting [59]. The wire is running from an upper guide to a lower guide traversing the specimen through its thickness (see Figure 2-7).

Prime et al [51] asserts that the contour cut using EDM wire must not recut previously cut surfaces, no plasticity [60] must occur at the cut tip, the cut width must be constant, and the stiffness of the part affected by the stress relaxation must be mirror-symmetric with respect to the cut plane.

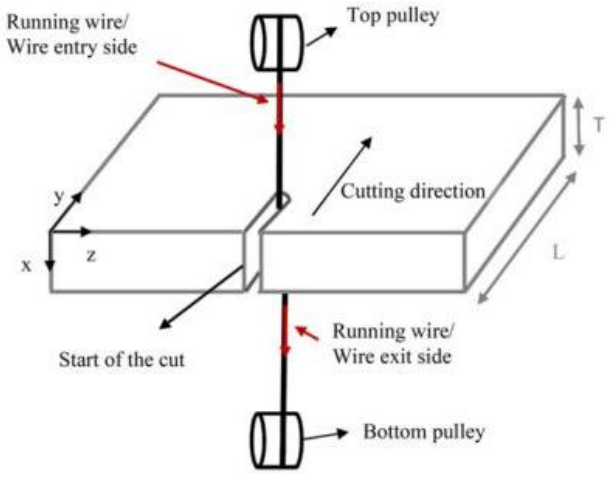

Figure 2-7 Schematic view of a sample cut using wire EDM [54].

However, cutting artefacts may occur during the contour cut [61]. Also the clamping configuration of the work piece during the contour cut [62] may have a significant impact on the quality of the cut surface and the contour method measurement results. The errors in contour method residual stress measurement due to cutting artefacts and the measures suggested by various practitioners to minimize and correct the errors [51] will be discussed later.

Step 2: Measuring the cut surface topography

The aim of the surface contour measurement step is to obtain the displacements due to the assumed elastic relaxation of residual stresses after the cut. This measured displacement is processed and used to calculate the original distribution of residual stresses prior to the cut. The perimeter of the cut surfaces is also measured and used in the data analysis step as will be discussed later.

Various tools can be used to measure the topography of surfaces [49], but for the contour method coordinate measuring machines (CMM) [58] are most widely used. The CMM is linked to a computer where the raw data from the CMM are processed through specially adapted software. Various sensors can be 'plugged-in' to the CMM machine to measure the specimen's deformation [63], including touch probes (see Figure 2-8) and laser based sensors (for example a triangulation laser, see Figure 2–9, [64]).

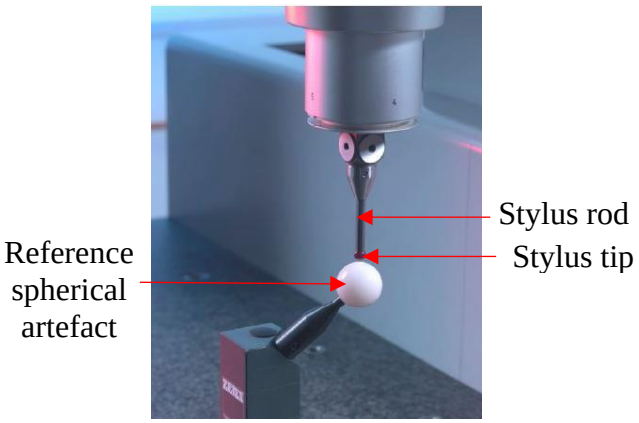

Figure 2-8 Illustration of an example of a touch probe stylus and a reference spherical artefact [63].

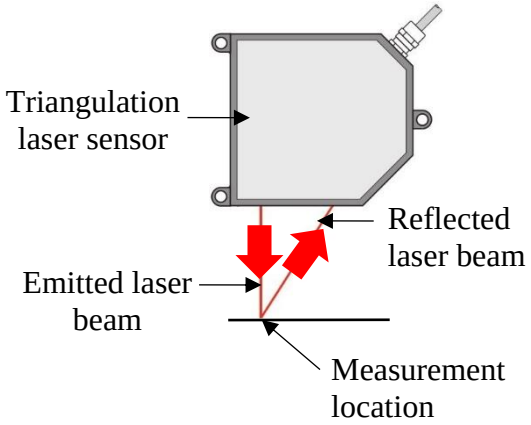

Figure 2-9 Schematic view of surface topography measurement using triangulation laser sensor, adapted from [64].

The working principle of the touch probe system is that when the stylus ball touches the specimen, the coordinates of the stylus tip are recorded. The stylus tip of a touch probe has a spherical shape and is made from ruby. The diameter of the stylus tip can vary from 1mm to 8mm [65]. The choice of the stylus tip diameter is sometimes important as a large diameter tends to smooth the surface topography [66] and this can be significant when the length-scale of the residual stress distribution being measured is small. Other limitations of the touch probe

sensor include the possibility of indenting the cut surfaces and wear of the stylus tip during the measurement.

The principle of the triangulating laser sensor is that the emitted laser beam hits the target surface topography measurement location and is reflected back and measured by a charge-coupled device (CCD) array enabling the surface position (distance from probe) to be calculated. The spatial resolution of triangulating laser sensors is higher than touch probes. Also triangulation laser sensors allow surface topography measurement near the edge of the cut surface to be done. Moreover, the speed of data acquisition is faster using triangulation laser sensors than with touch probes. Laser probe systems are more sensitive to the quality of surface finishing than touch probe, although surface measurements made by laser sensors tend to be noisier than those measured using touch probes. But the main limitation of the laser triangulation sensor is that is cannot measure dark or highly reflective surfaces.

Step 3: Data analysis

The aim of the data analysis step is to process displacement measurements (i.e. the deformation "contour") of the cut surfaces. Then this processed displacement contour is used to back calculate the original residual stresses that were present over the cut plane of interest prior to the contour cut. The measured perimeter of the cut surfaces, as mentioned earlier, is also used to facilitate the data analysis. The key sub-steps of data analysis [61] are detailed below.

Mirroring and aligning the two sets of data

As mentioned earlier the surface contour of the two cut surfaces is averaged to remove the effect of shear stresses and possible asymmetric cutting artefacts. However, the two cut surfaces are measured in two different coordinate systems. In order to average the two measured contour displacements point by point, the two sets of data must be in the same coordinate system. Hence one set of data is mirrored about the Y axis (see 'Mirroring' in Figure 2-10), then rotated and translated in the XY plane in order to get the two data sets aligned in one common coordinate system (see 'Alignment' in Figure 2-10). The measured perimeters of the cut parts are used to align the two data sets [67].

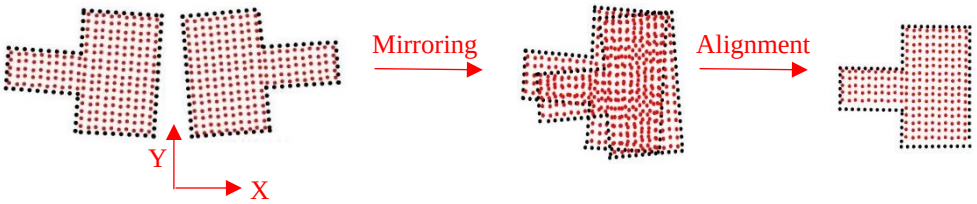

Figure 2-10 Mirroring and alignment of the two sets of data. Red dots refer to cut surfaces' displacement data while black dots refer to cut surfaces' perimeter data.

Interpolating the two data sets into a common grid

During the surface topography measurement, positioning uncertainties across the XY plane arise owing to instability of the measurement instrument (usually a CMM), or caused by other sources such as the misalignment of the cut surfaces [68]. These uncertainties may result in a mismatch between the locations of the points measured on the cut surfaces. This mismatch between the measured points cloud on the mating cut surfaces is tackled by interpolating the two data sets onto a common grid.

Extrapolating the data to the cut surface perimeter

The measurement of displacement near the edge of the cut surface can be prone to error [68]. In addition, cutting artefacts may occur near the edge of the cut surface as will discussed later. Moreover, measurement close to the edge of the cut surface is often not practical. However, the displacement contour across the entire cut surface including up to the perimeter has to be defined for the stress back calculation step. The missing data is dealt with by extrapolating the measured profile to the perimeter. The "measured" residual stresses calculated from extrapolated data have to be interpreted with caution and are often not reported.

Averaging the displacement contours of the two cut surfaces

Displacements caused by stress relaxation acting normal to the cut plane are mirror-symmetric across the cut plane [51], (see Figure 2-11), for mirror-symmetric stiffness and restraint conditions during cutting. On the contrary shear stresses, or cutting artefacts (as mentioned earlier) can cause asymmetric displacements (Figure 2-11). Averaging the contour displacements of the two cut surfaces can cancel the effect of shear stresses and asymmetric

cutting artefacts (although cutting artefacts can also cause symmetric errors as will be discussed later).

The arithmetic average of the contour displacements on the two cut surfaces is given by:

$$U_{Average}(x,y) = \frac{U_{Left}(x,y) + U_{Right}(x,y)}{2}, \quad \text{Equation 2-7}$$

Where $U_{Average}(x,y)$ refers to the displacement averaged at location (x,y) on the cut surface, U_{Left} refers to the displacement on one of the cut surfaces, and U_{Right} refers to the displacement on the opposing cut surface. The averaged displacement $U_{Average}$ is obtained after translation and rotation of displacements on one of the cut surfaces with regards to the mating cut surface.

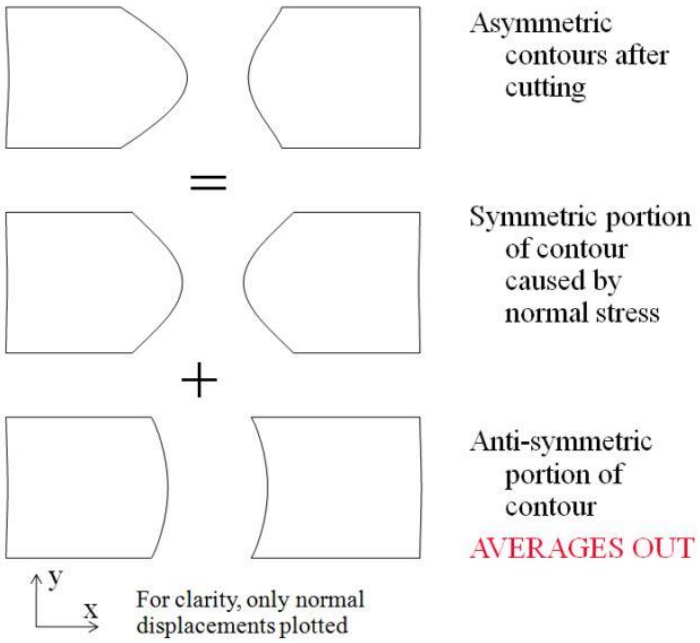

Figure 2-11 Schematic view of symmetric and asymmetric displacements after the contour cut [51].

Cleaning the raw contour displacements data

At this stage evident 'outliers', which refers to the data clearly isolated from the main underlying features of surface deformation (see Figure 2-12), are removed. This subjective step is sometimes referred to as "data cleaning".

The reference plane, related to the zero position within the measured contour displacement data set, is defined arbitrarily. In fact, the zero position is defined as an average of the whole data set. Therefore, the reference plan is located in the middle of the measured points cloud.

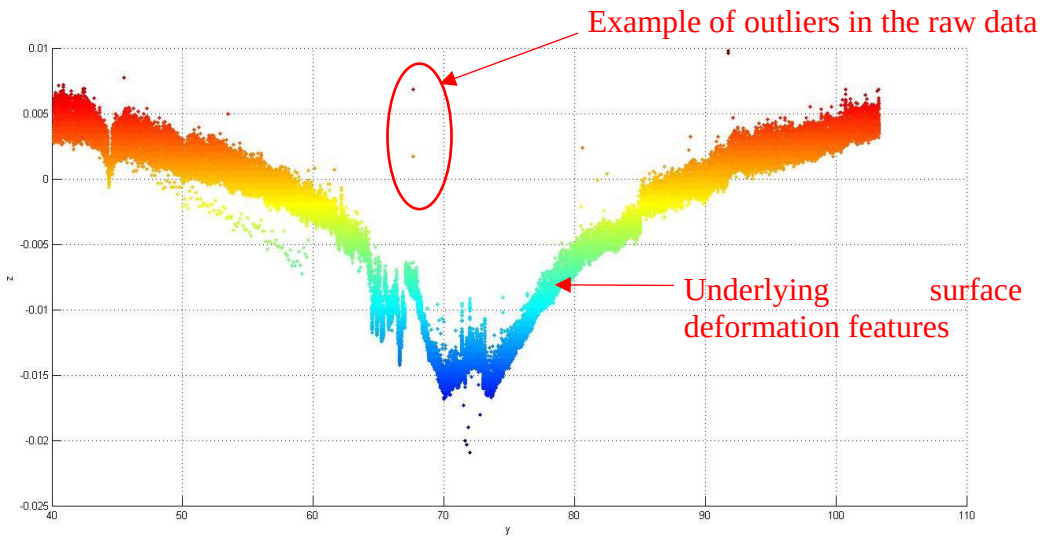

Figure 2-12 Illustration of outlier and main raw data. The colors refer to different displacement magnitudes.

Smoothing the data sets

Surface contour measurement data include inherent noise. The noise is undesired data that can be generated by different sources such as for example dust on the measured locations, surface roughness, or measurement instrument errors. The noise is amplified during the stress back calculation and therefore must be dealt with prior to the stress analysis step of the contour method. As such the averaged and cleaned data needs to be smoothed whilst capturing the main features of the surface deformation. Hence smoothing the data is necessary. Different smoothing methods can be used for the contour method. The most common smoothing methods used are polynomial fitting [69], bivariate Fourier series [70], and two dimensional splines [68]. Prime et al [68] reported that smoothing using the Fourier series method may fail to capture important features on a surface topography during a contour method measurement. Two dimensional spline smoothing is the most widely used smoothing method for the contour displacement data analysis. A spline is a mathematical function defined on intervals between data points. Each interval is bounded by ‘knots’. The spline function must be continuous in

particularly at each knot. The spacing between the knots defining the spline and the order of the mathematical function are important parameters impacting the smoothing results. A coarse knot spacing over-smooths the data whereas a fine knot spacing tends to under-smooth the data. The knot spacing parameter value is often chosen subjectively, that is according to the judgement of the practitioner based on the difference between the raw data and the fitted interpolation function [71].

A more objective approach would be to optimize the knot spacing based on the resultant error in the residual stress measurement result. Prime et al [68] suggested to incrementally increase the knot spacing within a specific range (see Figure 2-13).

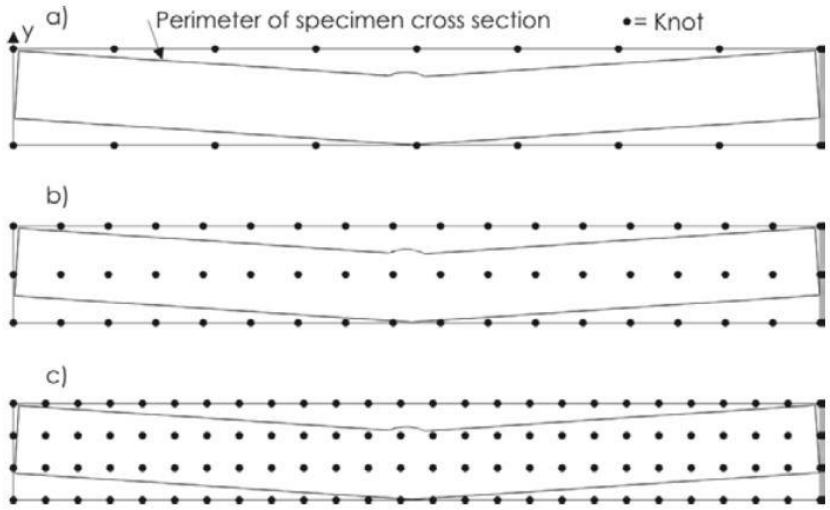

Figure 2-13 Example showing incremental refinement of knots for the smoothing splines. The top (a) shows the coarsest grid, the middle (b) and bottom (c) shows the two next incrementally finer grids [68].

Then for each increment nodal residual stresses are extracted from the finite element (FE) model used for the back calculation of residual stresses. The standard deviation (STD) of the residual stress results between each two successive increments is given by Equation 2-8:

$$\partial\sigma(i,j) = \frac{1}{\sqrt{2}}\,|\sigma(i,j) - \sigma(i,j-1)|, \qquad \text{Equation 2-8}$$

Where $\sigma(i,j)$ is the stress at node i using a spline j, j-1 refers to previous coarser smoothing spline solution.

Finally the global stress uncertainty is given by Equation 2-9:

$$\overline{\partial\sigma}(j) = \frac{1}{\sqrt{n}}\sqrt{\sum_{i=1}^{n}[\sigma(i,j)]^2}, \quad \text{Equation 2-9}$$

Where n is the number of finite element nodes on the cut surface in the model.

The optimum knot spacing is chosen based on the minimum averaged uncertainty in the calculated stresses using Equation 2-9. This approach is more objective since the optimal knot spacing is chosen as the one minimizing the error in the computed residual stresses. However, this approach can be time consuming, since the back calculation of stresses using FE analysis must be processed for each increment of knot spacing parameter.

Step 4: Back calculation of stresses

For the stress back-calculation a three dimensional FE model of one of the cut parts is created. Only one half of the specimen is modelled because the specimen is cut symmetrically. The back calculation of stresses involves forcing back the deformed topology of the cut surface to its assumed original flat shape. However, for convenience the cut part is modelled having a flat cut surface. Then the reversed contour displacements are applied as boundary conditions on the modelled flat cut surface. Because the surface deformations are small in comparison with engineering components dimensions and the FE model is elastic, having a flat cut surface as starting point for the analysis doesn't impact the back calculation of residual stress results.

The elastic material properties (Young's modulus and Poisson's ratio) are used as input to the FE model. The material is assumed to have isotropic behaviour. It was assumed that the Young's modulus value was the same at the parent and weld regions in the material as no filler metal was used in the autogenous welding process.

The mesh is usually generated by linear 8-nodes or quadratic 20-nodes elements with reduced integration. The FE element size must not induce additional smoothing of the contour displacement. Hosseinzadeh et al [54] asserts that the element size must be smaller than one quarter of the knot spacing used for the smoothing model.

Minimal constraints must be applied to the FE model to avoid perturbing the stress distribution resulting from the applied displacement boundary conditions, but must stop rigid body motion. Figure 2-14 shows an example of constrained translations in Z and Y directions in order to prevent rigid body motion.

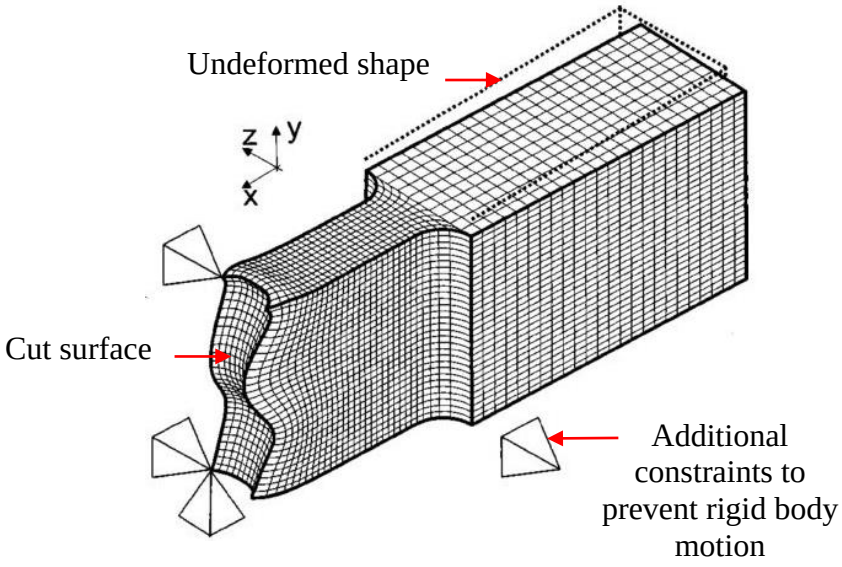

Figure 2-14 Example of a deformed view of a finite element model, after contour displacements were applied as boundary conditions on the cut surface. Additional constraints preventing rigid body motion are also illustrated. Adapted from [35].

Linear elastic stress analysis is then performed to generate a two dimensional map of residual stresses acting normal to the plan of the cut (see Figure 2-15).

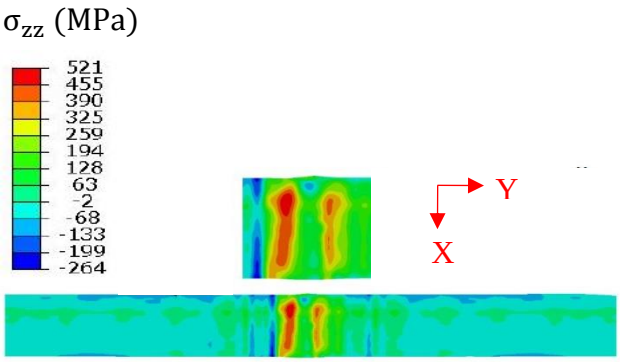

Figure 2-15 Example of two dimensional map of residual stresses acting normal to the plane of the cut in the contour method [72].

Recently analytical solutions have been proposed as a new alterative to the FE method for back calculation of stresses [73]. In this approach the displacements are applied as boundary

conditions in basic geometries for example a semi-infinite strip or finite rectangle. Analytical solutions for back calculation of residual stresses are derived for both plane stress (where the stress state can be represented by a tensor of dimension 2) and plain strain (where the strain state can be represented by a tensor of dimension 2) conditions. The results of residual stress measurement using this new 'analytical contour method' were validated against 'conventional contour method' and neutron diffraction measurements and very good correlation was found between the three approaches [73]. The new alternative analytical solutions for back calculation of stresses removes the dependency of the contour method on the FE method. However, the approach is limited to simple rectangular shapes.

2.3.3 Fracture surface approach for the contour method

The contour method can be also adapted to measure residual stress on a fractured specimen [74]. The main difference between this 'fracture surface method' and the conventional contour method is that the specimen is not cut using wire EDM rather the two parts were separated as a result of a brittle fracture. The fracture surface method can provide valuable information about residual stress for forensic failure analysis. Prime et al. [75] invented this new approach and validated it numerically and experimentally. A 7000 series aluminium alloy forging specimen was fractured into two parts having similar sizes. The brittle type of fracture ensured that relaxation of residual stress along the fracture path was elastic in nature. Then the displacements normal to the fractures faces were measured and averaged. The fractured faces would perfectly match if no residual stress was relaxed along the fracture path. Hence the mis-match between the mating faces was used to back-calculate the original residual stress that was present prior to the specimen fracture. This approach was successfully extended by Oliveira et al. [76] to measure the residual shear stress in addition to the direct residual stress acting normal to the fracture path on the specimen. The shear stress components were obtained by measured the relaxed in-plane displacements using digital image correlation (DIC) [77]. Then the negatives of both the in-plane and out-of-plane displacements were applied as boundary conditions during the back-calculation step [74].

2.3.4 Uncertainties and errors related to the contour method

There are various sources of uncertainties and errors associated with each step of the contour method including cutting the work piece, surface measurement, data analysis and back

calculation of residual stresses. However, in this section the focus will be on plasticity induced errors associated with the cutting step of the contour method that is directly relevant to the investigative work of this thesis.

Cutting errors

As mentioned earlier an ideal contour cut doesn't introduce additional stress within the material, has zero width, is planar, doesn't recut previously cut surfaces and any surface deformation arising is entirely due to the elastic release of residual stress.

However, in practice the contour cut deviates from the ideal conditions described above and therefore can introduce errors in the measured contour method residual stress results. In fact, additional cutting artefacts such as wire breakages may occur and introduce other errors in the residual stress measurement results. Cutting errors are categorized as symmetric or antisymmetric geometric features in the topography of the created cut surfaces. The sources of cutting errors can be either stress dependent or stress independent.

The main sources of symmetric and asymmetric errors are summarized in Figure 2-16.

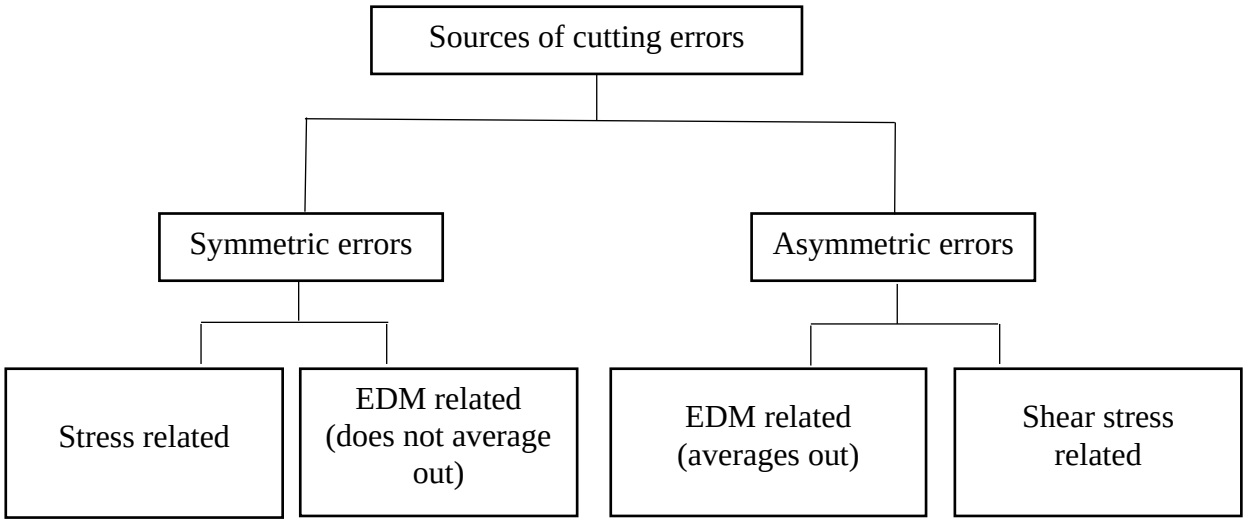

Figure 2-16 Diagram summarizing the main sources of cutting errors.

Asymmetric errors cancel out when the contour displacements of the cut surfaces are averaged during the data analysis step. In contrast symmetric errors don't cancel out and introduce errors in the results of the contour method. Therefore, symmetric errors are problematic for the contour method. As shown in Figure 2-16 symmetric errors are either stress dependent or could be introduced due to the nature of wire EDM process.

Hosseinzadeh et al [54] have discussed extensively EDM related symmetric cutting artefacts and suggested measures to mitigate them. The two main symmetric errors owing to the stress state in the material are the 'bulge error' [51] (related to the violation of the assumption of a constant cut width during the cutting step) and the 'plasticity error' [51].

Bulging error

Sometimes during cutting, the material in the remaining ligament can be elastically stretched or compressed due to residual stress redistribution associated with previous cutting increments [51]. This can change the width of the material cut, although the nominal cutting frame is still assumed to be constant (see Figure 2-17). Hence, during the back-calculation step, where the deformed cut faces are forced back to their assumed flat nominal shape, errors can arise in the contour method results [78]. This so-called 'bulging' error can be assessed and corrected for using an iterative FE approach first proposed by Prime [51]. In his approach Prime [51] maps the back-calculated stresses into a two dimensional FE model of the sample. Then the cut is simulated by removing elements incrementally along the cut line. The displacements are recorded and used to estimate the bulge error. Hence the measured contour displacements can be corrected using the estimated bulge error and whole approach is repeated until the back-calculated stresses converge.

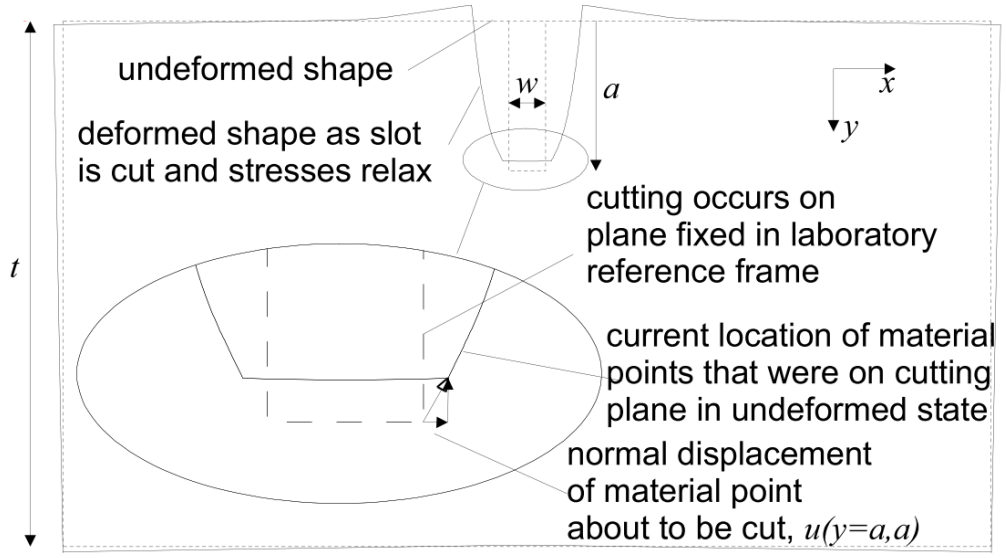

Figure 2-17 Illustration of the bulging error in the contour method [51].

Plasticity error

While the specimen is being cut by wire EDM, the residual stresses along and normal to the cut plane are rebalancing in reaction to the new boundary conditions (free cut surfaces where the cut has been done). Also stress concentration develops at the cut tip. The accumulated localised stresses can cause yielding if the stress magnitude is high enough. If significant yielding occurs (i.e. the yielding zone expands sufficiently far from the cut tip,) this violates the contour method assumption of elastic stress relaxation and will introduce errors in the measured residual stress results. For example, Mahmoudi et al [79] reported that residual stress measurements using the contour method showed plasticity effects. Plasticity errors in contour residual stress measurement results can give a distorted distribution and reduce the magnitude of tensile peaks [79].

Wire EDM cutting is similar to introducing an edge crack into a body. Based on the concept of fracture mechanics the stress field as well as plastic zone size ahead of the cut tip can be characterized using the mode I stress intensity factor (SIF) [80]. Hence, the severity of stress at the cut tip (SIF) can be used to assess the likelihood of plasticity during the contour cutting process. Reducing the SIF and its associated crack opening helps to reduce the effect of plasticity [30,31] for example by introducing more rigid clamping conditions during cutting. Traore et al [81] proposed a novel approach to help mitigate plasticity errors in contour method measurement by using an “embedded cut” configuration combined with secure clamping of the sample (8 holes for fitted bolts) and using a large wire diameter, all of which reduced the stress intensity at the cut tip (see Figure 2-18). An embedded cut configuration involves defining a cut path joining two holes (start and finish) previously drilled in the material. This generates a smaller SIF than that generated by an edge crack [82].

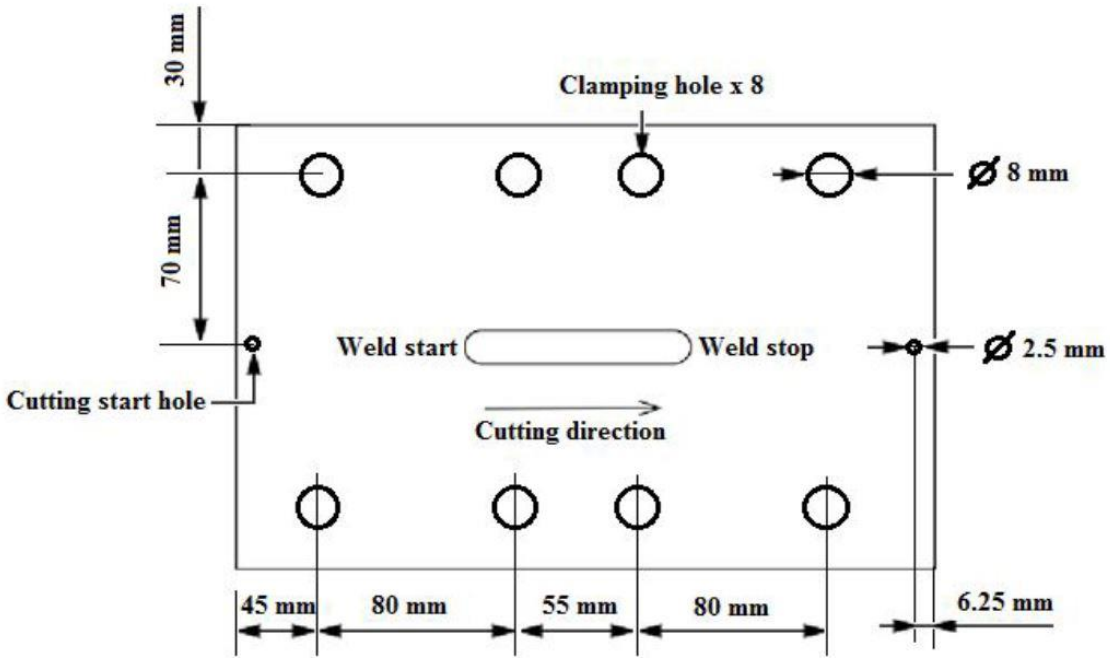

Figure 2-18 Example of embedded cut configuration with secure clamping approach applied on a benchmark specimen [81].

The size and location of the cutting start and finish holes, as well as the position and number of clamping holes, was optimized using FE simulations in order to minimize the SIF at the cut tip and thereby reduce the measured residual stress plasticity error. This approach was examined and validated numerically by Muransky et al. [83] and experimentally by Hosseinzadeh et al. [84].

2.3.5 Contour method needs and gaps

Uncertainties assessment

The contour method is one of the youngest residual stress measurement techniques and no standard has yet been established, especially with regard to uncertainty assessment of the results [2]. Prime suggested a novel approach to quantify the uncertainty on the stress calculation caused by the smoothing step during the data analysis [68]. However, this approach

can be cumbersome as the back-calculation step needs to be done for each different smoothing configuration until the error is minimized. Also, the calculated error is related only to the smoothing of the measured contour displacements. Hosseinzadeh et al. [85] assessed the uncertainty on the contour method results caused by the contour displacement measurement step. The same contour displacements were measured by two different instruments and the differences between the measurements were used to assess the uncertainty in the stress results. This approach involves using different instruments during the measurement step which can be time consuming. Uncertainty caused during the cutting step was also assessed using stress-free reference contour cuts [86] [87]. A more general approach that takes into account various sources of errors in the contour method was proposed by Olson et al. [88]. He quantified the 'displacement' errors caused by noise during contour displacement measurement using a Monte Carlo approach. Also, he took into account the 'model' error caused by the choice of smoothing parameters by calculating the standard deviation of the back-calculated residual stress using a range of different smoothing configurations. Then, the two sources of errors were combined to a single total uncertainty estimator. However, this approach can be challenging to implement in practice as it is cumbersome.

Plasticity induced errors

The novel approach suggested by Traore et al [81] and mentioned in the previous section was implemented by Hosseinzadeh et al [82]. Although the contour results were in reasonable agreement with neutron diffraction measurements, there was evidence of significant plasticity error in the contour method results despite the measures taken. The plasticity errors were manifested by lower than expected stress peaks magnitude and an asymmetric stress profile across the weld. Also, Muransky et al [89] examined optimal cutting configurations to mitigate plasticity cutting induced errors. However, although the approach proposed by Traore et al [81] and Muransky et al [89] helps to reduce the risk of plasticity errors, plasticity induced errors can still be problematic and limit the capability of the contour method

Single stress component measurement

The contour method only measures one direct stress component. However extensions of the conventional contour method including multiple-cuts [9] [90], the multiaxial contour method

[90] [91], and multiple-method approaches [92] that allow multiple stress components to be measured.

In the multiple-cut contour method [93], a first cut is done along a symmetry plane on the sample. Then, using the conventional contour method the residual stress acting normal to the cut plane is obtained. A second cut can then be done along another symmetry plane of one (or both) of the cut parts in direction normal to the first cut plane. The relaxed residual stress in the first cut half component acting normal to the second cut plane is then obtained using the conventional contour method (this is not the original residual stress prior to any cutting). However, using the principle of superposition, the back-calculated stress from the second cut can be superposed with the relaxed stress from the first cut along the second cut plane to obtain the original stress. The main limitation of this technique is that the shear stress relaxed from the first cut can change the stresses measured by the second cut. Hence errors can be introduced in the results from the second cut, and this error can propagate in the results from any additional cut. Another limitation is that the second cut gives information about residual stress along a plane different from the one of the first cut. Hence, additional stress components cannot be obtained along the same measurement plane using this technique, although two direct components of stress are determined along the line where the cut planes intersect.

The multiaxial contour method [90] [91] allows multiple residual stresses to be measured using multiple contour cuts. However, the multiaxial contour method is mainly limited by the assumption that the process introducing residual stresses in the material is continuous. Here, this means that residual stress is generated from a plane strain state in the body. Such a process can be for example welding starting from one edge until the opposite edge of a body. The start and end welding effects are neglected so that the strain along all the weld location is assumed to be the same.

Combining the contour method with other residual stress methods [94] allow multiple residual stress components to be measured. For example, Hosseinzadeh et al. [85] proposed a new approach to measure hoop stress along a symmetry plane on a pipe after a contour cut, then did X-Ray measurements to obtain axial and radial stress components along the cut faces.

Symmetric and planar cuts

The conventional contour method is limited by the use of planar cut configurations dividing a component into mirror symmetric parts during the cutting step as mentioned earlier in this

chapter. This restricts its capability to measuring residual stresses acting normal to a mirror symmetric cut plane in a body. But most engineering components have a complex geometry and locations of interest where residual stress information is required often do not sit on a convenient mirror symmetric plane.

There is therefore a need for a contour method procedure which can determine residual stresses on a cut plane where the cut parts have asymmetric elastic stiffness. Figure 2-19 illustrates two different materials which have been joined, perhaps by diffusion bonding, and for which it is imagined that a contour cut is made across the join plane. In this case, the cut path is along a geometric symmetry plane, but the cut parts have different stiffnesses owing to the different elastic moduli of the materials. The term 'flat asymmetric cut' is used in this thesis to cover production of contour method cut parts having asymmetric elastic stiffness (in a direction normal to the cut plane) whether owing to material elastic properties or geometric asymmetry. Figure 3-20 illustrates a flat cut path passing by the edge of a central embedded weld in a flat plate. This gives cut parts having asymmetric stiffness across the cut plane owing to both geometry and potentially elastic modulus (of the weld metal).

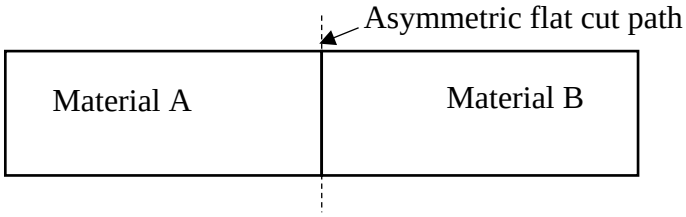

Figure 2-19 Example of a flat asymmetric cut path creating two parts that are geometrically symmetric but the elastic stiffness is asymmetric owing to the material properties

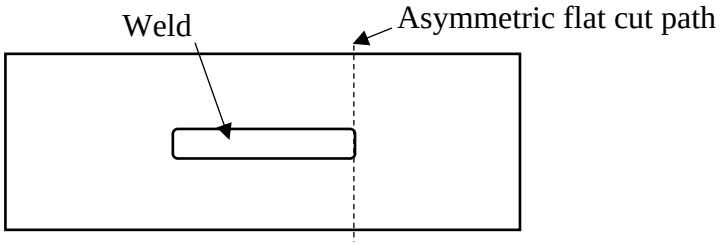

Figure 2-20 Example of a plate with a central weld where the asymmetric cut path passes by the edge of the weld giving asymmetry of geometry, stiffness and residual stress field.

The significance of using asymmetric cutting for contour residual stress measurement was explored by Zhang et al [95] and more recently by Mahmoudi [96]. Zhang used 2D linear elastic FE simulations of the asymmetric cutting process by removing elements along the cut path. The two cut surfaces deformed asymmetrically as expected (see Figure 2-21). The original residual stresses prior the cut were back calculated separately for the two mating cut surfaces, then averaged. The averaged residual stress profile matched with the known residual stress profile (see Figure 2-22). However further work is required to demonstrate the validity of this approach and validate it experimentally against independent residual stress measurement such as ND. Also the left cut part deformations at the cut surface are unexpectedly higher than the ones on the right cut part. This might be caused by the original stress field prior to the cut. The effect of the stress field on the asymmetric cut is explored and discussed in chapter 3.

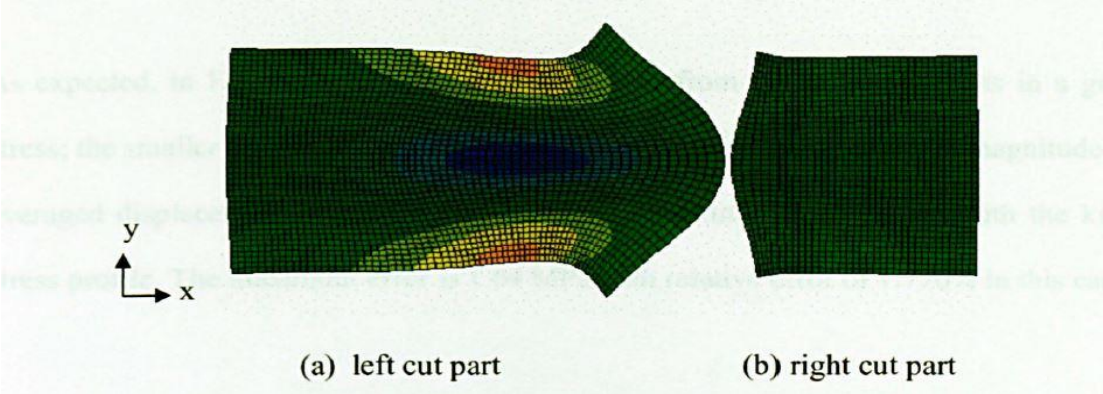

Figure 2-21 Deformed view of the 2D linear elastic FE model (the deformation magnification is 643) showing the shear stress contour [95].

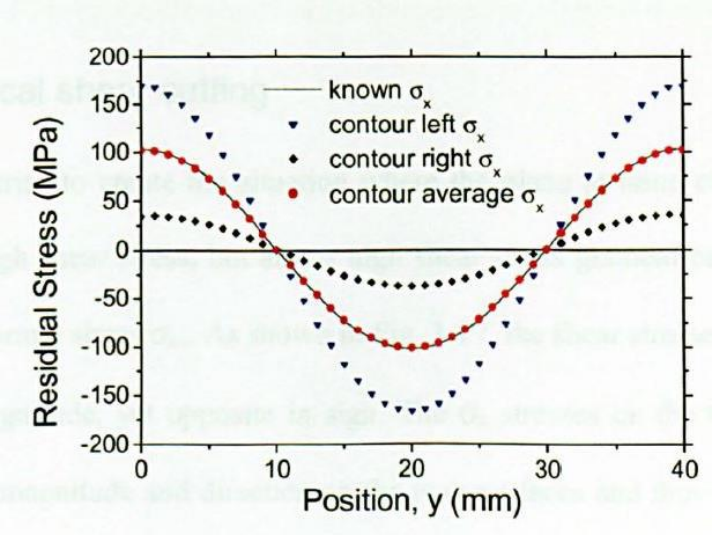

Figure 2-22 Stress line profiles measured on the cut surfaces after an asymmetrical cut [95].

Mahmoudi [96] suggested a novel approach to deal with an asymmetric cut in the contour method. He states that averaging the contour displacements is still a requirement for eliminating the effect of shear stress [96]. So, in his approach, the deformations from both mating cut surfaces are averaged, then the back calculated stresses from each cut part are averaged again to obtain the original stress acting out of the cut plane. However, for an asymmetric contour cut, the stiffness of the mating cut parts will be different from each other. Hence, the displacements of the mating cut parts will differ in magnitude. Thus Mahmoudi's approach [96] is incorrect in that averaged displacements will be incorrectly applied to the mating parts resulting in an incorrect calculation of stress for each part, for which final averaging of stresses from the two parts will not correct.

Non planar cuts

The conventional contour method is restricted to flat cuts. However, non-planar cuts could allow the normal stress component to be calculated at each single point measured on the cut surface. Hence residual stress components could be measured in multiple directions using a single cut. Extending the capability of the contour method to deal with asymmetric flat cuts might be a first step towards using non planar cuts.

2.4 Summary

Residual stresses can be introduced within engineering structures by almost any engineering process [3]. Also residual stresses can arise within materials during the life cycle of an engineering component like for example owing to a weld reparation. Residual stresses can combine with in-service stresses during the life cycle of an engineering component increasing the chances of premature failures. Hence information related to residual stresses retained within materials must be accurately known. In fact residual stresses must be taken into account for safety structural integrity and life assessments [97]. However residual stresses are very complex to predict [1]. Hence reliable residual stress measurement methods are indispensable tools for acquiring knowledge of the residual stress state retained in materials and structures.

Various residual stress measurement methods are available [2] as described earlier in this chapter. XRD and ND are the most used non-destructive techniques. As for any other non-destructive methods XRD and ND allow the specimen to be used after residual stress measurement but are mainly limited by their sensitivity to the microstructure of materials. Moreover, XRD can measure only near surface in-plane residual stresses. Although ND can measure all the stress tensor components it is only available in specialist facilities and has limited depth penetration within materials [3]. Strain relaxation methods, including semi-destructive and destructive methods, are not sensitive to microstructural variation but damage the specimen during residual stress measurement. The most common semi-destructive methods are ICHD and DHD. ICHD is limited to near surface residual stress measurement. DHD can measure in plane residual stresses through the thickness of large engineering components but like ICHD generates only a one dimensional stress profile. The most common destructive methods are slitting and contouring. Slitting allows residual stresses to be measured through the thickness of the specimen but only a one dimensional stress profile can be generated.

The contour method is a powerful residual stress measurement method owing to its unique advantage of providing a two dimensional map of stress on a cut plane of interest. Moreover, the operational cost related to the contour method is relatively cheap. Also the tools and instruments required to implement the contour method are available in most of universities and industrial workshops and laboratories.

However, the contour method is still an emerging method that requires further investigations for improvement. Like any other strain relaxation method, the contour method is limited by plasticity. Also the specimen must be cut across a symmetry plane and only one stress component can be measured using the conventional contour method. The requirement of using

a symmetric flat cut limits the range of candidate components and structures for contour method measurement. No work has been done so far exploring asymmetric flat cuts apart from Zhang [95] and Mahmoudi [96]. However only 2D linear elastic FE simulations were used by Zhang to explore asymmetric cuts and no analytical demonstration or experimental validation of asymmetric cuts was done. Mahmoudi's [96] approach involves averaging deformations from both cut surfaces, which is assumed to introduce errors as the deformations from the mating cut parts have different magnitudes because of the stiffness difference between the cut parts due to the asymmetric cut.

2.5 Research aims and methodology

The aims of this PhD project were to advance the contour method in several ways. The first aim was to develop and validate a novel adaptation of the contour method applicable to asymmetric flat cuts. The second aim was to use this approach to explore shear stress and in-plane displacement effects on contour measurements for a more general case. The third aim was to explore how asymmetric flat cuts could be implemented in an incremental way to relax stresses at a location of interest thereby preventing plasticity errors in the contour method results. The aims were addressed by first considering theoretical approaches and numerical investigations. Once a robust approach was developed and understood, it was validated by experimental measurements using the well-established neutron diffraction technique.

Chapter 3: Investigating the contour method using asymmetric cuts

The conventional contour method is limited to sectioning a component in two cut parts that are identical (mirror-symmetric) in terms of geometry and material properties. In this chapter, a new approach having the potential to extend application of the contour method to cutting a body into asymmetric parts is presented. An asymmetric cut is defined as sectioning a body in which the two cut parts don't have the same geometry or material properties or stress field. Developing an approach for asymmetric sectioning of components will indirectly bring new opportunities to overcome some of the other limitations of the contour method. For example, cutting induced plasticity is one of the main limitations of the technique. Using asymmetric cuts will allow for example exploring new cutting strategies for the contour method to mitigate cutting induced plasticity and its associated errors in contour method measurements following recent work dealing with this matter [98] [83] [84] [99]. In addition, the contour method is limited to planar cuts. Enabling the contour method to deal with asymmetry of the cut parts is the first step towards advancing the technique using non-planar cutting paths [99]. Another new capability of asymmetric cuts is that it will extend the application of the contour method from simple geometries to complex structures.

The need to measure residual stresses using the contour method on a plane that results in asymmetric cut parts frequently arises owing to the position of interest in a component, an irregular shaped geometry, varying elastic properties and potentially the nature of the stress field. For example Figure 3-1 illustrates a planar asymmetric cut used in a specimen having two different materials welded together. Figure 3-2 illustrates an example of a flat asymmetric cut path in which the location of interest is at the weld start/stop position. Therefore, the cut plane must pass by the edge of the weld generating two geometrically different cut parts, one big part which includes the weld and one small part. In this case the elastic material properties may also differ in the two parts as well as the stress-field. Figure 3-3 shows a third case where the parts have mirror-symmetric geometry and properties (at least close to the cut), but strongly asymmetric residual stresses. The approach presented in this chapter aims to overcome the cut-parts mirror-symmetry limitation of the contour method.

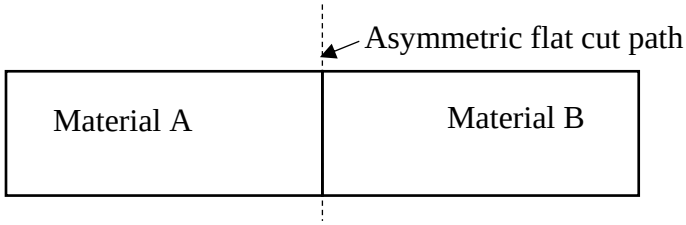

Figure 3-1 Example of a planar asymmetric cut path in a specimen comprising two different materials welded together.

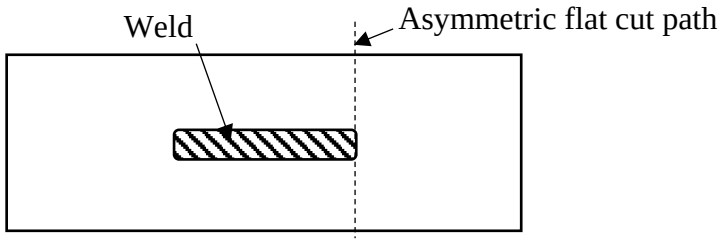

Figure 3-2 Example of a planar asymmetric cut path creating two geometrically different cut parts that may also possess asymmetric elastic properties and asymmetric residual stresses

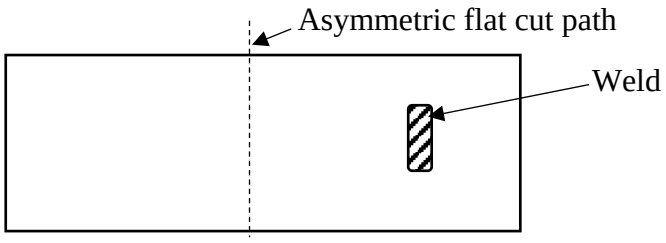

Figure 3-3 Example of a planar asymmetric cut path where only the stress field differs from side to side of the cut plane (ignoring any geometric or stiffness differences associated with the weld)

First, the theory and assumptions used to develop a new data analysis approach for dealing with asymmetric cuts are presented. Then finite element modelling is used to introduce a well-defined residual stress field into carefully designed benchmark specimens and the entire contour method process simulated for symmetric and various asymmetric cuts. The resulting surface deformations for the various cases considered are extracted to explore the robustness of proposed data analysis approaches for dealing with asymmetry.

Experimental asymmetric contour cuts are conducted on manufactured benchmark specimens and the new data analysis approach is implemented to back-calculate the residual stresses. The results of numerical contour method simulations and experimental contour method measurements are then compared and validated against experimental measurements made using the neutron diffraction technique.

3.1 Analysis of asymmetric cut data

The theory and assumptions of the conventional contour method for symmetric cuts are detailed in [52] [35] [51] [61]. When a symmetric contour cut is made to section a component the resulting out of plane surface displacements of the created cut surfaces can be decomposed into symmetric and anti-symmetric features (see Figure 3-4) [52] [35] [51].

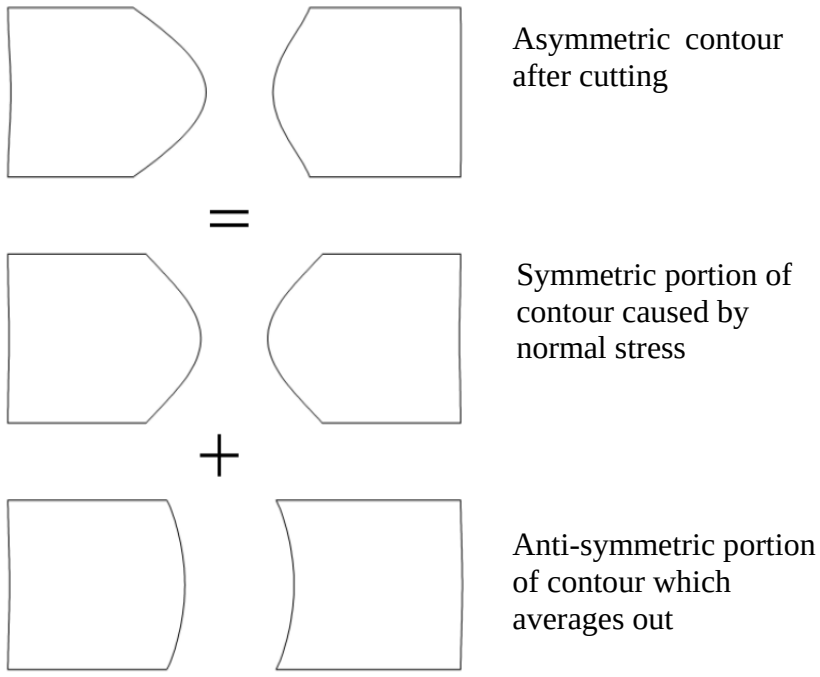

Figure 3-4 Diagram showing the decomposition of out-of-plane displacements after a cut into symmetric and asymmetric features [51].

For an ideal contour cut, in the absence of cutting induced artefacts or cutting induced plasticity, the release of normal stress results in out of plane displacements of the cut surfaces that are mirror-symmetric about the cut plane. The relaxation of shear stresses on the plane of the cut surface also affects the out of plane surface displacements and gives rise to asymmetric features.

For a symmetric contour cut where the stiffnesses of the two halves are the same, the effect of shear stress and its associated asymmetric features are cancelled out by averaging the out of plane displacements of the cut surfaces. For an asymmetric cut, however, where the stiffness of the cut parts is different the resulting out of plane surface deformation scales according to the stiffness of the corresponding cut part. Hence the release of normal stress does not create symmetric out of plane displacements and the release of shear stress does not result in anti-symmetric features which completely cancel. Therefore, averaging surface deformations of the cut parts will not remove the effect of shear stress and this gives rise to errors in the back-calculated stresses for the contour method. The following section explains the proposed underlying theory and assumptions for a new approach to analyse surface displacement data for asymmetric contour cuts.

3.1.1 Theory and assumptions

Consider a thin plate of length L and width W that contains an arbitrary residual stress field and is completely unrestrained at its boundaries. The distribution of normal residual stress, σ_{yy} (x), along section AA' at mid-length and at an arbitrary section BB' at αL from one end are indicated in Figure 3-5a. Also shown in Figure 3-5a are the distributions of shear stress, σ_{xy} (x).

When a cut of certain length is introduced in a body, which contains residual stress, the normal and shear stresses on the cut surface are relaxed. Based on the extension of Bueckner's principle [100] for a cracked body this stress relaxation is the same as imposing a stress field of the same magnitude of the original stress field with reverse sign on the cut faces.

Likewise, Bueckner's principle of elastic superposition is used to consider the residual stress field (Figure 3-5b and Figure 3-5c) and displacement field (Figure 3-5d and Figure 3-5e) introduced by the contour cut, that is similar to introducing an edge crack at sections AA' and BB'.

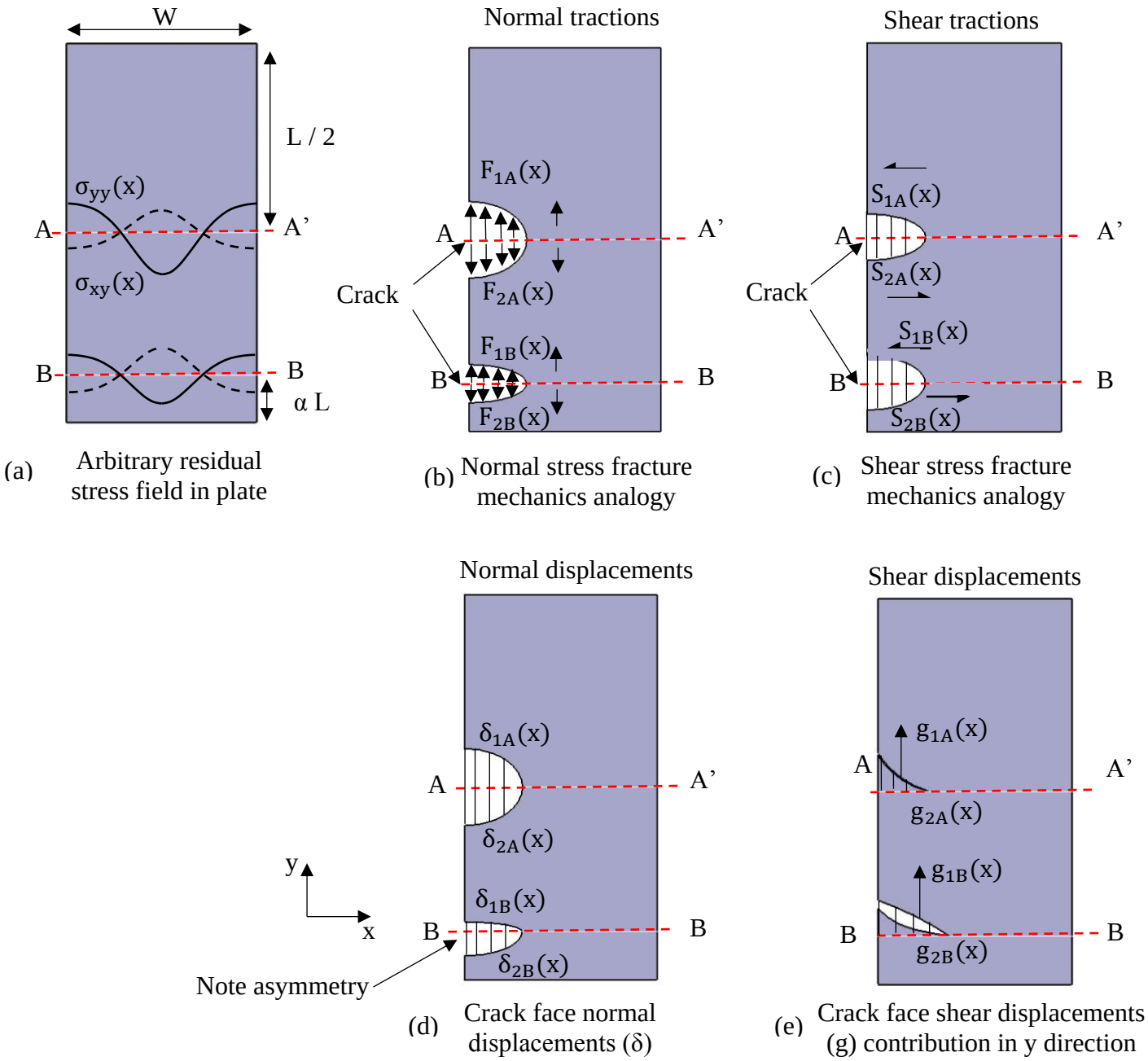

Figure 3-5 Bueckner's principle of elastic superposition for a rectilinear thin plate containing an arbitrary residual stress field and completely unconstrained at its boundaries: (a) the distribution of normal stress, $\sigma_{yy}(x)$ along sections AA' at mid-length and at an arbitrary section BB'. Also shown are the distributions of shear stress $\sigma_{xy}(x)$, (b) normal stress fracture mechanics analogy, (c) shear stress fracture mechanics analogy, (d) crack face normal displacement (δ) and (e) crack face shear displacement (g) contribution in y direction.

Normal and shear stress components are considered separately before adding effects using the principle of elastic superposition.

a) Normal stresses for a crack at mid-length AA': symmetric contour cut

Considering Bueckner's superposition for normal stresses, the imposed stresses on the crack faces as indicated in Figure 3-5b should be the same.

$$F_{1A}(x) = - F_{2A}(x) \qquad \text{Equation 3-1}$$

For the conventional contour method when the cut parts are symmetric, the resulting surface deformation of the cut parts is averaged. That is inversing the displacement of one of the cut parts and then adding it to the displacement from the other side and divide by two.

$$\delta_{con} = \frac{\delta_{1A}(x) + (-\delta_{2A}(x))}{2} \qquad \text{Equation 3-2}$$

For an ideal contour cut in the absence of cutting induced artefacts and elastic relaxation of stresses the out of plane displacements due to the release of normal stresses should be identical for the two cut parts. Therefore

$$\delta_{1A}(x) = -\delta_{2A}(x) \qquad \text{Equation 3-3}$$

The averaged out of plane displacement, δ_{con}, can be applied to an FE model of one of the cut parts to back calculate the normal stresses; $F_{1A}(x)$ and $F_{2A}(x)$.

b) Normal stresses for a crack at section BB': asymmetric contour cut

Likewise using Bueckner's superposition principle, the imposed stresses on the crack faces as indicated in Figure 3-5b should be the same.

$$F_{1B}(x) = - F_{2B}(x) \qquad \text{Equation 3-4}$$

However, the out of plane displacements due to the release of normal stresses, $\delta_{1B}(x)$ and $\delta_{2B}(x)$, are no longer identical due to differences in the compliance of the cut parts (Figure 3-5d); $\delta_{1B}(x)$ depends on the compliance of the bigger part and $\delta_{2B}(x)$ depends on the compliance of smaller part.

$$\delta_{1B}(x) \neq -\delta_{2B}(x) \quad \text{Equation 3-5}$$

Applying the out of plane displacement of side 1, $\delta_{1B}(x)$, to an FE model of side 1 and conducting an elastic stress analysis gives the imposed stress on the crack face of side 1, $F_{1B}(x)$. Likewise, applying $\delta_{2B}(x)$ to an FE model of side 2 and performing an elastic stress analysis gives the stress imposed on the crack face of side 2, $F_{2B}(x)$.

Therefore, in the absence of shear stress, applying the out of plane displacements of each cut part to the corresponding FE model of the cut part leads to the correct stress answer. However, averaging displacements and using the averaged displacements to infer stresses gives wrong stress on both sides.

c) Shear stresses for a crack at mid-length AA': symmetric contour cut

For the shear stress component the imposed stresses on the crack faces as indicated in Figure 3-5c should be the same.

$$S_{1A}(x) = -S_{2A}(x) \quad \text{Equation 3-6}$$

The release of shear stress introduces displacements normal to the crack face, $g_{1A}(x)$ and $g_{2A}(x)$ (see Figure 3-5e) as well as in-plane displacements along the crack direction. In practice the in-plane component of shear displacements along the crack direction cannot be readily measured, hence, they are ignored here.

However, the shear displacements normal to the crack face can introduce error in the back-calculated stress results. For the conventional contour method where the compliance of the two cut parts, side 1 and side 2, are the same this component of shear displacement is anti-symmetric (i.e. $g_{1A}(x) = g_{2A}(x)$) as shown in Figure 3-5e. The effect of shear stress and hence the resulting displacement normal to the crack face is cancelled out when displacements from both sides of the cut are averaged using Equation 3-2.

d) Shear stresses for a crack at section BB': asymmetric contour cut

Likewise, the imposed shear stresses on the crack faces for section BB' as indicated in Figure 3-5c should be the same.

$$S_{1B}(x) = -S_{2B}(x) \quad \text{Equation 3-7}$$

As explained earlier shear displacements along the crack direction are ignored. However, the displacements normal to the crack face as a result of shear stress relaxation, g_{1B} (x) and g_{2B} (x), are important to consider and their magnitudes depend on the compliance of side 1 and side 2 accordingly. Averaging the displacements and using the averaged displacements leads to error in the back calculated stresses.

Instead, applying g_{1B} (x) as surface boundary condition to the FE model of side 1 and performing an elastic stress analysis gives the stress error for side 1. That is equal and opposite to the stress error introduced on side 2 by applying g_{2B} (x) on the FE model of side 2 and conducting an elastic stress analysis. Averaging the back-calculated stresses on both sides should cancel out the effect of shear stress and its introduced error in the contour method analysis.

Now the back calculated stresses resulting from normal and shear stress relaxations can be added together for a symmetric cut (that is step a and c) or for an asymmetric cut (that is step b and d).

Therefore, based on the elastic principle of superposition a new data analysis approach is proposed for asymmetric cuts for the contour method as described in the following:

1. Apply the out of plane displacement of the cut surface from cut part 1 (U_1 in Figure 3-6) to the corresponding FE model of cut part 1 and perform elastic stress analysis ($\sigma_{1,u1}$).
2. Apply the out of plane displacement of the cut surface from cut part 2 (U_2 in Figure 3-6) to the corresponding FE model of cut part 2 and perform elastic stress analysis ($\sigma_{2,u2}$).
3. Average the resulting stresses from step 1 and step 2 ($\sigma_{1,u1}, \sigma_{2,u2}$) using the following equation:

$$\sigma_{contour} = \frac{\sigma_{1,u1} + \sigma_{2,u2}}{2} \qquad \text{Equation 3-8}$$

The averaged stress gives the back-calculated stresses measured using the contour method when asymmetric cuts are used.

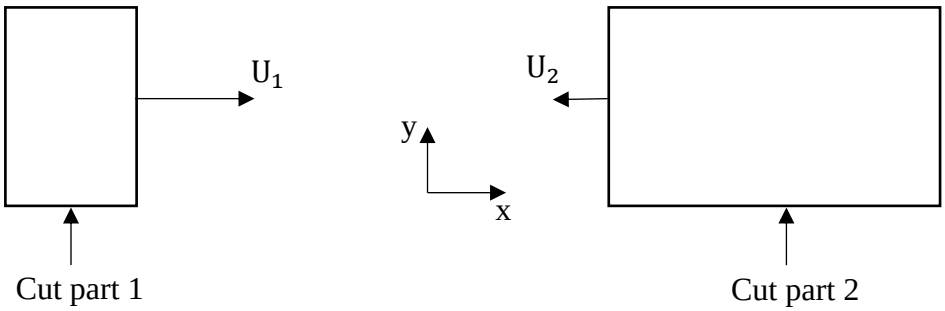

Figure 3-6 Schematic view of cut parts and displacements normal to the cut surfaces, U_1 and U_2 are the out of plane displacements of the cut surfaces of part 1 and 2, respectively.

In the following sections, extensive finite element simulations are used to design benchmark test specimens, simulate the entire contour method procedure and finally to validate the proposed data analysis approach.

3.2 Finite element modelling

Finite element simulation was implemented to explore the proposed data analysis approach for asymmetric contour cuts. Firstly, extensive FE modelling was conducted to design a suitable benchmark sample for this project. A well-defined residual stress field was introduced into virtual benchmark test specimens. Then the entire contour measurement method was simulated on the benchmark samples. The cutting step of the contour method was simulated for a symmetric cut and a number of asymmetric cuts. Following contour cutting simulations the out of plane displacements of the cut surfaces were recorded and the proposed data analysis approach was implemented to reconstruct the original residual stresses. The reconstructed residual stresses were compared with the initial stresses to demonstrate the accuracy of the proposed method.

3.2.1 Exploring the design of benchmark samples

A residual stress field was introduced in benchmark test specimens by simulating a high energy autogenous (no added filler material) laser welding process. First, a tramline weld configuration was evaluated (see Figure 3-7). Two laser line weld were modelled using the finite element method as shown in Figure 3-7. The commercial FE code Abaqus was used [101]. Weld residual stress generation was simulated using a two dimensional uncoupled

thermo-mechanical analysis. An initial temperature of 1300°C was applied to nodes on the weld lines (see Figure 3-7). It was assumed that this temperature is the melting point of the material as detailed later. Then an air cool down to 20°C was simulated using a transient analysis with applied surface heat transfer losses. A free convection coefficient of 7.9 W/m²K for mild steel in air was assumed [102]. The model was meshed using 17 400, 8-node quadratic heat transfer quadrilateral elements (DC2D8). A global mesh size of 2 mm was used with finer mesh elements having a size of 1 mm in the weld and the surrounding areas. The mesh size was further refined to 0.3 mm during the cut simulation as detailed later. Physical properties from the MPC data base were used as developed for the ASME Div II_Rewrite [103] (Table 3-2).

Once the thermal analysis was completed, the nodal temperature history on the sample was mapped onto a new FE model for a mechanical analysis. The FE models from the thermal and mechanical analysis were the same except for the FE element type and material properties. 8-node bi-quadratic plane stress quadrilaterals with reduced integration elements were used (CPS8R). Also, temperature dependant mechanical properties of the material [104] were used including Young's modulus and yield strength.

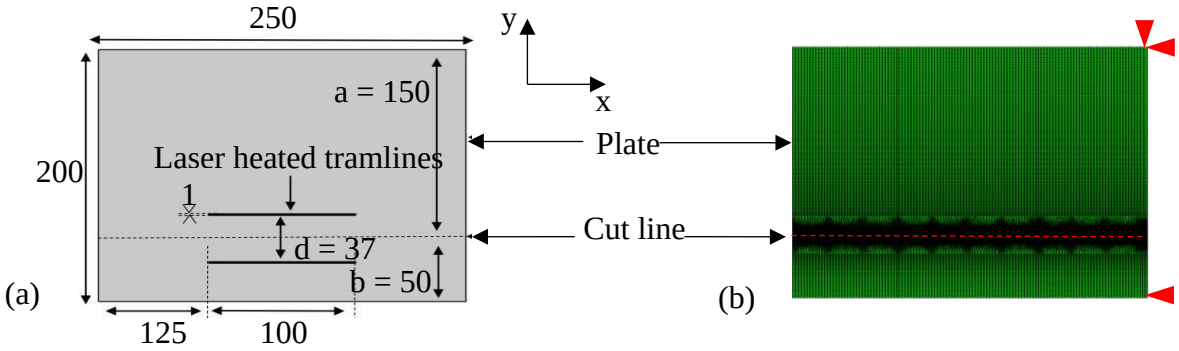

Figure 3-7 Schematic diagram showing a proposed benchmark specimen containing laser heated tramlines (a). FE model of the proposed benchmark specimen for contour simulation showing the very fine mesh along the proposed plane of the cut together with the applied boundary conditions (b). Dimensions are in mm.

After residual stress was generated in the benchmark specimen, the entire contour method process was simulated. The predicted residual stress was mapped onto a new FE model where the mesh was refined along the cut line and the surrounding area (see Figure 3-7) using a mesh size of 0.3 mm. The cut was simulated by incrementally removing elements with model change

along the cut line. Elastic-plastic material properties were used as detailed in section 3.2.2. To prevent rigid body motion, displacements were constrained in both X and Y direction on the top left corner of the plate and in X direction of the bottom left corner (see Figure 3-7b).

During the contour method simulation, the magnitude of the equivalent plastic strain (PEEQ in Abaqus) was extracted along the cut plane (see Figure 3-8a) at the cut tip after each cut increment. The equivalent plastic strain in Abaqus is a scalar that measures the accumulated plastic strain. It contains the initial value of equivalent plastic strain plus any additional equivalent plastic strain due to plastic straining during the analysis [101]. The equivalent plastic strain is Abaqus is defined as [101]:

$$PEEQ = \int_0^t \sqrt{\frac{2}{3}\ \dot{\varepsilon}_{pl} : \dot{\varepsilon}_{pl}}\, dt \qquad \text{Equation 3-9}$$

Where t is the total duration of the analysis and $\dot{\varepsilon}_{pl}$ is the plastic strain rate.

Also the original elastic stress distribution at 20^{o}C along the cut plane prior to cutting was compared to the back calculated stress (see Figure 3-8b) using the new data analysis approach dealing with asymmetric cuts.

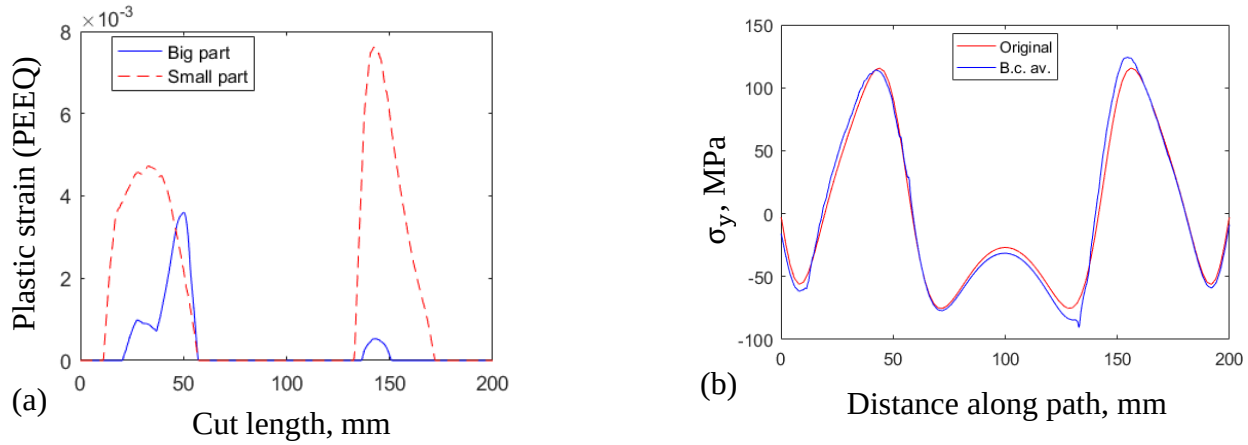

Figure 3-8 Variation of the equivalent plastic strain along the cut plane (a) and comparison between the original stress prior to the cut and the back-calculated one (b).

The correlation between the original stress profile and simulated contour results based on the new analysis approach is good. However, the contour method simulation results showed evidence of some plastic deformation during cutting which violates the requirement for strict elastic relaxation. This probably accounts for the small differences in stress profile shown in Figure 3-8b. The plastic strains of about 1 % contributing to the stress error was considered unacceptable. Therefore, the design of the test specimen was updated from having a weld tramline to a single weld line.

Different design strategies were explored via a series of FE studies that included changing the length of the weld line, the positioning of the weld line relative to the plate ends and the options for where to introduce asymmetric cuts (see Figure 3-9). The shear stress along the measurement line was also examined for each case as it was deemed important for the new data analysis approach to work in extreme cases of high shear. Only elastic material properties were used during the contour method simulations as the aim was to assess the effect of stress field on the contour results.

The final selected benchmark designs are shown in Figure 3-9. In 'Plate 1' the cut creates geometrically symmetric parts having the same stiffness (see Figure 3-9a). A predicted 2D map of stress acting in Y direction (σ_y) in 'Plate 1' is shown in Figure 3-10a. Here, the weld is located in the bottom half. The displacement misfit introduced by the weld zone increases the displacement of the bottom half as shown in Figure 3-10b. But, by averaging the

displacements in contour method simulations, the effect of the asymmetric stress field is cancelled as illustrated in Figure 3-10c.

In 'Plate 2' the cut is geometrically asymmetric, that is the 'Big part' is stiffer (see Figure 3-9b). The 2D map of stress acting in the Y direction (σ_y) in 'Plate 2' is shown in Figure 3-11a. The displacement magnitudes extracted on the cut surfaces of both cut parts are similar as shown in Figure 3-11b. However, since the 'Big part' is stiffer, the back-calculated stresses using the new data analysis approach dealing with asymmetric cut on it are higher than the one on the 'Small part' as shown in Figure 3-11c.

Similarly, in 'Plate 3' the cut is asymmetric and the 'Big part' is stiffer (see Figure 3-9c). However, the weld is located in the 'Small' part. The 2D map of stress acting in Y direction (σ_y) in 'Plate 3' is shown in Figure 3-12a. The displacement misfit associated with the simulated weld has increased the displacement on the bottom half. Figure 3-12b shows that the displacement from the bottom half is the largest. As a result, the stresses from the 'Small part' are higher than the one from the 'Big part' as shown in Figure 3-12c. Therefore, when the cut is symmetric the asymmetry in stress field impacts only the displacements at the cut surfaces. However, the asymmetry of the cut as well as stress-field will affect both the displacement at the cut surfaces and the back calculated stress on each cut part.

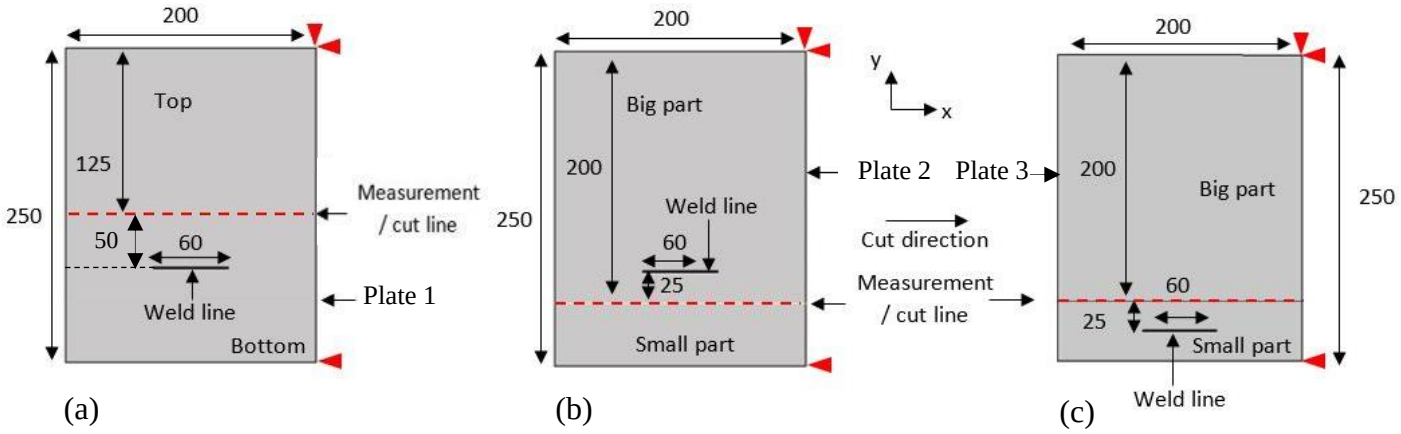

Figure 3-9 Schematic view of the boundary conditions, and weld locations of the laser welded plate for a symmetric cut (a) and asymmetric cuts (b) and (c). Dimensions are in mm.

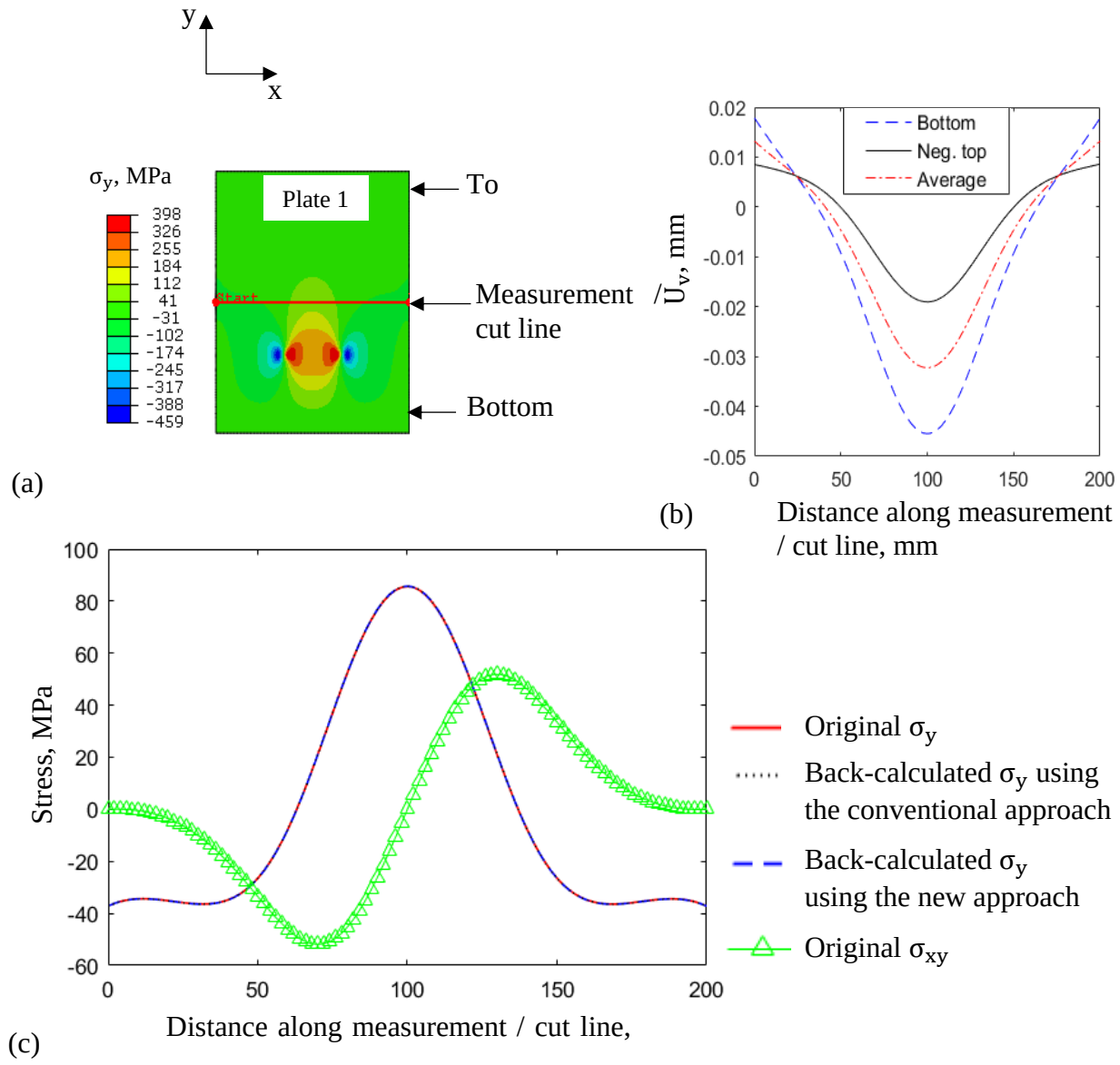

Figure 3-10 Comparison of line profiles of the original and back calculated stresses (a) and the out of plane displacements of cut surfaces (b) along the measurement / cut line extracted from the stress map (c) of the stress acting in Y direction in 'Plate 1'.

The design of 'Plate 3' (see Figure 3-9c) was chosen to be manufactured for experimental validation studies because the residual stress along the measurement / cut line (see Figure 3-9c) was found by analysis to remain the same while changing the length of the big part from 200 mm to other values (see Figure 3-9c). Thus the effect of stiffness asymmetry could be studied in a systematic way by changing the relative size (length ratio) of the big and small parts of the specimen as detailed in section 3.2.2 that follows.

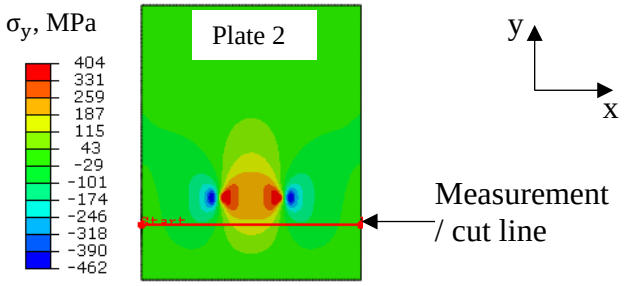

(a)

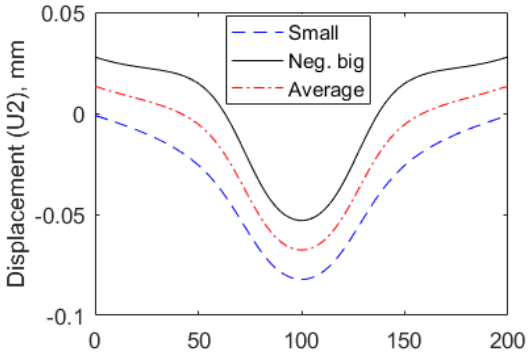

Distance along measurement / cut line, mm

(b)

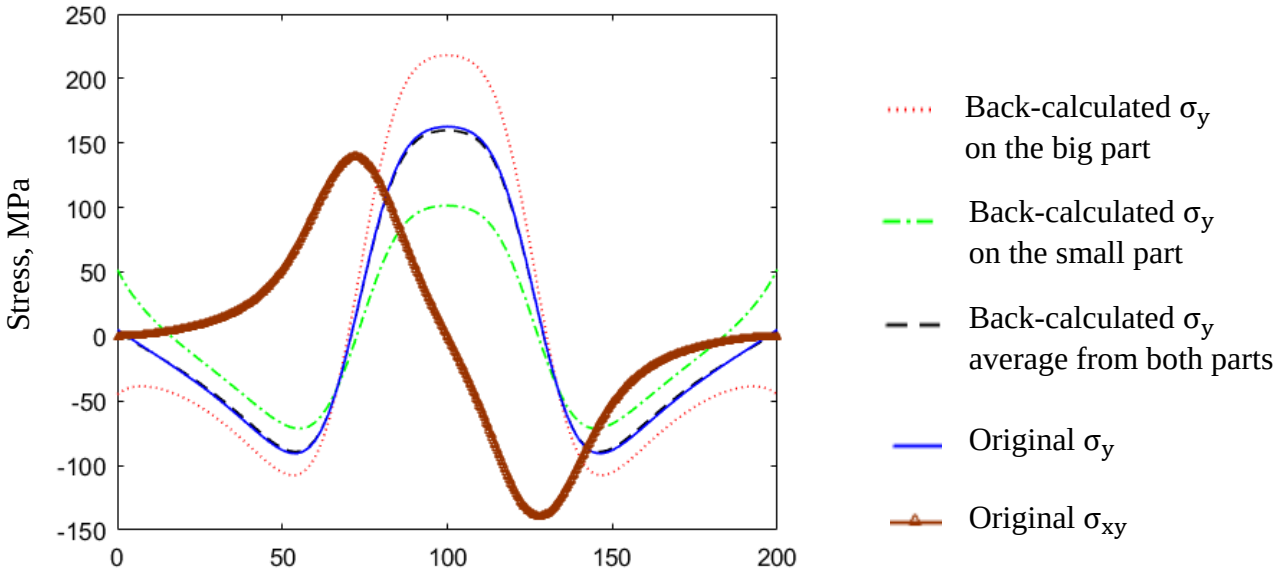

(c) Distance along measurement / cut line, mm

Figure 3-11 Comparison of line profiles of the original and back calculated stresses (a) and the out of plane displacements of cut surfaces (b) along the measurement / cut line extracted from the stress map (c) of the stress acting in Y direction in 'Plate 2'.

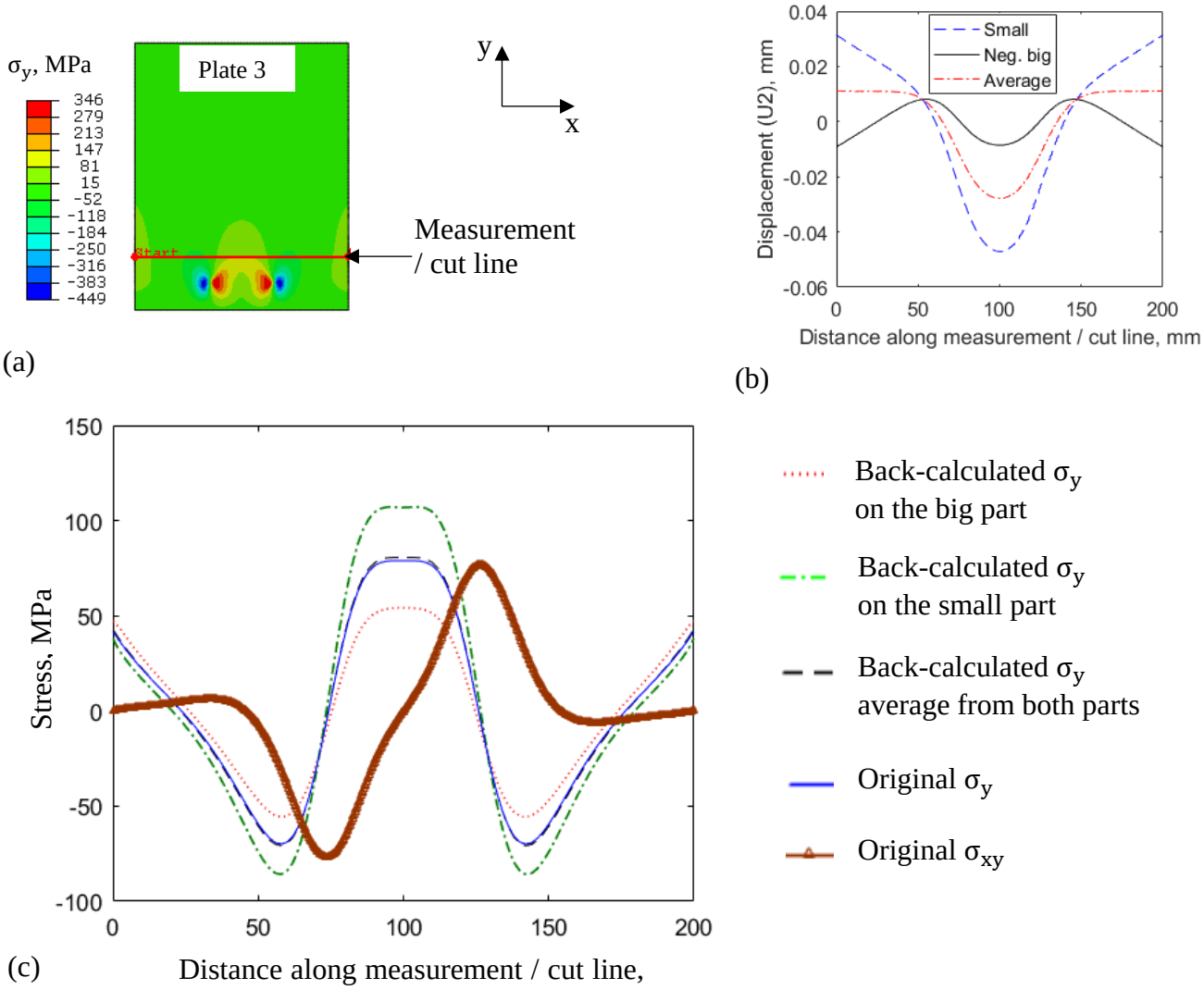

Figure 3-12 Comparison of line profiles of the original and back calculated stresses (a) and the out of plane displacements of cut surfaces (b) along the measurement / cut line extracted from the stress map (c) of the stress acting in Y direction in 'Plate 3'.

The design of plate c in see Figure 3-9c was selected with the weld located in the small part. In fact, using this design the length of the plate can be changed by increasing or decreasing the length L (see Figure 3-14a) while the stress profile along the cut/measurement line remains similar. This allows the effect of different ratios of stiffness asymmetry to be explored as discussed later.

3.2.2 Material properties

The level of residual stresses introduced in the proposed benchmark design depend on the choice of the material. Bright mild steel was chosen for the base plate material as this is very suitable for ND measurements. Bright steel material was procured and the grain size measured (Figure 3-13) using an optical microscope LEICA CTR6000 and the module 'grain expert' of the software LAS 4.2. Also, the ASTM E112 intercept method [105] was implemented. The grain size was found to be smaller than 13 µm.

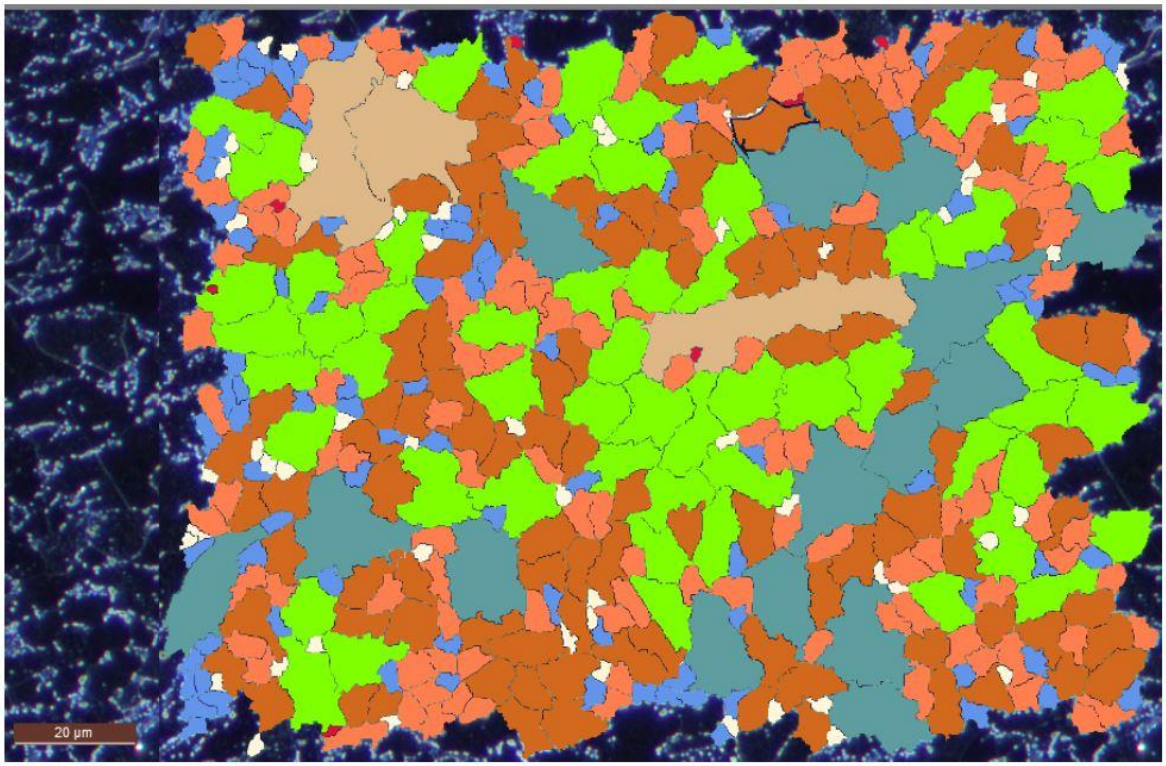

Figure 3-13 View of the grains of the bright steel material used for manufacturing the test specimens

The as-received (200 x 250 x 6) mm plates from Bright Steel material were heated in a oven at 600°C for stress relief heat treatment. This temperature was maintained for 10 hours to obtain a uniform temperature distribution in all the plates. Then the plates were air-cooled until room temperature was reached.

The material properties were assessed by doing room temperature tensile tests (see Figure 3-14) using an Instron 5969 Universal machine equipped with a 50 KN load cell, as detailed in

[106][67]. 6 tensile test specimens were extracted from a spare plate, including 3 specimens oriented in the x direction and 3 oriented in the y direction (i.e. the length direction of the tensile test specimen was parallel to x and y axis, respectively). The strain was measured using an extensometer attached and centred on the test specimens. Also Young's modulus was measured using the flexural vibration frequency method using a 50.1 x 6.85 x 9.99 mm^3 beam cut from the material as detailed in [67][107].

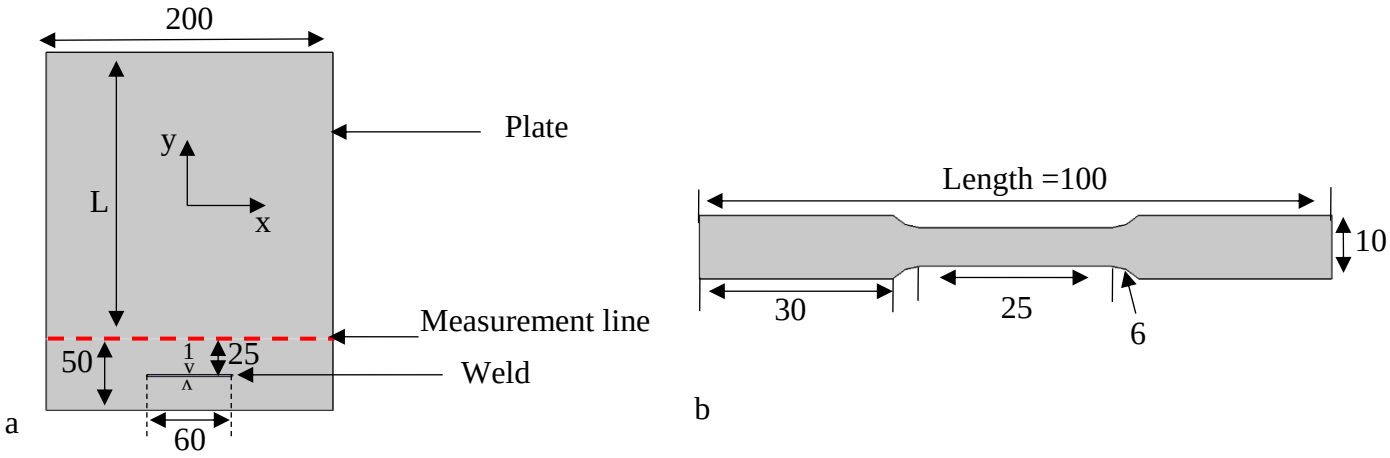

Figure 3-14 Test specimen geometry (a) and tensile specimen design (b). Dimensions are in mm.

The stress-strain curves from the specimens oriented in the Y direction (see 'T1O1', 'T2O1', 'T3O1' in Figure 3-15) were averaged. The average yield stress from the measurements on the specimens oriented in Y direction was 280.7 MPa. The value of the elastic Young's modulus measured using the flexural vibration frequency method was found 223.0 GPa.

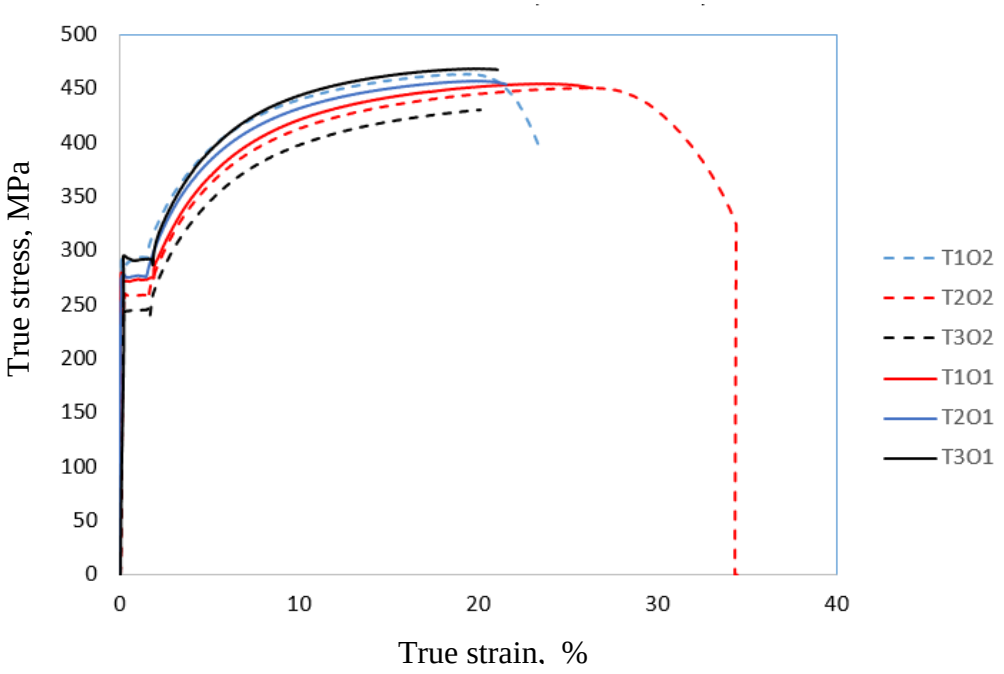

Figure 3-15 Tensile test stress-strain curves at 20°C for the 080A15 material after heat treatment.

The chemical composition of the material received is presented in Table 3-1:

Table 3-1 Table presenting the chemical composition of the 080A15 material.

C	Si	Mn	P	S
0.22	0.20	0.67	0.018	0.007

General physical-thermal properties of Bright Steel from the open literature documented in the MPC database developed for ASME Div II_Rewrite [103] have been assumed for the material and are summarised in Table 3-2.

Table 3-2 Thermal properties assumed for the 080A15 material [103]

Temperature (°C)	Conductivity (W / mm.K)	Specific Heat (J/Kg.K)	Expansion coefficient (/K)	Young's Modulus (MPa)
20	0.0586	460	1.18E-005	222980
100	0.058	480	3.75E-005	
200	0.052	500	3.9E-005	

300	0.049	550	4.1E-005	
400	0.0435	635	4.255E-005	
500	0.04	710	4.35E-005	
600	0.035	790	4.45E-005	
700	0.03	880	4.65E-005	
800	0.026	990	4.8E-005	
900	0.021	1050	5E-005	
1000	0.018	1140	5.2E-005	
1100	0.015	1200	5.4E-005	
1200	0.01	1300	5.5E-005	
1300	0.008	1400	5.65E-005	2229.8

Note:

- ✓ Constant density was assumed: 7.85 x 10^{-06} Kg.mm^{-3}
- ✓ Poisson's ratio: 0.3
- ✓ Latent heat of fusion: 300 KJ/Kg, absorbed/released between 1275 °C and 1300°C.

3.2.2 Benchmark test specimens

Extensive finite element simulations were conducted to design a suitable benchmark test specimen for the project, some of which have already been described. Different sample design strategies were examined to ensure that a) the level of introduced residual stress and the resulting out of plane displacements after contour cuts were large enough to be captured from an experimental measurement point of view and b) the relaxation of residual stress during contour cuts was elastic. The main stages of this process are detailed below including residual stress generation, material and geometry selection, and cutting induced plasticity error mitigation.

Two-dimensional plane stress FE modelling implementing uncoupled thermal-stress analysis was conducted to simulate the laser welding process introducing an initial residual stress state

into the benchmark test specimens. ABAQUS 6.13 software [108] was used for the FE simulations.

Temperature-dependent properties of Bright Steel with the hardening behaviour obtained from the tensile tests (Figure 3-15) were used as inputs to the FE models. The value of the Young modulus and yield strength measured at room temperature were divided by 100 to estimate their value at 1300°C. For the thermal analysis the models comprised heat transfer quadrilateral elements (ABAQUS designation DC2D8). The temperature of elements at the weld location was instantaneously set to 1300°C and the temperature of the remaining elements of the plate was set to 20°C. Then the entire plate was left to cool down to reach temperature equilibrium equal to 20°C. Free convection boundary conditions were applied on the external edges of the plate during the cooling phase. For the thermal analysis temperature dependent physical-thermal properties were taken from the data reported in [67] and are summarised in Table 3-2.

The nodal temperatures from the thermal models were mapped into the same number of bi-quadratic plane stress quadrilateral with reduced integration elements (ABAQUS designation CPS8R) of the stress analysis models. Likewise, the stress analysis model comprised a 1 mm mesh size adjacent to the weld and 2 mm mesh size elsewhere.

Displacement boundary conditions were applied on the stress analysis model to avoid rigid body motion. The displacements were constrained in X and Y directions at the top right corner and in X direction at the bottom right corner (see Figure 3-16b). The other boundary conditions that were used for the cutting step will be discussed later.

Three virtual benchmark test specimens were simulated for (a) a symmetric cut where the stiffness ratio of cut parts is 1 (SR1), L=50 mm, (b) an asymmetric cut with stiffness ratio 2 (SR2), L=100 mm and (c) an asymmetric cut with stiffness ratio 4 (SR4), L=200 mm (see Figure 3-17). To avoid rigid body motion, additional boundary conditions to the one used during the laser heating simulation were added. So, during the simulation of the cutting step the displacements were constrained in both X and Y directions at the right corners and in Y directions at the right corners of the plate (see Figure 3-16b).

The predicted distribution of the stress component σ_y introduced into the virtual specimens as a result of the welding process is shown in Figure 3-17.

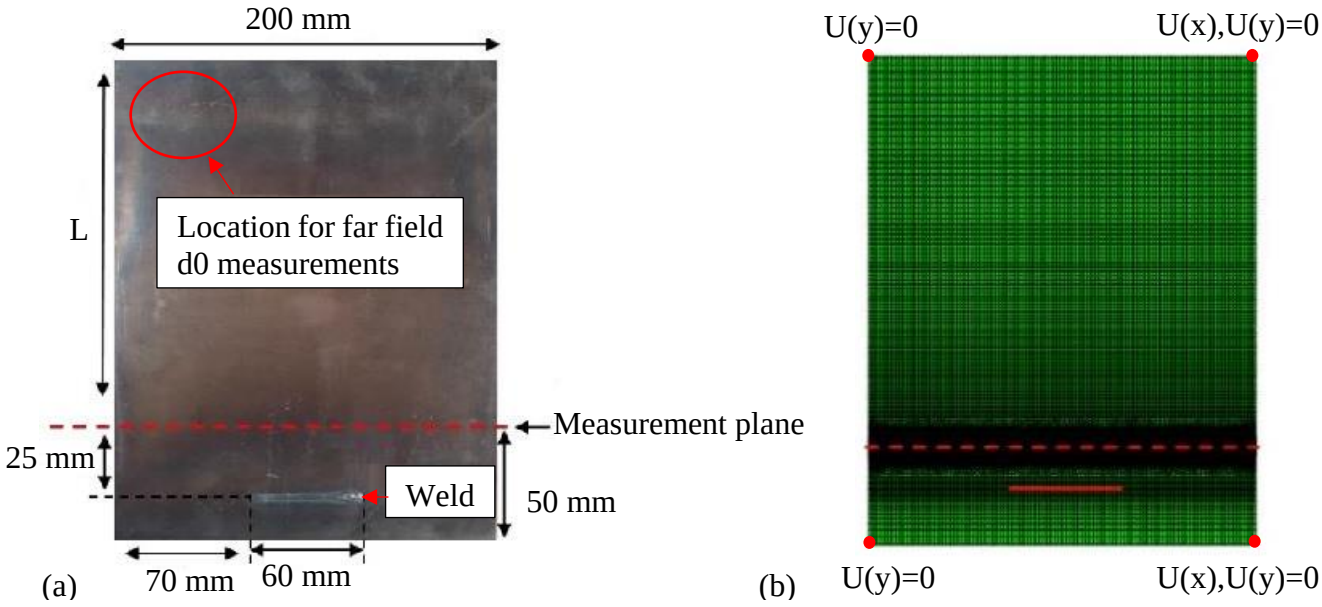

Figure 3-16 (a) An example of benchmark test specimens showing the dimensions, location of the laser weld and measurement plane. For a symmetric contour cut L = 50 mm. For asymmetric cuts with stiffness ratio 2 and 4 L was increased to 100 mm and 200 mm respectively. (b) 2D finite element model of the benchmark test specimen with stiffness ratio 4.

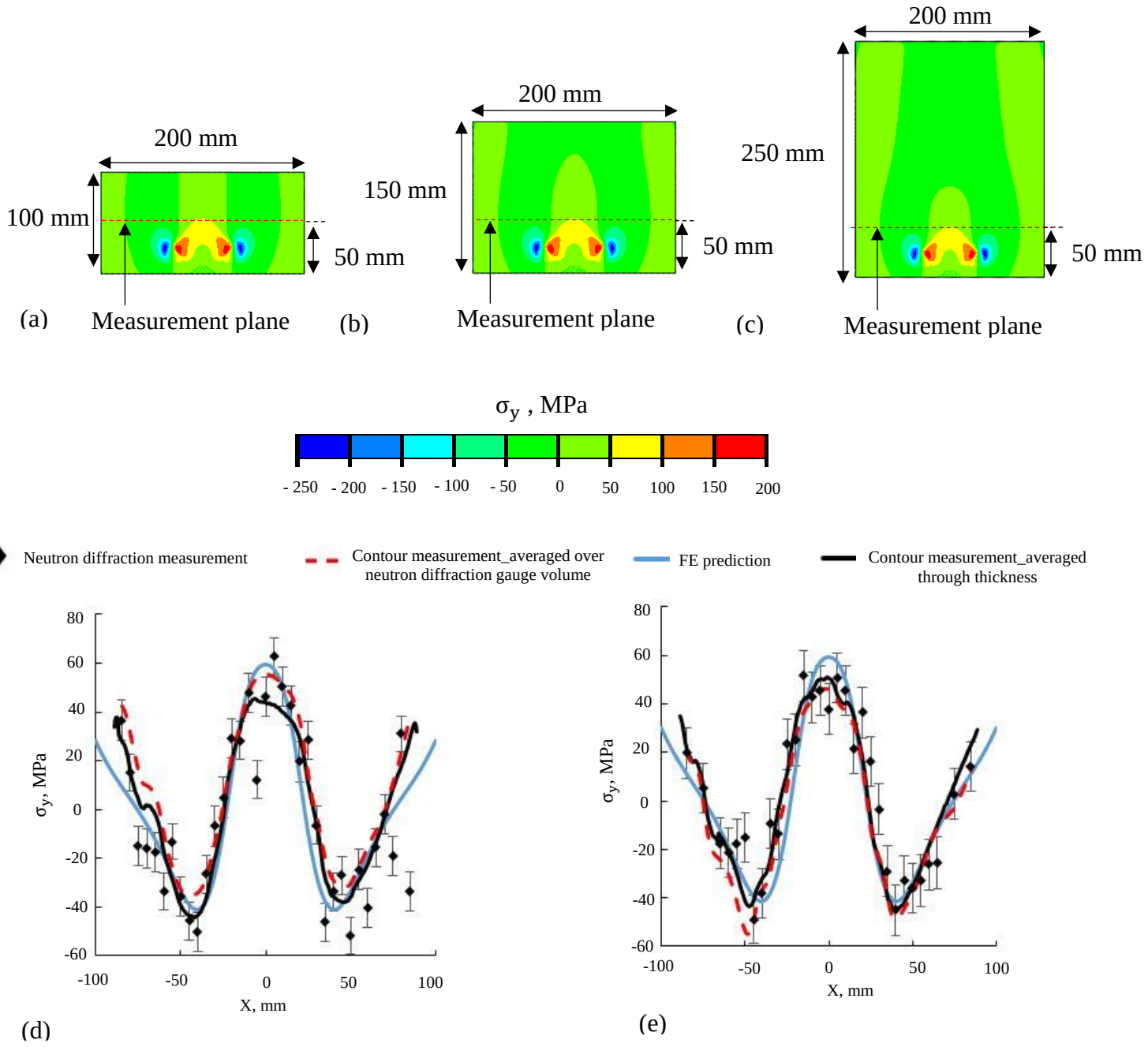

Figure 3-17 Predicted map of the plate (a) with stiffness ratio 1, (b) with stiffness ratio 2 (c), with stiffness ratio 4 (d) line profile of neutron diffraction σ_y stress for the plate with stiffness ratio 2 and (e) line profile of neutron diffraction σ_y stress for the plate with stiffness ratio 4. Also shown in (d) and (e) are line profiles of FE predicted transverse stress and measured transverse stress for asymmetric cuts using the contour method. The experimental data is discussed later in the thesis.

3.2.3 Plasticity mitigation

The contour method like most mechanical relaxation residual stress measurement techniques is based on the assumption that the material relaxation is elastic. However, if during cutting the deformations of the cut surface causes stress redistribution that exceeds the yield stress of the material then the deformation is no longer purely elastic which violates a fundamental assumption of the contour method. This leads to error in the measurement which is referred to as plasticity error.

Traore [67] developed a correlation between the normalized plastic zone size (NPSZ) at the cut tip and the estimated error in the contour method. There are different techniques to simulate the contour cut step. However, the correlations were developed for symmetric cuts and the NPZS was calculated for only one half of the sample assuming symmetry of the NPZS. But for an asymmetric contour cut there are two NPZS relating to respective sides of the cut. Therefore, Traore's approach to estimate plasticity induced errors is not applicable when the contour is asymmetric. This is demonstrated by simulating the contour method on 'Plate 3' where a weld line is introduced close to one edge of the plate (see Figure 3-9c) and considering plastic material properties. In fact, Figure 3-8a clearly shows that PZS is different on the small and big parts. The plastic radius along the cut edges reached maximum values of 3 mm and 1.5 mm on the small and big parts, respectively. Those maximum values are reached at 80 mm from the cut start. Hence another approach was required to assess the plasticity induced error in the contour method for asymmetric contour cuts. This involved modelling the entire contour method for different weld lengths and locations and for different cut locations.

The plastic radius or plastic zone size was defined as the area where plastic deformation of the material occurred due to cutting at the cut tip (see Figure 3-18).

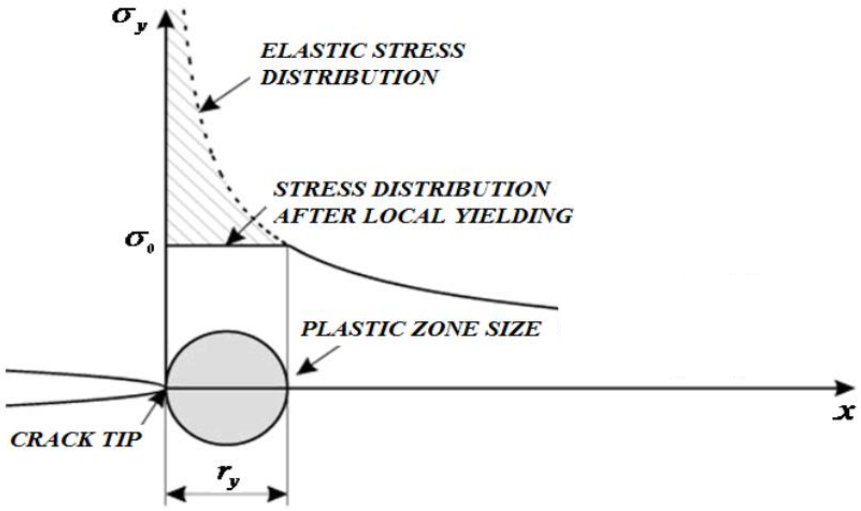

Figure 3-18 Schematic view of the plastic zone size generated at a crack tip [113].

The plasticity induced stress error was calculated using a root mean square (RMS) average stress error between the original and the back-calculated stress profile and was given by:

$$\bar{\sigma}_{\text{Error}}^{\text{RMS}} = \sqrt{\frac{1}{n}\sum_{i=1}^{n}(\sigma_{\text{Original}}(i) - \sigma_{\text{Back calculated}}(i))^2} \qquad \text{Equation 3-10}$$

Where n is the number of nodes on the cut line in the given FE model and σ_i the stress acting in the direction out of the cut plane at a given nodal position.

The process was repeated for a number of sample designs including different weld lengths, weld locations and cut locations until the cutting induced plasticity error was found to be lower than 5%. This was achieved for the sample design shown in Figure 3-9c in 'Plate 3'.

3.2.4 Simulation of the contour method

Once the initial residual stress field was introduced in the virtual benchmark specimens the simulation of the contour method procedure was carried out.

The FE models to simulate the cutting step of the contour method requires a different mesh and a set of boundary conditions than those used in the laser weld simulation FE model. Therefore, the residual stress fields from the weld FE models were mapped onto their corresponding FE contour cutting models using the command 'map solution' within ABAQUS. The FE contour cutting models contained bilinear plane stress quadrilateral, reduced integration and hourglass control elements (ABAQUS designation CPS4R). The mesh was refined around the cut line for each plate using 0.3 mm mesh size. The number of elements increased from 10400 to 43186 for the "SR2" plate where the stiffness ratio between the big and small parts is 2, and from 17400 to 48081 for the "SR4" plate where the stiffness ratio between the big and small cut parts is 4. The mapping step used the same boundary conditions as explained for the simulation of residual stress (Figure 3-16b).

The contour cutting process was simulated introducing a blunt cut by removing a series of 0.3 mm x 0.3 mm element sets along the cutting path representing the cut width. Hence the width of the simulated contour cut was 0.3mm. Additional boundary conditions were applied in the Y direction (see Figure 3-16b) at the top and bottom left corners and at the bottom right corner of the plate for the cutting step of the contour method to prevent rigid body motion.

Once the cutting process was simulated, the predicted out of plane displacements on both cut surfaces were recorded and used to back calculate the residual stresses using the proposed new approach presented in Section 2.1. To implement the new data analysis approach, the following procedure was followed:

1. The recorded out of plane displacement of each cut surfaces was applied as surface boundary condition to a new FE model of the corresponding cut part and fully elastic stress analyses were conducted.

2. The resulting stresses for each part were then averaged. The averaged stresses present the back-calculated stresses reconstructed using the contour method (see Figure 3-19).

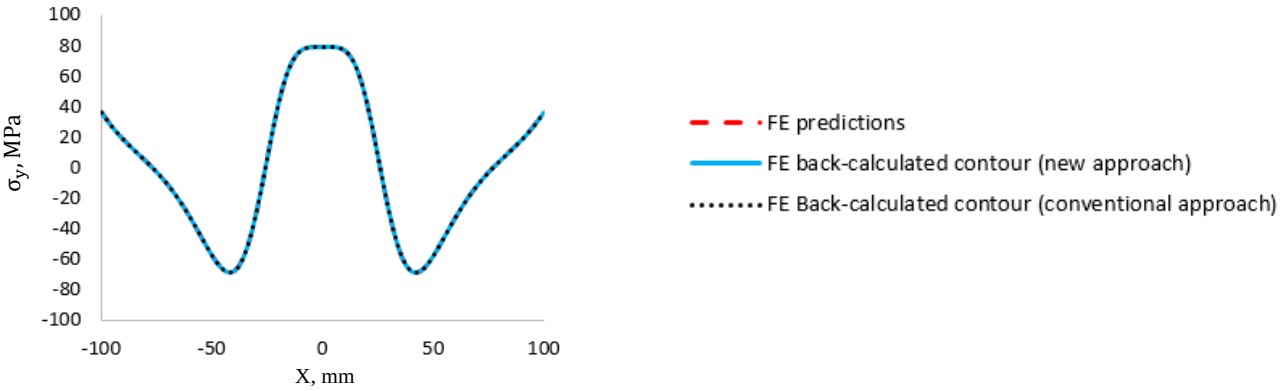

(a) Symmetric contour cut with stiffness ratio 1 (L=50)

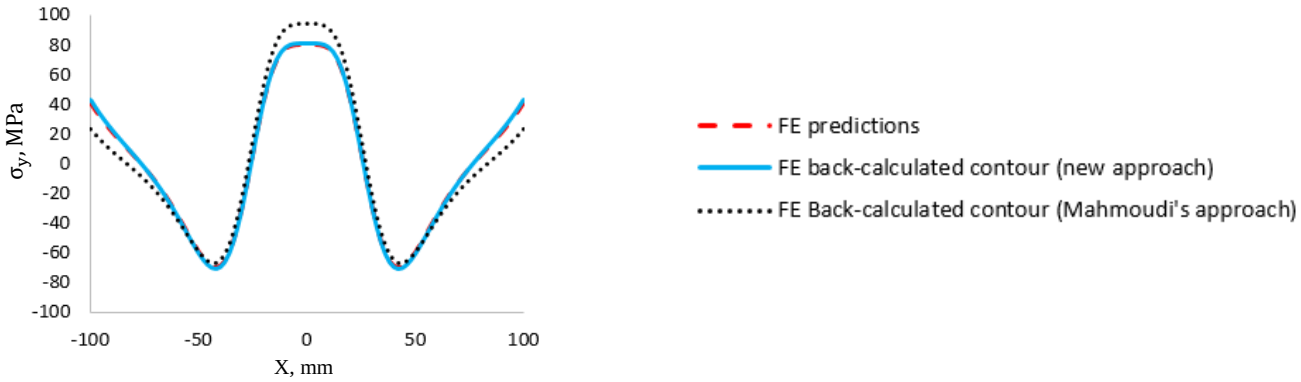

(b) Asymmetric contour cut with stiffness ratio 2 (L=100)

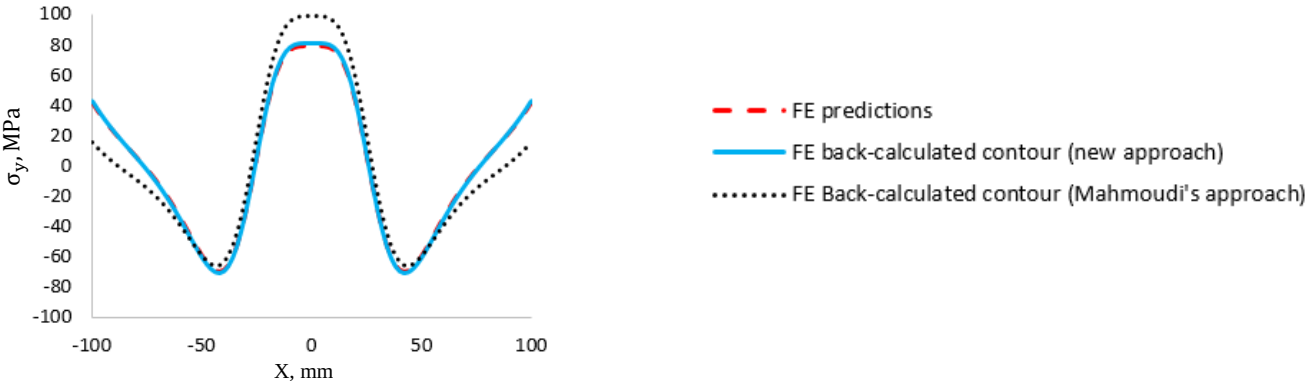

(c) Asymmetric contour cut with stiffness ratio 4 (L=200)

Figure 3-19 Comparison of the FE predicted residual stress component σ_y with back calculated residual stress from FE contour simulations using the proposed new data analysis approach, conventional [35] contour data analysis approach and Mahmoudi's approach [96]: (a) symmetric contour cut with stiffness ratio 1 (L=50), (b) asymmetric contour cut with stiffness ratio 2 (L=100), (c) asymmetric contour cut with stiffness ratio 4 (L=200). See Figure 3-16a for the geometry of the samples.

It is important to note that all of the cutting simulations were carried out using elastic models in order to rule out the possibility of introducing cutting induced plasticity errors when assessing the reliability of the new proposed data analysis step of the contour method.

The accuracy of the proposed data analysis approach was calculated using a root mean square (RMS) average stress error between the original and the back-calculated stress profile as detailed in Equation 3-10.

It is worth noting that although high shear stress magnitude was acting along the cut line prior to the cut (see Figure 3-20 for the extreme case where the stiffness ratio between the cut parts is 4) an excellent agreement was obtained between the back calculated stresses using the new data analysis approach and the reference stress prior to the cut (see Figure 3-19). The in-plane stress and its potential effect on the contour method will be discussed in the next chapter 4.

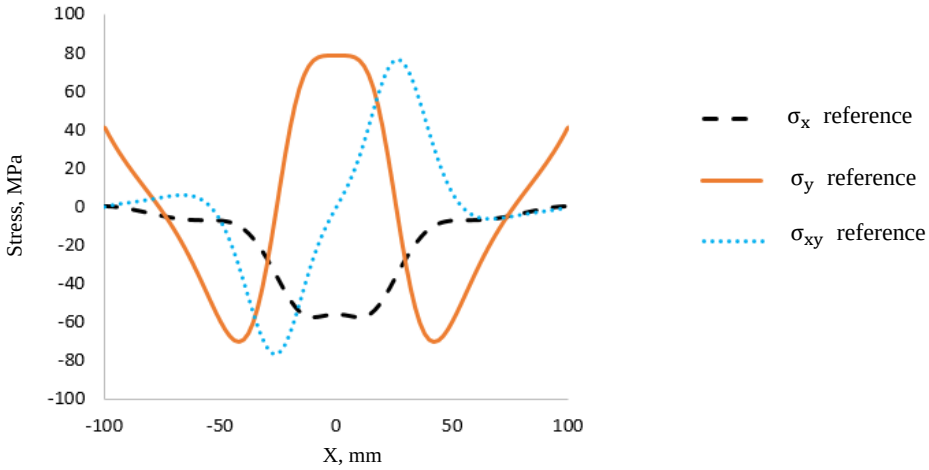

Figure 3-20 Line profile distributions of direct and shear stress along the cut line of the laser heated plate with a stiffness ratio of 4.

The displacement line profiles on the cut lines for the extreme case where an asymmetric cut was done on the laser heated plate with a stiffness ratio of 4 is shown in Figure 3-21. The range of displacements on the big part is smaller than the one for the small part as expected. In fact, the big part is stiffer than the small part and the weld is located on the small part.

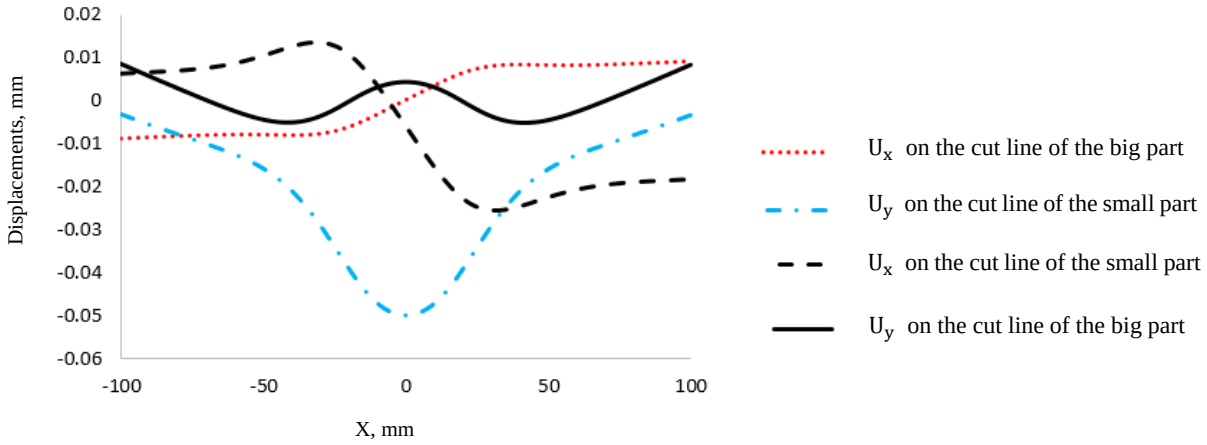

Figure 3-21 Displacement line profiles on the cut lines after an asymmetric contour cut on the laser heated plate having a stiffness ratio of 4.

Also the RMS and normalized RMS errors of the new data analysis approach dealing with asymmetric cuts were found to be lower than 1 MPa and 1%, respectively, for all different stiffness ratios explored (see Figure 3-22). However, the RMS and normalized errors of Mahmoudi's data analysis approach were found to be proportional to the asymmetry stiffness ratio. In fact, the error increased with the increase of the asymmetry stiffness ratio of the cut parts (see Figure 3-22). It can be inferred from these two sets of results that the new data analysis approach cancels the error owing to the shear stress contribution. In fact although the asymmetry stiffness ratio was changed from 1 to 4 during this study the stress distribution remained unchanged as shown in Figure 3-19. Hence the error in Mahmoudi's approach is most likely to be caused by the shear stress contribution that becomes more and more asymmetric when the asymmetry stiffness ratio increases. Averaging the contour displacements cancels out the shear stress contribution only if this contribution is anti-symmetric from both mating cut parts. When the asymmetry stiffness ratio increases the shear stress contribution from both mating cut parts the associated displacements become less and less anti-symmetric and therefore the error owing to shear stress increases.

Also, this study shows that the small error observed in the new data analysis approach is not caused by shear stress contributions as the error remains constant when the asymmetry stiffness ratio increases. This error may be caused by in-plane stress as discussed in the next chapter 4.

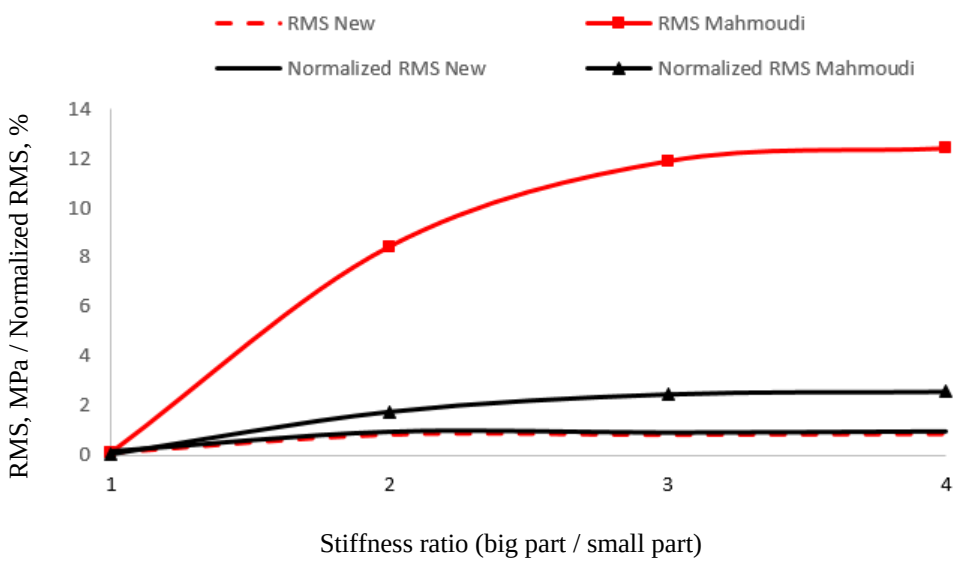

Figure 3-22 Comparison of the RMS and the normalized RMS errors between the new data analysis approach and Mahmoudi's approach to back calculate residual stress for different asymmetry stiffness ratios of the cut parts

3.3 Experimental validation

In order to experimentally validate the proposed new data analysis approach and the numerical analyses two of the proposed benchmark test specimens with stiffness ratios of 2 and 4 were manufactured. First, the residual stresses along the proposed contour cut plane were measured using the neutron diffraction technique. Then the samples were sectioned for contour method measurements. The contour method simulation and experimental results were compared with neutron diffraction measurements.

3.3.1 Manufacturing the test specimens

The benchmark test specimens were made from 200 mm x 250 mm x 6.5 mm blocks of bright steel (see Figure 3-16a). Prior to welding, the plates were stress relief heat treated up to 600°c and maintained in this temperature for 10 hours. Then the plates were air cooled to ambient temperature. A CO_2 fibre laser source of type IPG YLR-8000 CW with 3 KW power and 1 mm diameter welding spot was used for the welding. Controlling the heat affected zone accurately was of importance for this project as the numerical simulations were done using 1mm width

laser welded line to generate residual stress. Hence, the keyhole [109] welding mode was used as this mode enables deep penetration of the heat source and minimizes the heat affected zone.

3.3.2 Neutron diffraction measurement

Neutron diffraction measurements were carried out at the ENGIN-X instrument at Appleton Rutherford Laboratory for validating the asymmetric contour method numerical simulations and experimental measurements. For each plate, at least 31 different locations were measured along the planned contour measurement plane at mid-thickness of the plate (see Figure 3-16a). The nominal gauge volume for all the three orthogonal directions x, y and z was 2 x 2 x 2 mm^3. Reliable neutron diffraction measurements rely on undertaking appropriate measurements on stress-free reference samples. The benchmark test specimens were carefully designed so that the contour and neutron diffraction measurements were made away from the weld region reducing the complexity of composition and spatial variations in microstructure for the measurement locations. The 'far-field' approach was used for measuring stress-free reference sample. The introduced stresses are expected to fall off with distance from the weld. Hence, a far-field stress-free sample was expected to obtain as far away from the weld as possible; top right corner of the plates as shown in Figure 3-16a. The stress-free lattice parameter (d0) was measured in three different locations and at three orthogonal directions. The d0 for x direction was averaged at the three different location. Then the d0 for the x direction was used for the strain calculation in the x direction. The same procedure was repeated for the y and z directions.

Fitting and analysing of the lattice parameter (d) was performed using a full-spectrum Rietveld refinement [39] with the General Structure Analysis System [110].

The stress at each measurement position, acting in a given direction (e.g σ_x), was calculated in the following manner:

$$\sigma_x = \frac{E}{(1+\nu)(1-2\nu)} [(1-2\nu)\varepsilon_x + \nu(\varepsilon_y + \varepsilon_z)] \qquad \text{Equation 3-11}$$

where E is the bulk elastic modulus for the material, υ is Poisson's ratio, and ε_x , ε_y and ε_z are the strains calculated in three orthogonal orientations. It was assumed that the material was isotropic and Poisson's ratio value was 0.3 [67]. The measured bulk Young's modulus was 223 GPa. The results of neutron diffraction measurements are shown in Figure 3-17d-e.

3.3.3 Contour method measurement

The experimental contour method measurements were conducted on two manufactured test specimens having stiffness ratios of 2 and 4.

For all the contour method measurements the cut was conducted using an Agie Charmilles CUT1000 EDM machine, a tungsten coated EDM wire diameter of 50 µm and a cutting speed of 1 mm per minute. The contour simulations were done using 0.3 mm cut width whereas the experimental cuts were done using 50 µm wire diameter because a cut width of 0.3 mm or smaller doesn't affect the simulation results [67]. Moreover, simulating a cut width of 0.3 mm required a smaller number of elements on the FE model of the sample than using a cut width of 50µm. Therefore, the simulations were done faster and were less cumbersome. 3 mm x 200 mm sacrificial layers were bonded on the top and bottom surface of the plates to prevent cutting induced artefacts close to the top and bottom surfaces of the sample [54]. Self-constrained clamping strategy was used to securely restrain the test components during cutting [83] [84] [67]. This was achieved by introducing 1.5 mm diameter pilot holes at 5 mm away from the edge of the specimens (see Figure 3-23).

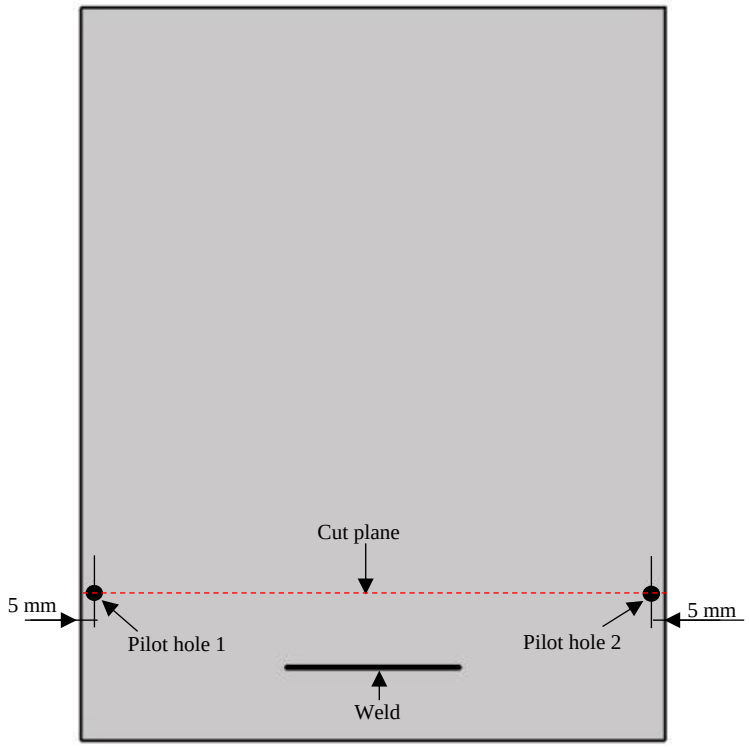

Figure 3-23 Schematic drawing of one of the benchmark test specimens illustrating self-constrained cutting strategy.

The wire EDM was threaded through one of the pilot holes and the cut was progressed to the other pilot hole. The remaining ligaments beyond the pilot holes were then severed. In addition, 'finger clamps' were used to prevent the specimen moving on the EDM bed table. Prior to performing cutting the specimen and the fixtures were left to reach thermal equilibrium conditions within the wire EDM deionised water tank. The cut parts were measured in a metrology laboratory and allowed to reach thermal equilibrium with the environment before the measurements were conducted. A Zeiss Eclipse Coordinate Measuring Machine (CMM), fitted with a Micro-Epsilon triangulating laser probe and a 4 mm diameter ruby-tipped Renishaw PH10M touch trigger probe was used for the measurements. The perimeter of the cut surfaces was measured with the touch probe at 1 mm pitch. The out of plane deformation of the cut surfaces was measured using the triangulating laser probe at 25 µm x 25 µm grid.

In addition to the welded benchmark test specimens, one plain plate after stress relief heat treatment prior to welding was also measured using the contour method. The two aims were first to assess the efficiency of the performed heat treatment process and characterise any remaining residual stresses in the plates prior to welding. Second, to identify cutting induced artefacts by wire EDM machining a stress-free sample. The un-welded plate measured 200 mm 250 mm 6.5 mm and was cut symmetrically at mid-length. For the symmetric cut on the un-welded plate, the conventional contour method data analysis and FE modelling steps were conducted using the standard approach described in [52] [68] and are summarised in the following.

The out of plane displacements (u_z) measured on both cut surfaces were mirrored, aligned and then averaged. The data from the ligaments beyond the pilot holes (see the dashed rectangles in Figure 3-24) was discarded because it showed clear evidence of cutting artefacts.

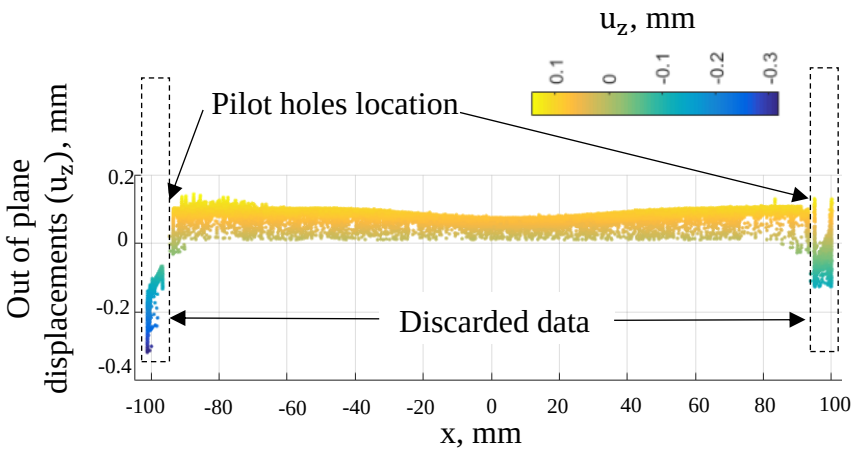

Figure 3-24 Figure showing the cleaned averaged out of plane displacements (u_z) and the discarded data from beyond the pilot holes.

Obvious outliers were removed from the averaged data set and bi-variate quadratic splines were used to fit the data to a smooth surface. The optimal amount of smoothing was chosen using the root mean square (RMS) misfit approached described in [68]. The smoothed displacements were inverted about the surface normal and were applied as displacement boundary conditions on a stress-free 3D FE model of half of the plate. Three additional point boundary conditions as described in [35] were applied to prevent rigid body motion and elastic stress analysis was conducted to back calculate the stresses.

For the asymmetric contour cuts on the welded plates with stiffness ratio 2 and 4 the new data analysis approach proposed in this thesis was used. For the asymmetric contour cuts the measured out of plane displacements of the asymmetric cut parts were mirrored and aligned but not averaged. The displacements of the cut parts were smoothed using quadratic bivariate splines. The level of smoothing was optimised for the data of each cut part independently. The smoothed data were then inverted and applied as boundary conditions to a 3D stress free FE model of the corresponding cut part. Rigid body motion was prevented using similar boundary conditions as for the back calculation step of the symmetric contour cut. Elastic stress analysis was performed and the resulting stresses for each cut part are shown in Figure 3- 25e and Figure 3- 25g for the sample with stiffness ratio 2 and in Figure 3- 25f and Figure 3- 25h for the sample with stiffness ratio 4.

Figure 3- 26a presents the measured stresses in the stress relieved sample (no weld present). Note that the stresses beyond the pilot holes where the displacement data were discarded are not presented. Hence a smaller FE model of the cut part was modelled discarding the ligaments beyond the pilot holes.

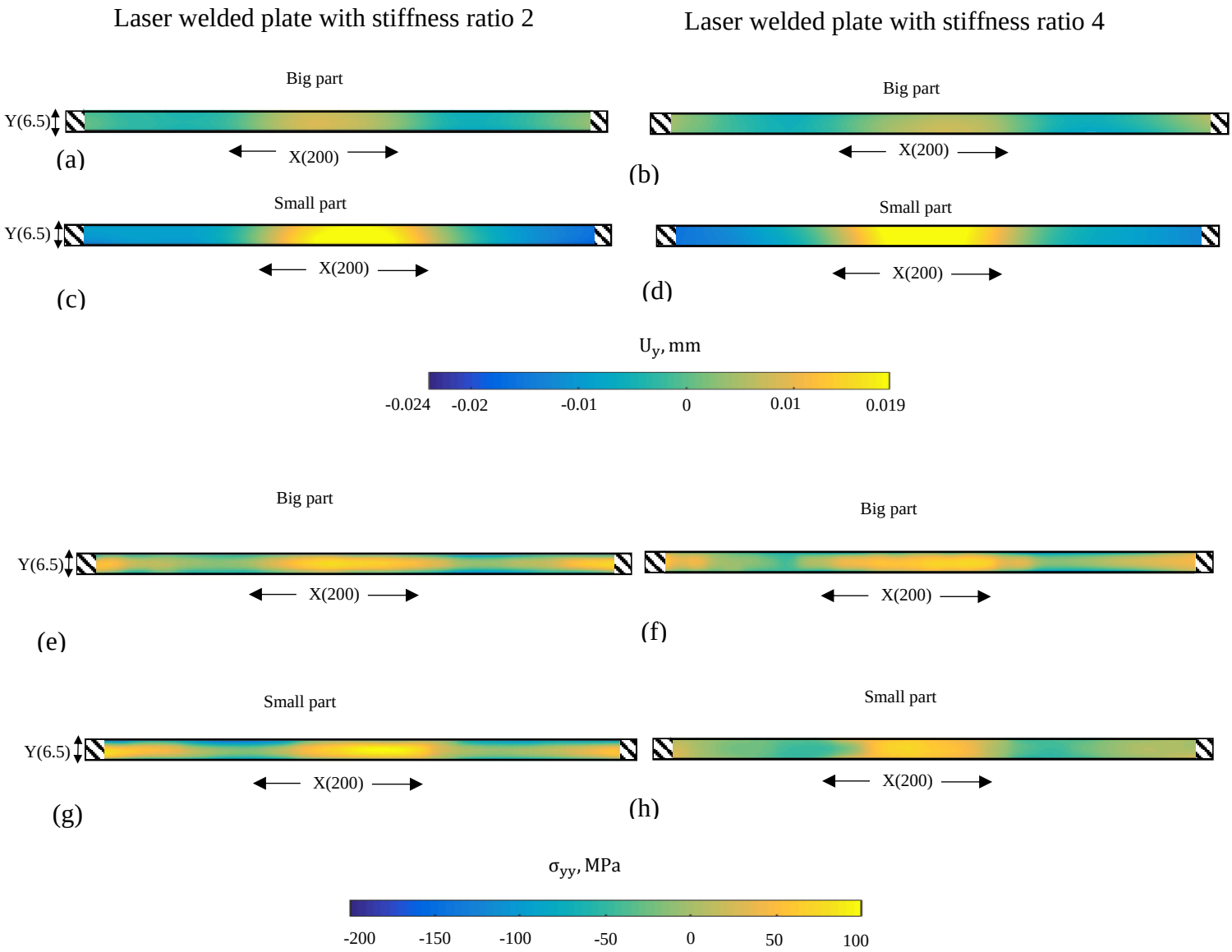

Figure 3- 25 Maps of measured out of plane displacements (a-d) and the resulting elastic stress analysis for each cut parts for the contour method measurements using asymmetric cuts (e-h).

The resulting stresses were then averaged and the map of averaged stresses shown in Figure 3-26b and Figure 3- 26c present the back calculated stresses measured using the contour method for asymmetric cuts.

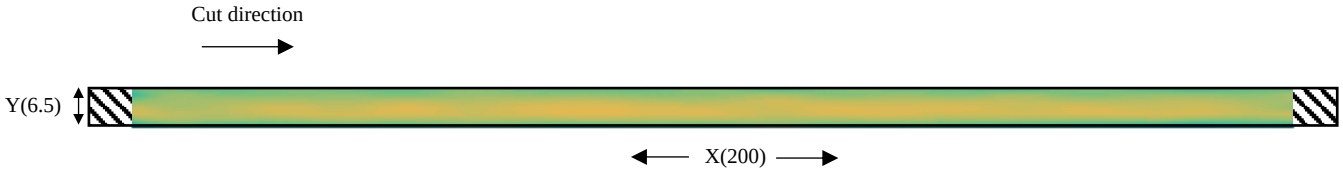

(a) Symmetric contour cut on a stress relieved un-welded plate with stiffness ratio 1 (L=50 mm)

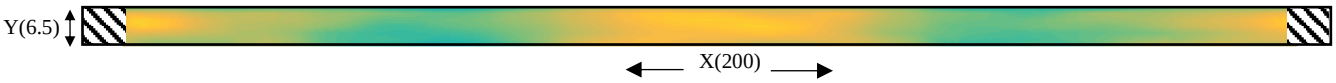

(b) Asymmetric contour cut on a laser welded plate with stiffness ratio 2 (L=100 mm)

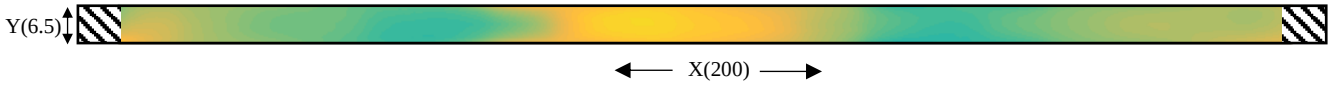

(c) Asymmetric contour cut on a laser welded plate with stiffness ratio 4 (L=200 mm)

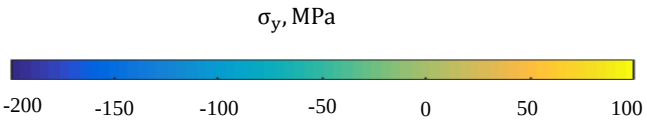

Figure 3- 26 Map of the stress component σ_y measured using the contour method: (a) symmetric contour cut on a stress relieved un-welded plate with stiffness ratio 1 (L=50 mm), (b) asymmetric contour cut on a laser welded plate with stiffness ratio 2 (L=100 mm) and (c) asymmetric contour cut on a laser welded plate with stiffness ratio 4 (L=200 mm).

3.4 Discussion of results

It was found that the shear stress effect is cancelled when the stress on one cut part is calculated using the displacement from the corresponding cut part without averaging it with the mating part. Then by averaging the back-calculated stresses from both cut parts, the shear effect is cancelled (Figure 3-5).

Also, the material stress-strain was not elastic perfectly plastic as expected. Thus the approach of Traore cannot be used to assess plasticity cutting induced error (Figure 3-15) but this is not the only reason as discussed later in this section.

The design of the sample was optimized from tramline to single weld line because when the entire contour simulation was done the plasticity cutting induced error was too high (Figure 3-8 and Figure 3-9).

To explore the effect of stress field on the contour method different weld design were explored one with a weld line on the bottom part and symmetric cut (asymmetry of stress field only), one with weld on the big part and asymmetric cut, and one with weld on the small part and an asymmetric cut (asymmetry of stress field and geometry) as shown in Figure 3-10.

The effect of the stress field was found to be important in the back calculation step for both symmetric and asymmetric contour cuts (from Figure 3-11 to Figure 3-12). Asymmetry of the stress field affects only displacement for the symmetric cut thus the conventional data analysis approach still works. For the asymmetric cut, displacements cannot be averaged but the effect of stress field is cancelled by averaging back calculated stress.

The design of plate 3 (Figure 3-10) was selected so that the stress profile remains similar by increasing the aspect ratio.

A comparison of the corrected contour results based on the stress-free sample measurements with the FE predictions and ND measurements is presented in Figure 3-17d and Figure 3-17e.

Figure 3-17d-e compare the FE predicted residual stress with the measured stresses using neutron diffraction and contour method for a line profile at mid-thickness of the plates. When comparing the stresses, it is important to account for differences in the gauge volume over which the stresses are presented. The FE prediction of initial residual stress state was made using 2D plane stress FE models. The predicted stresses are assumed to be uniform through the thickness of the plates. The neutron diffraction measurements are stresses averaged over the neutron diffraction gauge volume and the contour results are from local points along mid-

thickness. Therefore, in order to compare the results, one line profile (Figure 3-17d-e) presents the contour results averaged through the thickness of the plates and another line profile shows the contour stresses averaged over the sampling gauge area of neutron diffraction at mid-thickness of the plates. The former is to compare with FE predictions and the latter to compare with ND measurements on a fair basis.

The difference between the FE predictions and experimental measurements (Figure 3-17d-e) may be reduced by using 3D FE models instead of 2D models due the plane stress assumption, and using more accurate material properties.

Figure 3-17d-e shows that, overall, there is a good agreement between the predicted and measured stresses despite the stress levels being low, which is challenging especially for both the contour method and neutron diffraction technique.

It is worth noting that this FE study and the experimental contour measurements were conducted on samples in plane stress conditions with stress levels having the ratio of shear to normal stress equal to 1 (see Figure 3-12a). The proposed approach will have to be further explored in the next chapter 4 on more generic cases especially for samples with higher levels of shear stress.

The out of plane displacements obtained from contour cutting simulations of the laser welded plates were analysed using the approach presented in [96] and the new data analysis approach proposed in this report. For the symmetric contour simulation, the data were also analysed using the conventional contour data analysis approach. The back calculated stresses are compared in Figure 3-19. As demonstrated in Section 2.1, for the symmetric contour cut, all of the data analysis approaches used lead to the correct back-calculated stresses (Figure 3-19a). It is evident from Figure 3-19b and Figure 3-19c that implementing the approach presented in [96] for asymmetric contour cuts results in incorrect back-calculated stresses. The present proposed data analysis approach, however, accurately back calculates the original residual stresses. Figure 3-19b and Figure 3-19c shows an excellent agreement between the predicted and back-calculated stresses using the new data analysis approach. The contour method simulation results, using the new averaging method, give an average RMS error less than 1 MPa against the reference stress prior to cutting in the virtual specimens for the different stiffness ratios of asymmetric contour cuts investigated in this study. Similarly the average RMS error using the approach detailed in [96] was found to be higher than 9 MPa. Therefore,

the error obtained using the new averaging method was considered to be negligible in comparison to the error obtained using the approach detailed in [96].

Following the numerical simulation of the contour method, demonstrating the robustness of the proposed data analysis approach for asymmetric contour cuts with different levels of stiffness ratios, the manufactured benchmark test specimens were measured using neutron diffraction and the contour method subsequently.

Asymmetric contour cuts were conducted on test samples with stiffness ratio 2 (L = 100) and stiffness ratio 4 (L = 200), see Figure 3-16a. The measured out of plane displacements of the cut surfaces for both cut parts are shown in Figure 3- 25a and Figure 3- 25c for the sample with stiffness ratio 2 and in Figure 3- 25b and Figure 3- 25d for the sample with stiffness ratio 4.

The cut surface of the smaller cut part with lower stiffness deforms more that the mating cut surface of the bigger cut part; the larger the stiffness ratio, the greater the difference between the resulting out of plane displacement of the cut surfaces.

It is clear that averaging the out of plane displacements of the two cut parts, as is done in the conventional contour method or as proposed in [68], does not take into account the difference in stiffness of the cut parts and would result in error in the back-calculated stresses. This was demonstrated through numerical simulation of the contour method in section 3.2.4 (see Figure 3-19).

For the data analysis method proposed in this thesis the out of plane displacements of each cut part is independently used in the FE elastic stress analysis step of the contour method. Therefore, the FE modelling and performing elastic stress analysis for each cut part takes into account the effect of stiffness of the cut part in the resulting stresses (see Figure 3- 25e-h).

Once the effect of cut parts stiffness is accounted for, the resulting stresses obtained from elastic stress analyses are averaged. The averaged stresses present the back-calculated stresses measured using the contour method (see Figure 3- 26b-c).

The contour method measurement made on the stress-relieved un-welded test component (Figure 3- 26a) showed stresses in the order of ± 20 MPa in the plate after heat treatment (prior to welding). This stress is potentially a combination of remaining stress after stress relief heat treatment and cutting induced artefacts manifested in the back-calculated stress. This measured stress was subtracted from the results of contour measurements in order to correct for cutting artefacts and to compare the measured stresses with FE predictions and neutron measurements on a fair basis.

3.5 Conclusions

The present work proposes a new data analysis approach extending the application of the contour method using asymmetric contour cuts. Extensive finite element simulations were conducted to design suitable benchmark test specimens. Laser welded plates, with a well-defined residual stress field were used to explore the contour method using asymmetric cuts. The level of introduced weld residual stress as well as the location of the contour measurement with respect to the laser weld were optimised in order to prevent cutting induced plasticity errors during the cutting step of the contour method.

The theory and assumptions of the proposed data analysis approach for asymmetric cuts was presented. The accuracy of the proposed method for asymmetric contour cuts against the conventional data analysis approach and the approach presented in [96] for asymmetric contour cuts was demonstrated using idealised contour method simulations on virtual benchmark test specimens. The FE reconstructed contour stresses were presented for three different levels of asymmetric contour cuts: (a) when the stiffness of the cut parts was equal presenting a symmetric cut, (b) for a contour cut where the stiffness of one cut part was twice the stiffness of the mating cut part and (c) for a contour cut where the stiffness of one cut part was four times greater than the stiffness of the mating cut part.

Asymmetric contour cuts were then implemented experimentally on manufactured benchmark test specimens for two different asymmetry levels and the measured out of plane displacements were analysed using the new proposed approach. Prior to conducting contour cuts the residual stresses were measured using the neutron diffraction technique in order to validate the FE predictions and the results of the contour method using asymmetric cuts.

The good agreement between the stresses obtained from asymmetric contour cuts and neutron diffraction measurements, despite measuring low level of stresses, was encouraging. However, the proposed approach was only demonstrated on a limited number of samples. The impact of other potential parameters for example the level of shear stress and the level of stiffness ratio of the cut parts on the results of the contour method for asymmetric cut using the proposed approach needs further detailed investigation. This is covered in chapter 4.

Chapter 4: 3D asymmetric contour analysis

In chapter 3 a new data analysis approach dealing with off-centre cuts was explored. It was shown that the effect of shear stress generates asymmetric 'error' in the out of plane displacements on both mating cut surfaces. But by averaging the back-calculated stress without averaging the contour displacements from both mating cut surfaces, errors owing to shear stress are cancelled out. Theoretical considerations were proposed and a good correlation was obtained between FE predictions, contour method experimental measurement and neutron diffraction results. However, the experimental part was done on thin plates having an essentially two-dimensional stress field. This chapter aims to apply the new data analysis approach to more general cases using 2D and 3D FE models.

4.1 Introducing the TG6 welded benchmark test component

The European Network on Neutron Techniques Standardisation for Structural Integrity (NeT) is working on the development of the state-of-the-art experimental and numerical techniques for the reliable characterisation of residual stress in structural welds. The experimental methods used include neutron diffraction, synchrotron diffraction, laboratory X-ray diffraction, deep hole drilling and the contour method. Each benchmark problem examined by the network is tackled by creating a dedicated Task Group (TG) comprising researchers from universities, central scientific facilities and industry, which undertakes measurement and modelling studies and the interpretation of the results. Task Group 6 (TG6) was formed to study residual stresses in a benchmark problem where three superimposed weld beads are laid in a finite length slot in an Alloy 600 nickel alloy plate (Figure 4-1). This benchmark test component was used in the present study to validate the new data analysis approach for dealing with asymmetric contour cuts.

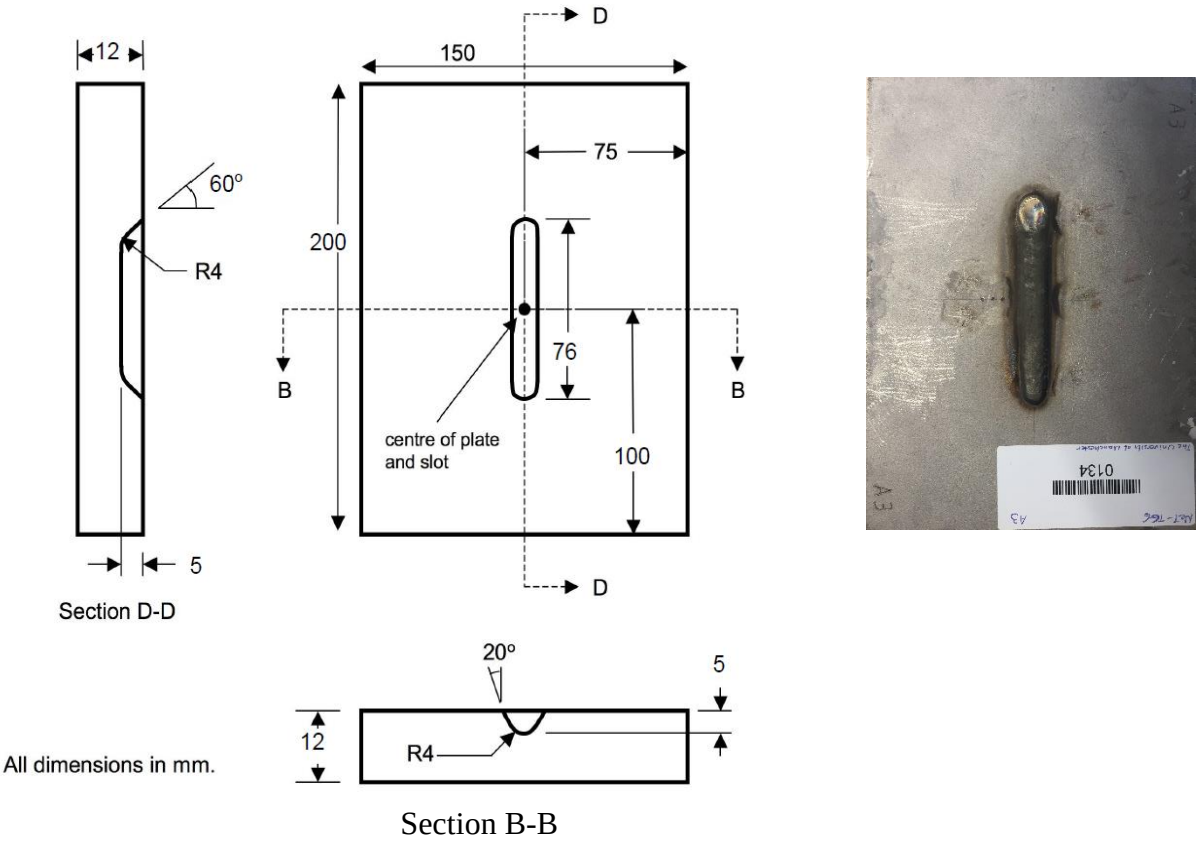

Figure 4-1 Schematic view of the TG6 weld benchmark design and a picture of TG6 plate A3.

The author was given a 3D FE model of one half of the TG6 welded benchmark specimen together with predicted residual stress results by Muransky [111]. In order to simulate asymmetric contour cuts using residual stress results predicted by this model, a full plate residual stress field solution had to be created first using mirror symmetry and then this was mapped onto a new 3D FE model (see Figure 4-2). Stresses and plastic strain were mapped using the command 'Map solution' in Abaqus and an equilibrium step was done after the mapping process. However, meshing the curved weld bead was found to be challenging and resulted in an irregular model, therefore it was simplified (flattened) to improve the quality of the mesh in the plate and avoid mesh artefacts. Also, the mesh had to be refined along the cut plane to capture any gradient of strain and stress during the contour cut stress relaxation and to accurately back-calculate the original residual stress prior to cutting. The procedure of contour simulation is detailed in the next section.

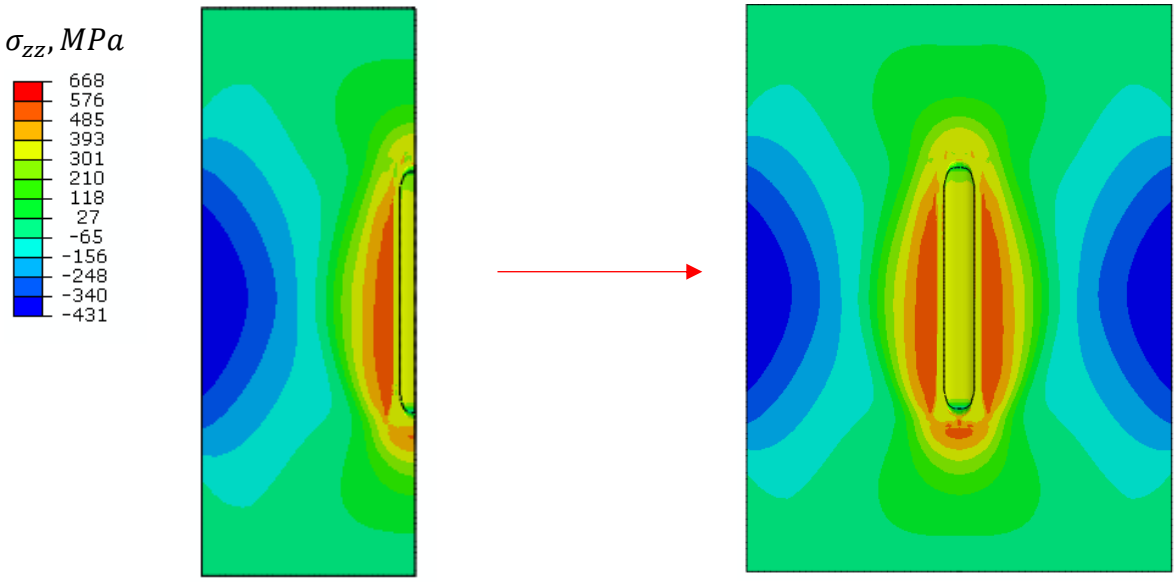

Figure 4-2 Diagram showing the half and the full mirrored TG6 predicted residual stress solutions for longitudinal stress

4.2 Symmetric contour cut on the TG6 sample

Once a simplified TG6 FE model had been generated and the results of Muransky mirrored to obtain a full residual stress simulation for the welded plate, a contour method simulation using a geometry symmetric planar cut was undertaken in order to validate the 3D procedure by comparing the simulated measured results with the original predicted stress field.

Only elastic material properties including the Young modulus (E = 213 700 MPa), and Poisson's ratio (μ = 0.31) of the parent material were used and applied to the material in the whole plate including the heat affected zone (HAZ) and the weld metal. This was done because the first stage the goal was to focus on validating the contour method simulation using the new data analysis approach for a 3D case, regardless of potential plasticity error. The conventional data analysis approach was compared with the new data analysis approach detailed in chapter 3.

The contour method simulation was done using a blunt instantaneous cut located at the centre of the plate (see Figure 4-3). The cut width was 0.3 mm. The elements along the cut plane were removed all at once. The effect of the cut width is discarded in the data analysis because the reference stress along the top and bottom cut surfaces is averaged and compared to the averaged back calculated stress from the top and bottom parts as detailed later.

The boundary conditions used were aiming only to stop rigid body motion. So, for each cut part one bottom corner was constrained in X,Y and Z directions, the other bottom corner was constrained in X and Z directions and one top corner was constrained in Z direction as shown in Figure 4-6.

An equilibrium step was done before extracting the out of plane displacements on the cut surfaces. Then the negative contour displacements of the small part were applied as boundary conditions on the cut surface of the small part. Similarly, the negative displacements of the big part were applied was boundary conditions on the cut surface of the big part. Then the back-calculated stresses from both mating cut parts were averaged as detailed in the previous section.

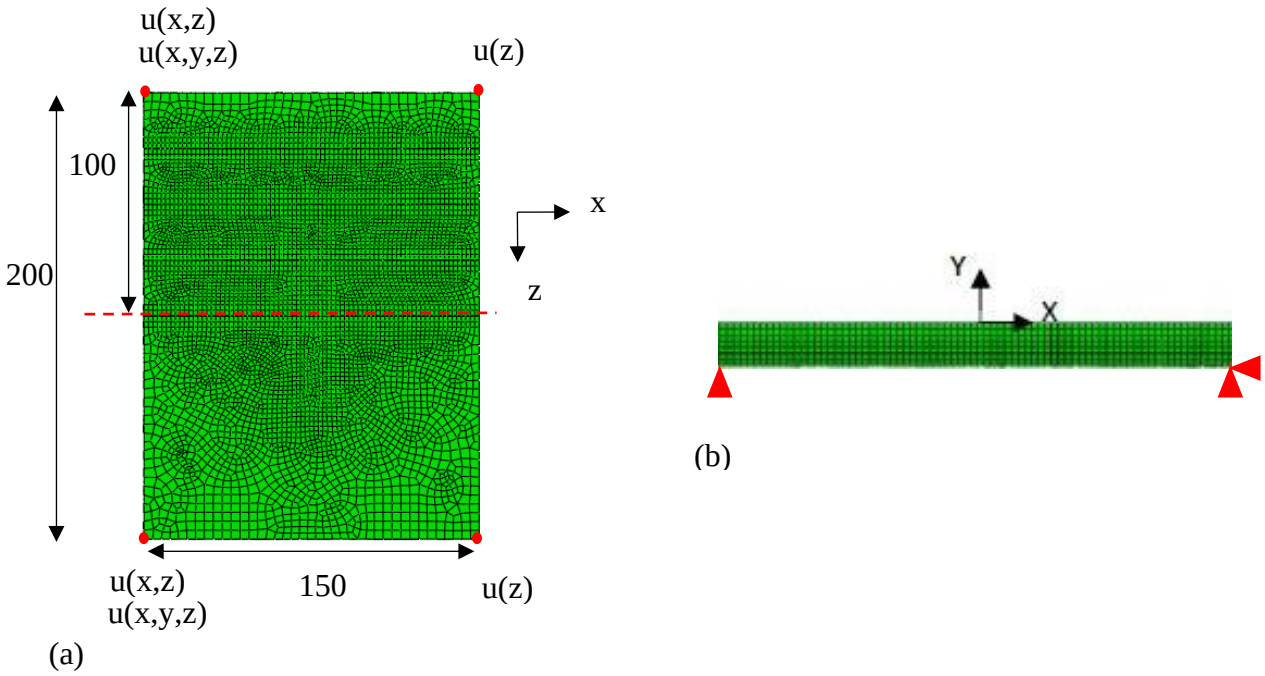

Figure 4-3 View of the meshed model and boundary conditions used during the cut step (a) and boundary conditions used during the back calculation step (b) for the TG6 sample.

The averaged back calculated stress from both mating cut parts were compared to the original stress along the cut plane prior to cutting the sample.

Also, the original stresses along the cut plane were averaged from each side of the cut plane in order to compare them with the averaged back-calculated stress. In fact, the width of the blunt cut was 0.3 mm so the cut surfaces were shifted by 0.15 mm from each side of the cut plane.

The error between the original and back calculated stress was assessed using the root mean square (RMS) of the differences between the reference and the back calculated stresses. This was then normalized using the range of the reference stress as detailed in Equation 4-1 and Equation 4-2.

$$Average\ RMS = \sqrt{\frac{1}{n}\sum_{i=1}^{i=n}\left(\sigma_z^{Reference}(i) - \sigma_z^{Reconstructed}(i)\right)^2} \qquad \text{Equation 4-1}$$

Where n is the number of nodes on the cut surface, $\sigma_z^{Reference}(i)$ is the value of the reference stress at the node i and similarly $\sigma_z^{Reconstructed}(i)$ is the value of the reconstructed stress at the node i.

$$\text{Normalized Average RMS} = \frac{Average\ RMS}{Max\left(\sigma_z^{Reference}\right) - Min\ \left(\sigma_z^{Reference}\right)} \qquad \text{Equation 4-2}$$

Where $Max\left(\sigma_z^{Reference}\right)$ and $Min\ \left(\sigma_z^{Reference}\right)$ are the maximum and minimum value of the reference stress.

The average RMS error was found equal to 2.9 MPa for both the conventional and new data analysis approaches. This gives a normalized RMS error of 0.28% which is negligible.

In fact, the stress maps of the back calculated stresses using both the conventional and the new data analysis approaches are very similar the reference stress map as shown in Figure 4-4. Also the stress line profiles extracted along the lines x = 0 mm, y = -12 mm, y = -6 mm, and y = 0 mm (see Figure 4-5) show an excellent agreement between the back-calculated stresses and the reference stress prior to the cut.

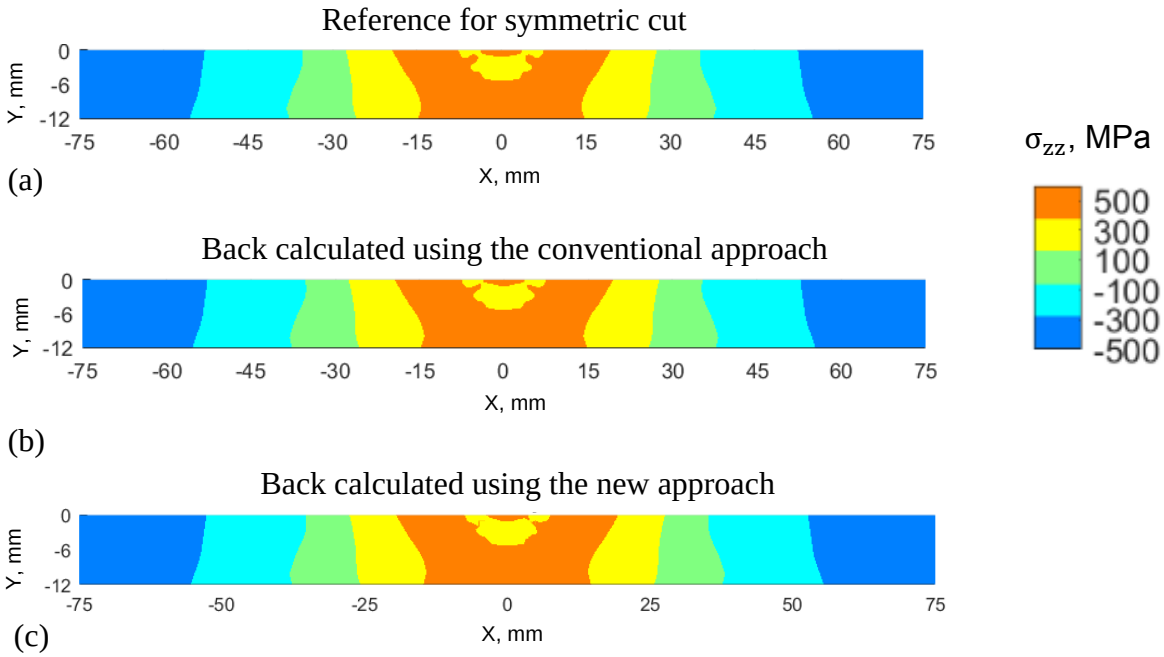

Figure 4-4 2D map of stress along the cut plan presenting (a) reference stress, (b) back calculated stress using conventional approach and (c) back calculated stress using the new approach.

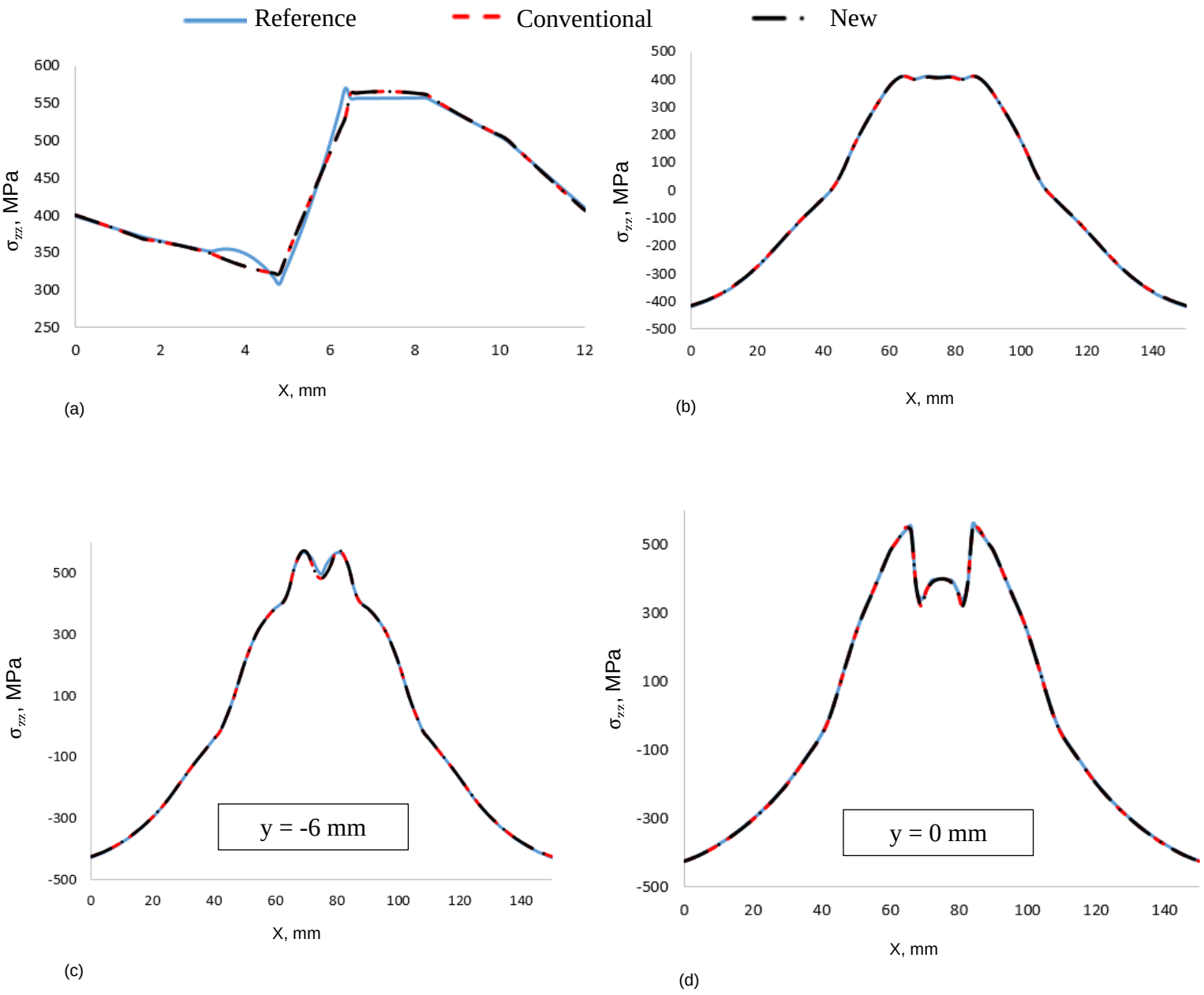

Figure 4-5 Comparison of stress line profiles between the reference stress prior to the symmetric cut, and the back calculated stress using the conventional and new data analysis approaches.

The maximum difference between the back calculated stresses using the new approach and the one using the conventional approach was found equal to 0.48 MPa which is negligible. Moreover, the error between the back calculated stresses using both approaches and the

reference stress was found to be negligible. Therefore, the new data analysis approach for simulating the contour method measurement for a 3D structure has been shown to be reliable.

4.3 Asymmetric contour cut

The contour measurement method was next simulated for the TG6 plate on a plane at 25 mm away from one edge of the sample (see Figure 4-6). This an asymmetric cut in terms of geometry (high aspect ratio) and residual stress field. The approach used here was similar to one used for the symmetric contour cut detailed in section 4.2. Elastic material properties including the Young modulus (E = 213 700 MPa), and Poisson's ratio (μ = 0.31) for the parent material were used for the entire component on both sides of the cut. Again this simplified model for material properties was used to avoid simulating potential plasticity effects during cutting.

The contour cut simulations involved modelling an instantaneous blunt cut by removing elements representing the cut width through the thickness, (see Figure 4-6). For this cutting step boundary conditions were chosen to just stop rigid body motion. So, for each cut part one bottom corner was constrained in X, Y and Z directions, the top corner was constrained in the X and Z directions and the other bottom corner was constrained in Z direction as shown in Figure 4-6a.

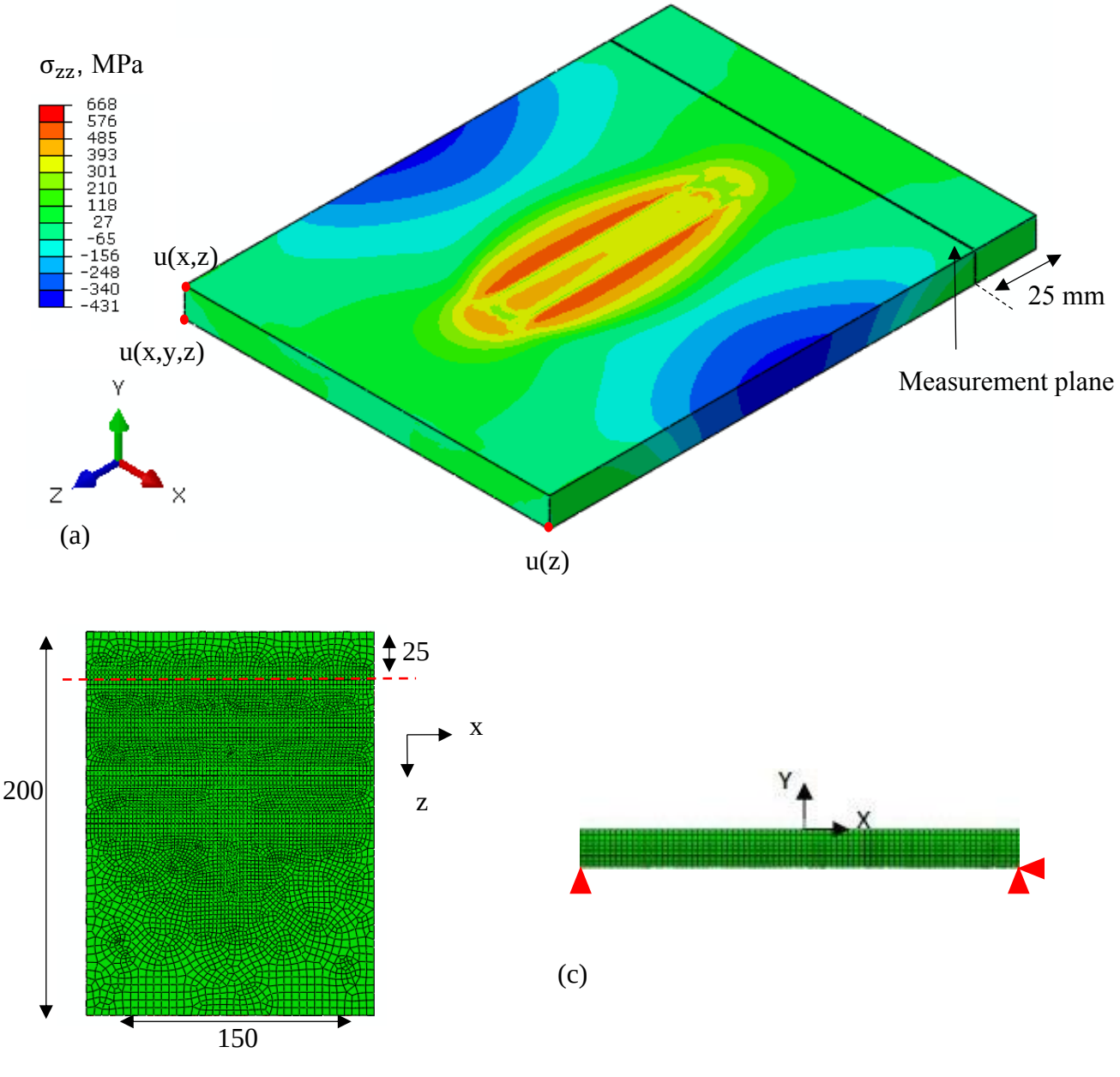

Figure 4-6 (a) View of the simulated residual stress field in the TG6 plate and the cut location, (b) the meshed model and boundary conditions used during the cut step and (c) the boundary conditions used during the back calculation step.

An equilibrium step was done before extracting the out of plane displacements of the cut surfaces. Then the negative of the out of plane displacements of the small part were applied as boundary conditions on the cut surface of the FE model of the small part. Similarly, the negative displacements of the big part were applied as boundary conditions on the cut surface of the FE model of the big part. Then the back-calculated stresses from both mating cut parts were averaged as detailed in the previous section.

The stress maps of the back calculated stress from both mating cut parts and their average were compared to the original stress along the cut plane prior to cut as shown in Figure 4-7. The averaged RMS error between the reference and back-calculated stress was found equal to 5.3 MPa which is 4.3% of the reference stress range.

Also, the conventional [35] and Mahmoudi's [96] data analysis approaches were implemented to back-calculate the residual stress. The conventional data analysis approach [35] involves averaging the contour displacements from both mating cut surfaces and applying the negative of the averaged contour displacements as boundary conditions on one half of the TG6 plate. The averaged RMS error between the reference and back-calculated stress using the conventional data analysis approach was found equal to 58.3 MPa which is 47.4% of the reference stress range. Mahmoudi's approach [96] involves averaging the contour displacements from both mating cut parts and applying the negative of the averaged contour displacements on each one of the mating cut surfaces. Then the back-calculated stresses from each cut surfaces are averaged. The averaged RMS error between the reference and back-calculated stress using Mahmoudi's [96] data analysis approach was found equal to 36.8 MPa which is 29.9 % of the reference stress range. Hence the error obtained using the conventional approach was 11 times higher and the error obtained using Mahmoud's approach was 7 times higher than the error obtained using the new data analysis approach.

The reference and the reconstructed stresses were compared along lines at x = 0 mm, y = -12 mm, y = -6 mm, and y = 0 mm as shown in Figure 4-8. The results show a mismatch between the reference and back-calculated stresses. Also, the reference stress map was averaged from both planes corresponding to the sides of the cut parts before comparing it to the back-calculated stress to discard errors owing to the cut width.

Therefore, different approaches were explored to mitigate this unexpected error as detailed in the next sections. The agreement between the back calculated contour stresses and the reference stress line profiles was not as good as that obtained in the 2D case presented in chapter 3 (Figure

3-19). The contour method simulation was done using elastic FE analysis. Therefore, the differences cannot be due to plasticity error.

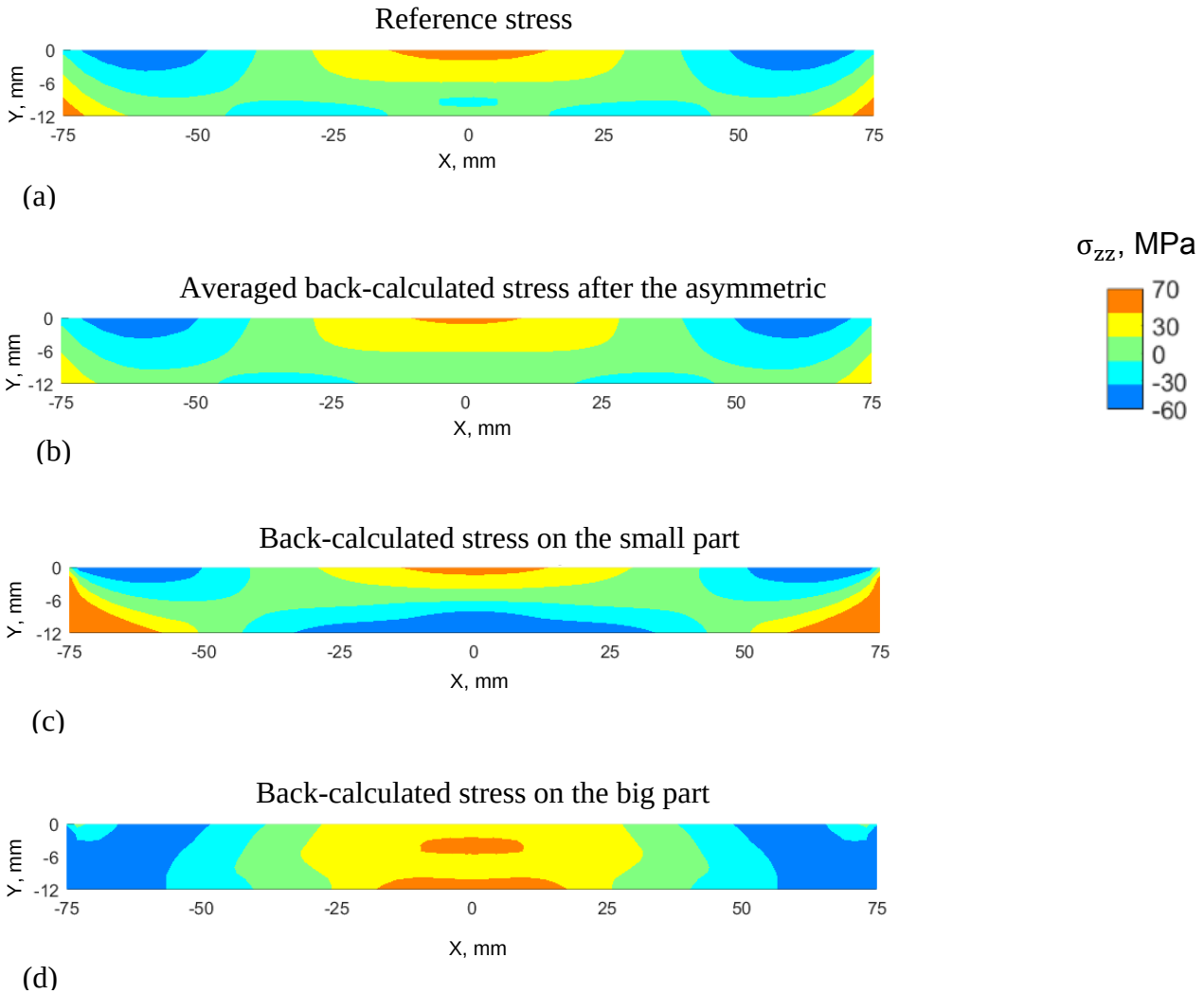

Figure 4-7 2D maps of (a) reference stress simulation over a transverse plan cut 25 mm from one edge of the sample, (b) averaged back calculated stresses, (c) back calculated stresses on the small part and (d) back calculated stress on the big part for an asymmetric contour cut simulation on the TG6 sample.

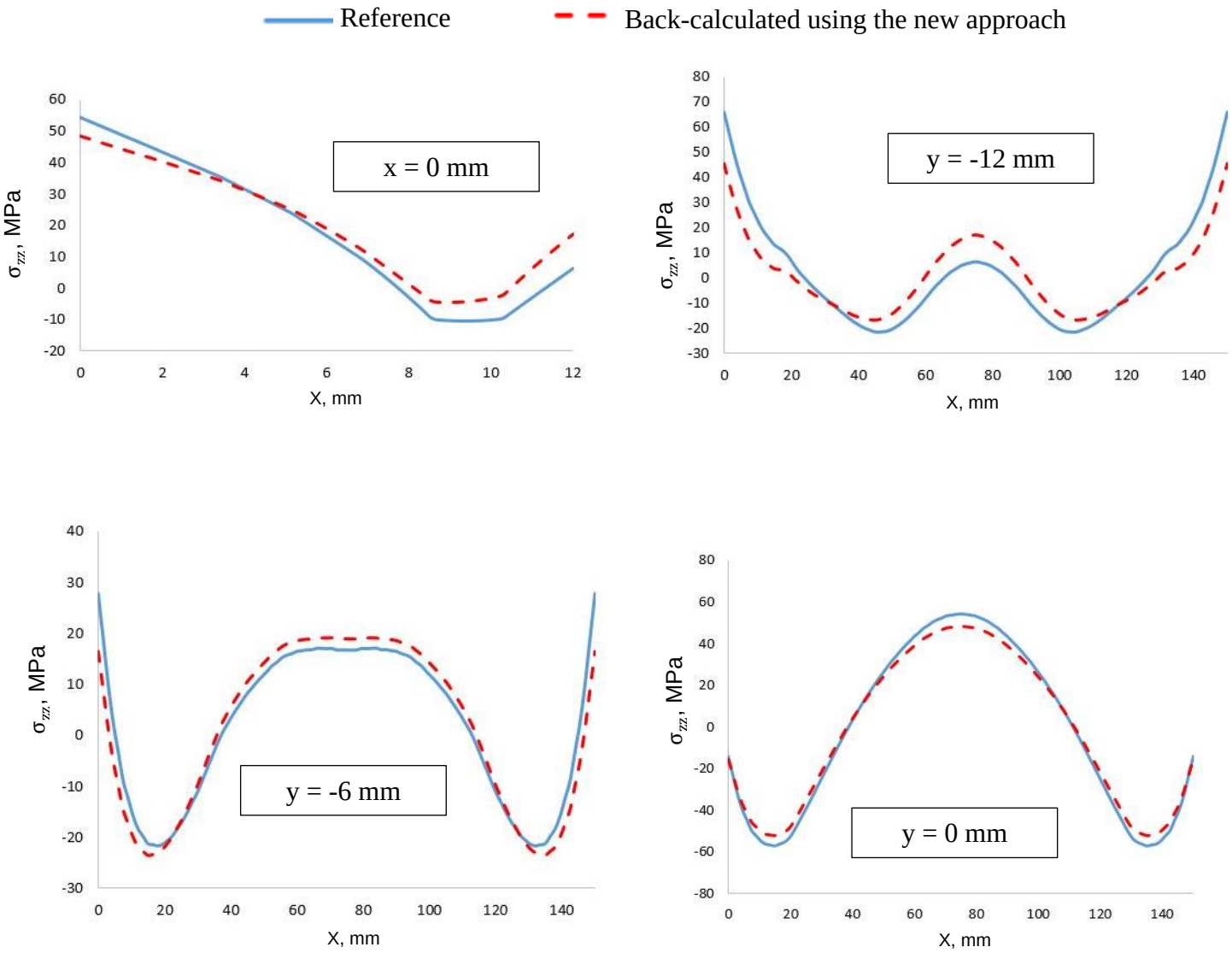

Figure 4-8 Comparison of stress line profiles between the reference stress prior to the asymmetric cut, and the back calculated stress using the new data analysis approach.

4.4 Investigating the error in the 3D asymmetric contour simulation

The 2D maps of residual stress components σ_{xx}, σ_{yy} and σ_{zz} along the cut plane prior to the cut on the TG6 plate are shown in Figure 4-9. It worth noting that the range of the reference in-plane stress σ_{xx} is more than three times higher than the range of the reference out-of-plane stress σ_{zz} . This may cause errors in the contour method as discussed later in this section.

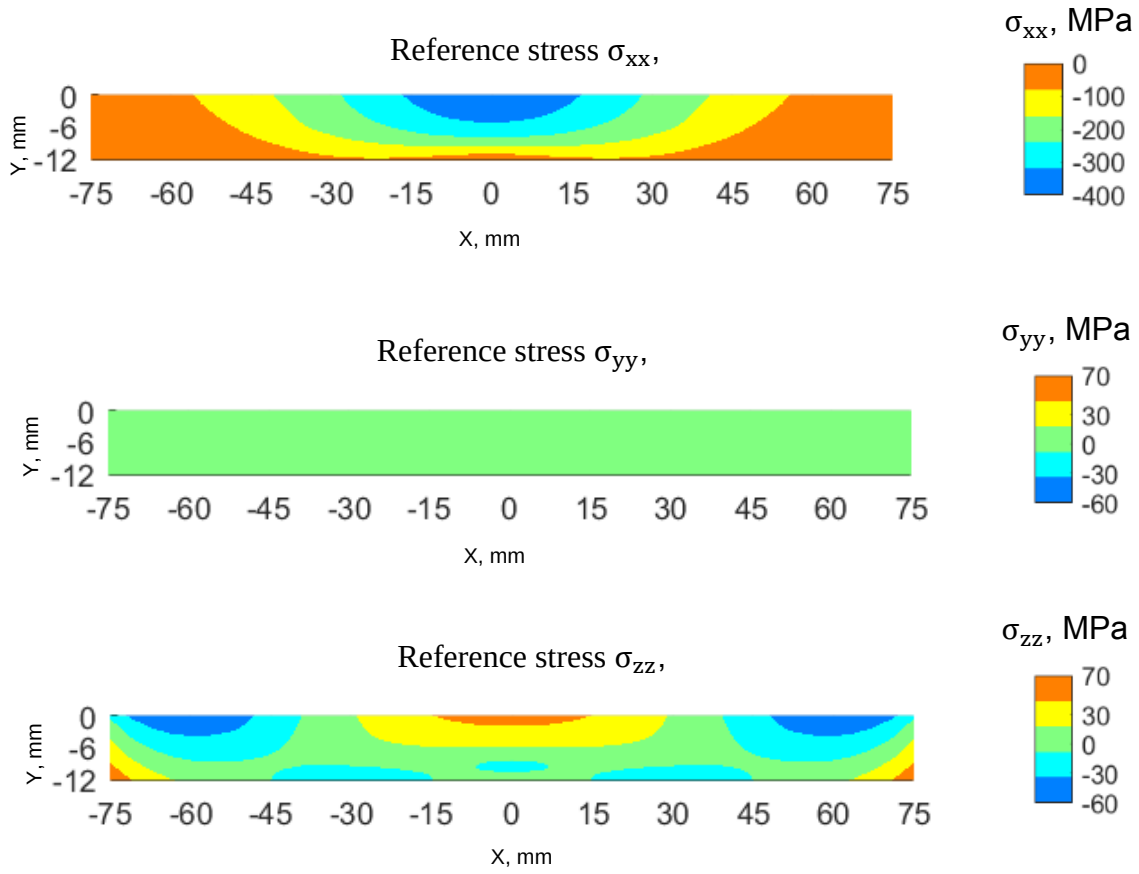

Figure 4-9 2D maps of the reference stress components σ_{xx}, σ_{yy} and σ_{zz} along the cut plane of the TG6 plate prior to the cut.

The 2D maps of residual stress components σ_{yz} and σ_{xz} along the cut plane prior to the cut on the TG6 plate are shown in Figure 4-10. The range of the shear stress component σ_{xz} is dominant as expected and is comparable to the range of the out-of-plane stress. However as discussed in chapter 3, the new data analysis approach cancels the error owing to shear stress during the back-calculation step.

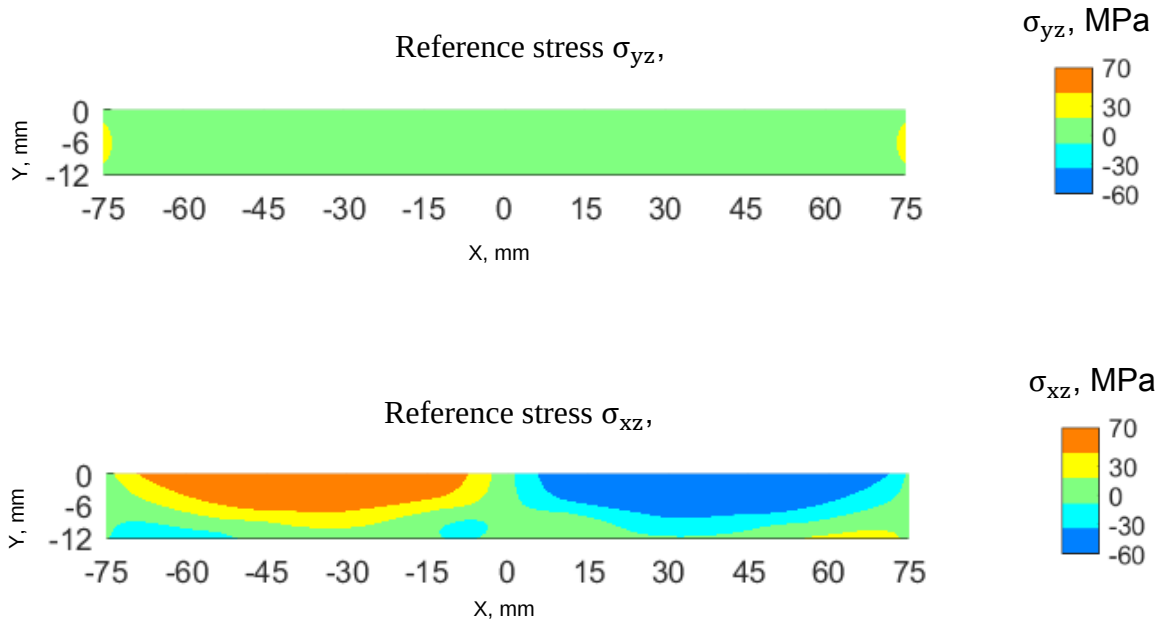

Figure 4-10 2D maps of the reference stress components σ_{yz} and σ_{xz} along the cut plane of the TG6 plate prior to the cut.

The relaxed out-of-plane displacements U_z on the cut surface of the big and small part after an asymmetric cut on the TG6 plate are shown in Figure 4-11.

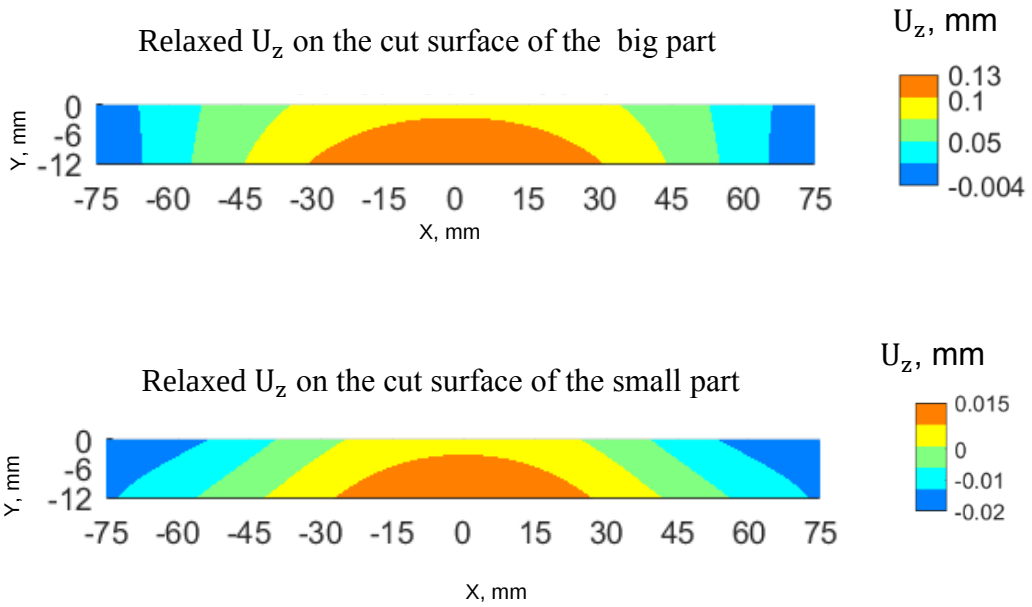

Figure 4-11 2D maps of the relaxed displacement U_z on the cut surfaces of the big and small after an asymmetric contour cut on the TG6 plate.

The relaxed in-plane displacements U_y on the cut surface of the big and small part after an asymmetric cut on the TG6 plate are shown in Figure 4-12.

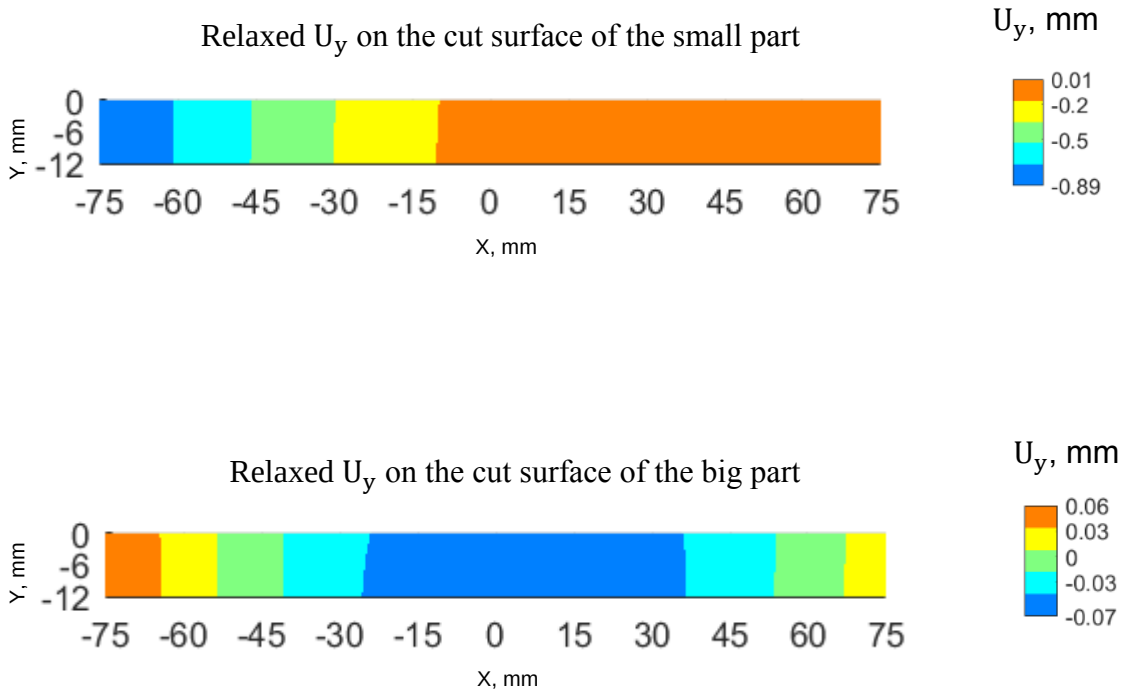

Figure 4-12 2D maps of the relaxed in-plane displacement U_y on the cut surfaces of the big and small after an asymmetric contour cut on the TG6 plate.

The relaxed in-plane displacements U_x on the cut surface of the big and small part after an asymmetric cut on the TG6 plate are shown in Figure 4-13.

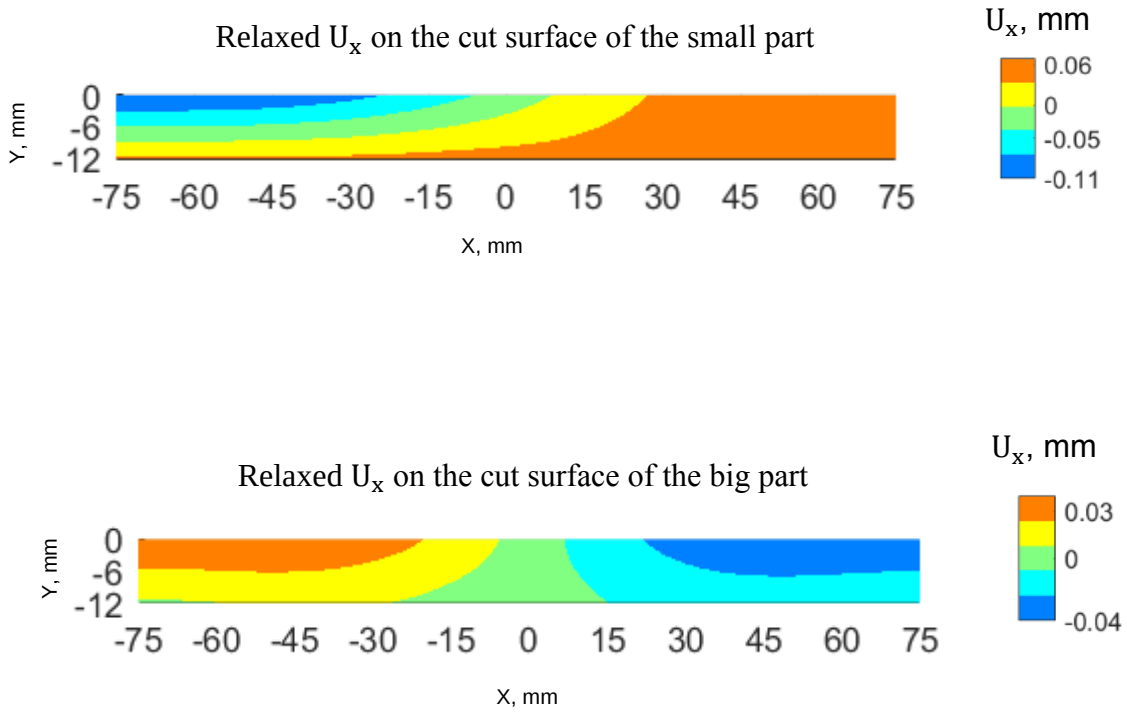

Figure 4-13 2D maps of the relaxed in-plane displacement U_x on the cut surfaces of the big and small after an asymmetric contour cut on the TG6 plate.

During the contour method only the out-of-plane displacement U_z is used during the back calculation step. It is worth nothing that the range of the in-plane displacement U_y is 6.9 times higher than the range of the out-of-plane displacement U_z. Also, the range of the in-plane displacement U_x is 1.3 times higher than the out-of-plane displacement U_z. The high range of the in-plane displacements with regards to the range of the out-of-plane displacement is consistent with the fact that the TG6 plate has a butterfly shape due to the retained residual stress field. The effect of in-plane displacements and in-plane stress in the contour method is investigated in this section.

Different approaches were explored to understand and mitigate the error in the contour results including:

- Applying the negative of all the relaxed displacements in the x, y and z directions (see Figure 4-6) as boundary conditions during the back-calculation step.
- Forcing the nodes on the cut surface to move in the same direction along the cut surface plane
- Exploring Hookes law to try to see where the error in the contour method results can come from.
- Conjecture about the generic influence of in-plane stress on the contour method

4.4.1 Exploring the effect of in-plane displacements

One hypothesis was that in-plane displacements, that are not considered in the back-calculation of the contour method, could have contributed to the error. In order to investigate this, both in-plane displacements u_x and u_y (see Figure 4-6), in addition to the out of plane displacements u_z (see Figure 4-6), were used in the contour simulation back-calculation step, for the full 3D FE model. The same asymmetric cut was simulated as detailed in section 4.3. The displacements on the cut surfaces in three principal directions X, Y and Z were extracted. The relaxed displacements were obtained by subtracting the displacements in the three principal directions before the cut from the corresponding displacements after the cut. Then the negative of the relaxed displacements in the 3 directions, was applied as a boundary condition on the cut surface of a new stress free model having the same mesh and geometry. Other boundary conditions were applied to prevent rigid body motion as detailed in the section 4.3. An elastic stress analysis was then carried out giving back-calculated residual stresses σ_{zz} that perfectly matched the reference map, as shown in Figure 4-14.

The averaged RMS error between the original and the back-calculated stress when all the in-plane displacements in addition to the out of plane displacements were taken into account during the back calculated step was found equal to 0.17 MPa, which is negligible.

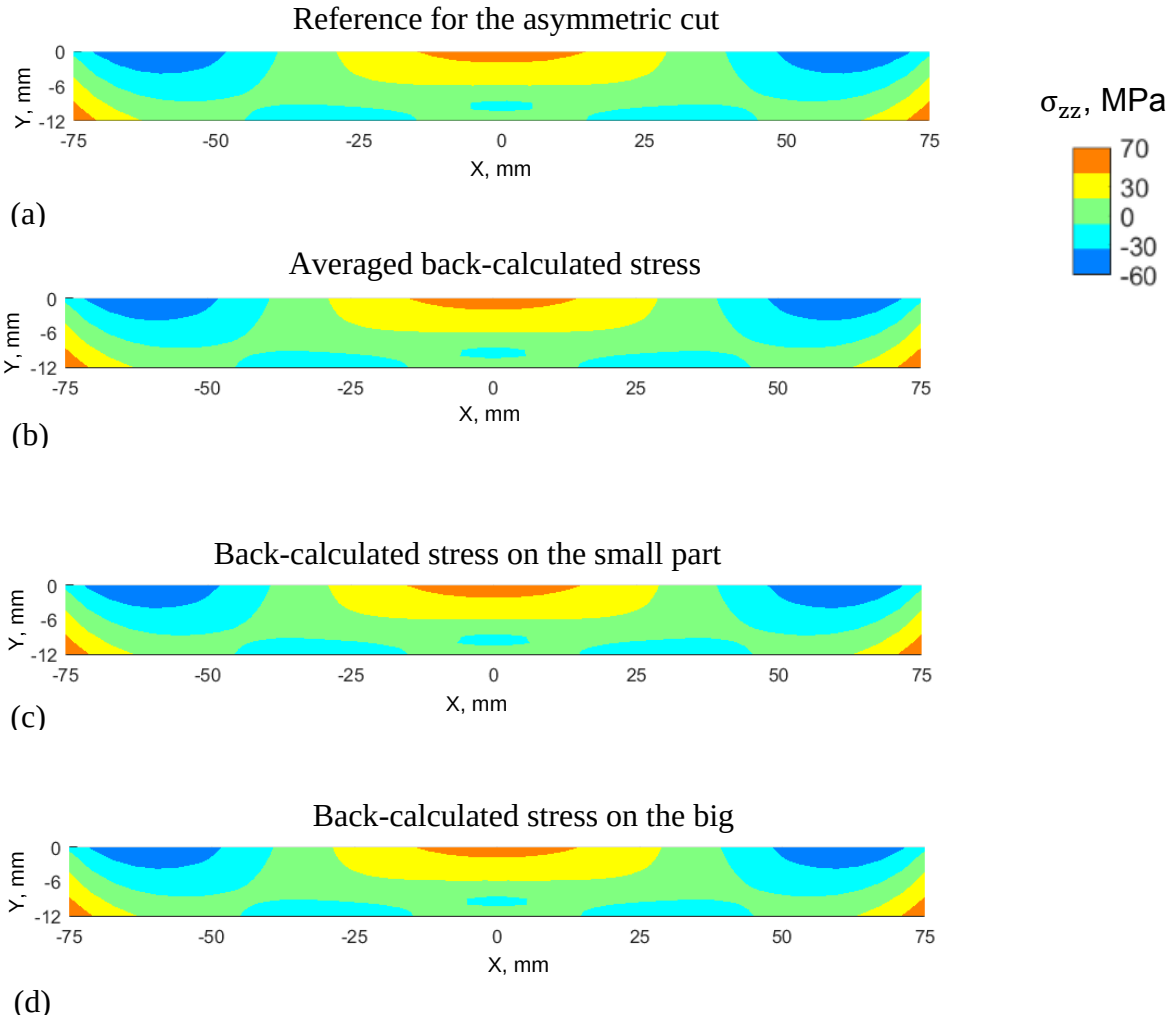

Figure 4-14 2D maps of reference (a), averaged back calculated (b), back calculated from the small (c) and big (d) parts after an asymmetric contour cut on the TG6 sample. The displacements in x, y and z directions were used during the back-calculation step.

4.4.2 In-plane displacements due to the effect of shear stress

In-plane displacements are defined as the displacements in the principal directions within the cut plane. On the contrary, out-of-plane displacements are defined as the displacements in the direction normal to the cut plane. The resulting in-plane displacements due to the presence of shear stress over the cut plane will be in opposite directions for the mating cut surfaces. In fact, when the shear stress is relaxed after cutting, the tearing forces should generate displacements on one cut surface that are in the opposite direction of the displacements generated on the mating cut surface. Thus all the nodes on the finite elements along one cut surface were tied to move in the opposite direction of the nodes on the finite elements along the mating cut surface during the back-calculation step. In the TG6 model, the cut is done in the plane normal to Z direction (see Figure 4-6). Therefore, the degrees of freedom of the nodes in X and Y direction along one cut surface were forced to be in the opposite direction with regards to their corresponding nodes in the mating cut surface.

A comparison of original and back-calculated residual stress maps when the mating nodes were tied to move in opposite in-plane directions (that is they have been forced to have anti-symmetric in-plane displacements) is shown in Figure 4-15. The average RMS error between the averaged back-calculated and the reference stress prior to the cut was found equal to 7.6 MPa which is 6.1% of the reference stress range. The resulting error in the back-calculated stresses is in fact higher than the earlier results. Hence the in-plane displacements due to the release of shear stress does not seem to have contributed to the observed error.

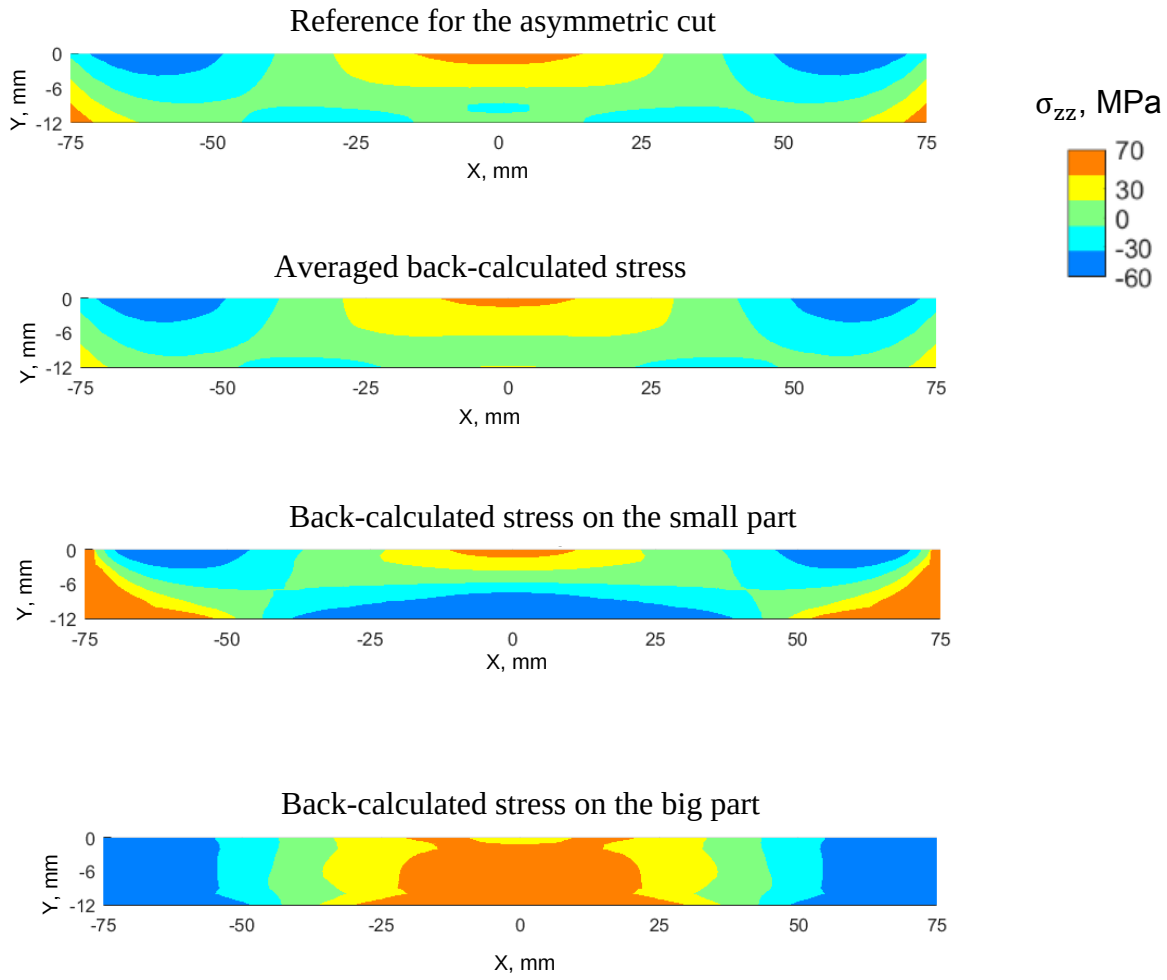

Figure 4-15 2D maps of reference (a), averaged back calculated (b), back calculated from the small (c) and big (d) parts after an asymmetric contour cut on the TG6 sample. The displacements in x, y and z directions were used during the back-calculation step. The motions of nodes on mating cut surfaces in the in-plane principal directions were constrained to be anti-symmetric.

4.4.3 Exploring Hooke's law

Another approach was to investigate Hooke's law and Equation 4-3 was used for a 2 dimensional case at a first stage.

$$\sigma_y = \frac{(1-\nu)E}{(1+\nu)(1-2\nu)}\left[\frac{\partial v}{\partial y} + \frac{\nu}{1-\nu}\frac{\partial u}{\partial x}\right] \quad \text{Equation 4-3}$$

Where E and ν are the Young's modulus and Poisson's ratio of the material, respectively.

The goal was to investigate Hooke's law in the contour method simulations for both symmetric and asymmetric cuts. The laser heated plates studied in the previous chapter gave a residual stress field that was asymmetric across cut planes. Thus the configurations studied effects of asymmetry with respect to geometry and stress field combined. Therefore, for the present study a new benchmark test specimen was designed, to simulate the contour method for cases dominated by symmetric and asymmetric geometry effects. The new design comprised a thin composite rectangular plate having a central band of material (see Figure 4-16a) having a different thermal expansion coefficient than the remainder of the model as detailed in [67]. The plate was heated from room temperature to 1000°C during a first step in Abaqus. Then an air cool down was simulated during a second analysis step by applying a temperature field equal to 20°C on the whole plate. Elastic-plastic material properties (Young modulus = 200 000 MPa, Poisson's ratio = 0.3 and yield strength = 400 MPa) were used during the residual stress generation step. Then the residual stress was mapped onto a new model having a similar geometry and mesh, but where only elastic material properties were defined. The contour cut location was fixed at 50 mm away from one edge of plates of different lengths representing for symmetric and asymmetric cases as shown in Figure 4-16. Then the displacements along the cut surfaces were extracted and the new data analysis approach dealing with asymmetric cuts was used to simulate measured residual stresses for both cases.

In the contour method only the out of plane displacements are measured. Therefore, the hypothesis was that the gradients of the in-plane displacements from both mating cut surfaces would correlate with the error between the reference and back calculated stresses for both symmetric and asymmetric cases

A comparison between the reference and the back-calculated stress along the cut line is shown in Figure 4-16b for both symmetric and asymmetric cases. Also the displacement gradients $\frac{\partial v}{\partial y}$ and $\frac{\partial u}{\partial x}$ are shown in Figure 4-16c. It is clear that for both the symmetric and asymmetric cases

the in-plane displacement gradients don't cancel out but there is still an excellent correlation between the reference and back-calculated stresses. No correlation was observed between the error in the contour method results and in-plane displacement gradients for both symmetric and asymmetric cases. Hence investigating Hooke's law doesn't seem to help to assess the effect of the in-plane displacement gradients. Moreover, in this approach the displacement gradients are investigated whereas in the contour method it is the displacements that are used.

Similar to the contour method simulations on the laser heated plates described in chapter 3, this supplementary study looking solely at geometric asymmetry with the proposed data analysis leads to correct back-calculated stresses for both symmetric and asymmetric contour cuts.

The initial hypothesis did not turn to be the main reason for not getting the correct back-calculated stress for the 3D case. In fact, for both symmetric and asymmetric cases, the in-planes displacement gradients did not cancel out when averaging stresses from both mating cut surfaces while an excellent correlation between the reference and back-calculated stresses was observed.

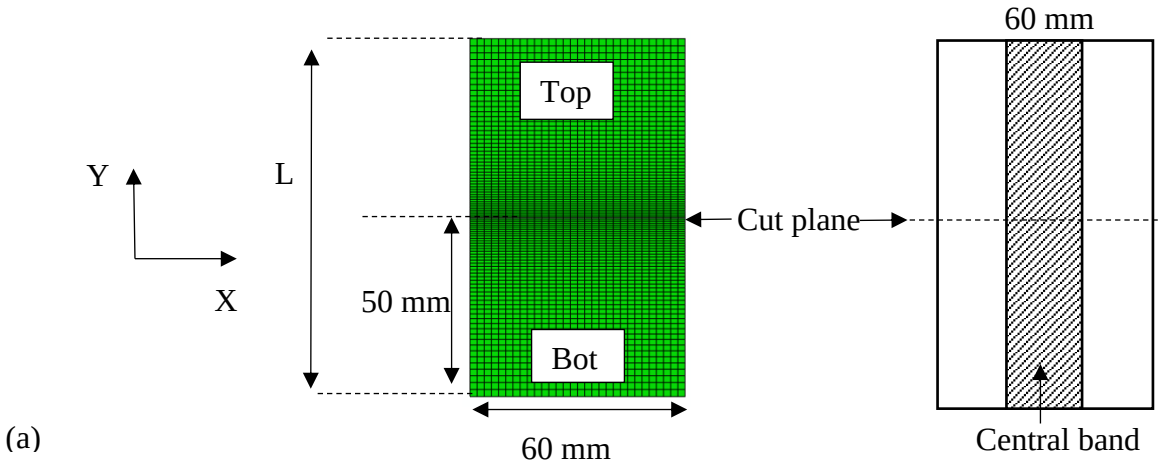

(a)

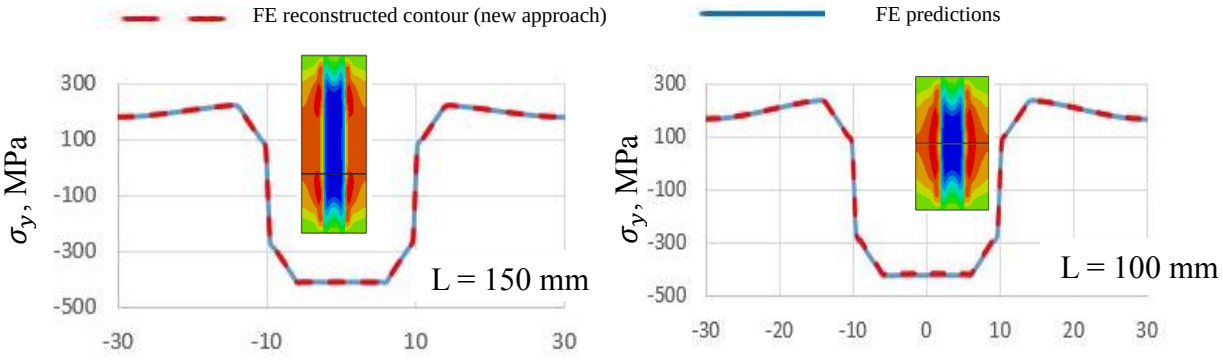

(b)

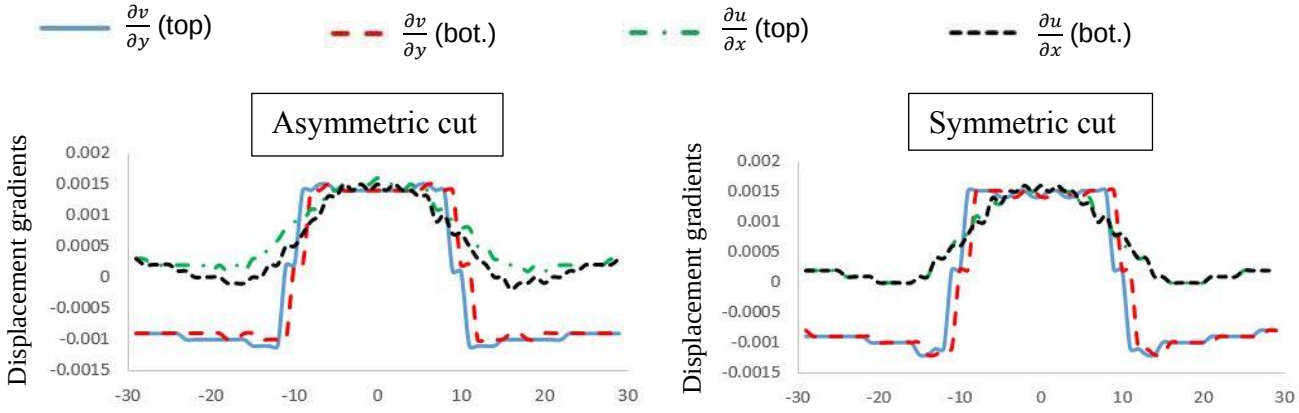

(c)

Figure 4-16 (a) Schematic drawing of the composite plate shown on the right. The FE mesh used for the FE modelling is shown on the left together with the location of the contour cut. (b) Comparison of the reconstructed contour stress with the original stress along the measurement line for asymmetric cut shown on the left and for the symmetric cut shown on the right. (c) Comparison of the displacement gradients $\frac{\partial v}{\partial y}$ and $\frac{\partial u}{\partial x}$ on both mating cut surfaces for the asymmetric cut shown on the right and for the symmetric cut shown on the left.

4.4.4 Conjecture about the effect of in-plane stress

In undertaking multiple contour measurement method simulations, it was noticed that errors arising in the contour method simulation appeared to be associated with the presence of high in-plane stress. This conjecture was investigated using a two dimensional problem for simplicity reasons, but can be extended to a three dimensional problem. Consider a plate having dimensions L × W and subject to traction forces in the x direction, T_x, as shown in Figure 4-17a. The extension of the plate in x direction is accompanied by a lateral strain component (Poisson contraction) [45] as shown in (Figure 4-17b).

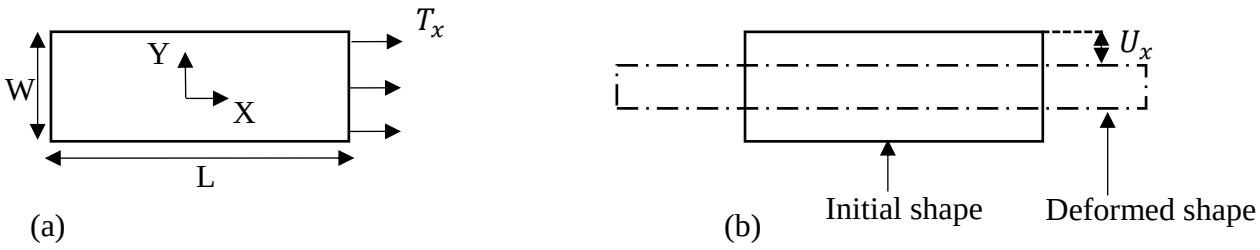

Figure 4-17 Illustration of a 2D L × W plate (a) subject to traction form in x direction T_x. (b) The extensions of the plate is accompanied by lateral strain component.

Stress in x direction is defined by Equation 4-4 [45].

$$\sigma_x = \frac{T_x}{A} \qquad \text{Equation 4-4}$$

Where A is a unit area.

If a contour cut along the x direction is introduced in the biaxial structure shown in Figure 4-17, the in-plane stress σ_x would be partially relaxed. Therefore the traction forces in the x direction T_x owing to the relaxation of in-plane stresses would generate out-of-plane displacements in the x direction U_x. This out-of-plane displacement may cause error in the contour method results because it can combine with the out-of-plane displacement caused by the relaxation of the out-of-plane stress σ_y.

A pilot study using a 2D FE model was done to investigate the effect of the in-plane stress on the conventional contour method. Two cases were explored, one where in-plane stress is negligible and one where in-plane stress is considerable with regards to the out-of-plane stress. In both cases the shear stress was negligible. A (50 x 20) mm plate was designed and an Abaqus [101] model created in order to introduce symmetric stress fields having different levels of in-plane stress for simulation of symmetric planar contour cuts. Elastic material properties were used including a Young modulus equal to 200 000 MPa and a Poisson ratio equal to 0.3. To prevent rigid body motion, displacements were constrained in X direction in both corners of the right edge of the plate and in Y direction at the bottom left edge (see Figure 4-18). The plate was meshed using 19 900 4-node bilinear plane stress quadrilateral with reduced integration and hourglass control. The mesh size was 0.1 mm in the whole plate. The residual stress field was generated by defining analytical expressions and using the subroutine SIGINI in Abaqus as detailed later. The cut was done by removing instantaneously all elements along the cut line (see Figure 4-18). Then the conventional contour method data analysis [35] was implemented. This involves averaging the out-of-plane deformations due to the cut on each node on the cut face with the corresponding nodes on the mating cut face. Then the negative of the averaged contour displacements is applied as displacement boundary conditions on a new stress free model of one half of the plate.

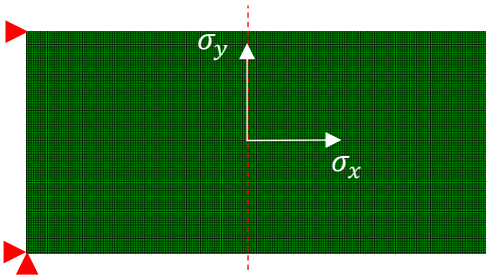

Figure 4-18 View of the mesh, boundary conditions and cut line on the plate.

Case 1: only out-of-plane stress is retained along the cut location with no in-plane and no shear stress.

The aim was to generate a residual stress field where only the out-of-plane component σ_x is retained along the cut location in the plate without in-plane σ_y and shear σ_{xy} components. This was done using a trial and error method and the subroutine SIGINI in Abaqus. Various analytical expressions were explored and used to generate a residual stress distribution in the plate. This process was iterated until a suitable residual stress distribution was obtained along the cut line. This was obtained using Equation 4-5.

$$\sigma_x = -200\cos(1.5y) \qquad \text{Equation 4-5}$$

The 2D residual stress map of the plate where the stress range of the components σ_y is negligible in comparison with the one for σ_x and where there is no shear stress σ_{xy} along the cut line is shown in Figure 4-19a. Residual stress line profiles of the components σ_x, σ_y and σ_{xy} acting along the cut line on this plate are shown in Figure 4-19b.

Case 2: both out-of-plane and in-plane stresses are retained and no shear stress is retained along the cut location.

A similar approach to the previous case was used to obtain a residual stress field on the plate where both residuals stress components σ_x and σ_y have a comparable magnitude along the cut line with no shear stress. The residual stress field for this case was generated on the plate using Equation 4-6 and Equation 4-7.

$$\sigma_x = -500\cos(y) \qquad \text{Equation 4-6}$$

$$\sigma_y = 500\cos(x) \qquad \text{Equation 4-7}$$

A comparison between the reference and back calculated stresses for both cases is shown in Figure 4-20. The stress line profiles are compared in Figure 4-20a, a zoom is shown in the location of the maximum error in Figure 4-20b and line profiles of the difference between the reference and back calculated stresses is shown in Figure 4-20c.

For case 1, where the in-plane stress σ_x range is negligible with regards to the out-of –plane σ_y stress range, the maximum difference between the original and back calculated stress was found equal to 0.3 MPa at x = -0.05 mm. This maximum difference represents 0.09 % of the reference stress at that location, which is negligible.

For case 2, where the in-plane stress σ_x range is similar to the out-of-plane σ_y stress range, the maximum difference between the original and back calculated stress was found equal to 7 MPa at x = -2.5 mm. This maximum difference represents 8.3% of the reference stress at that location, which is not negligible.

For both cases, no shear stress was acting along the cut line and the conventional data analysis approach was used to back calculate the stress. Hence the error cannot be caused by shear stress. Moreover, only elastic material properties were used during the contour method simulation so the error cannot be caused by plasticity.

Also the range and profile of the out-of-plane stress along the cut for case 1 was similar to the one of case 2. The only difference between case 1 and case 2 was the presence of in-plane stress along the cut line. Therefore, it is believed that the in-plane stress contributed to the observed error during the contour method simulation.

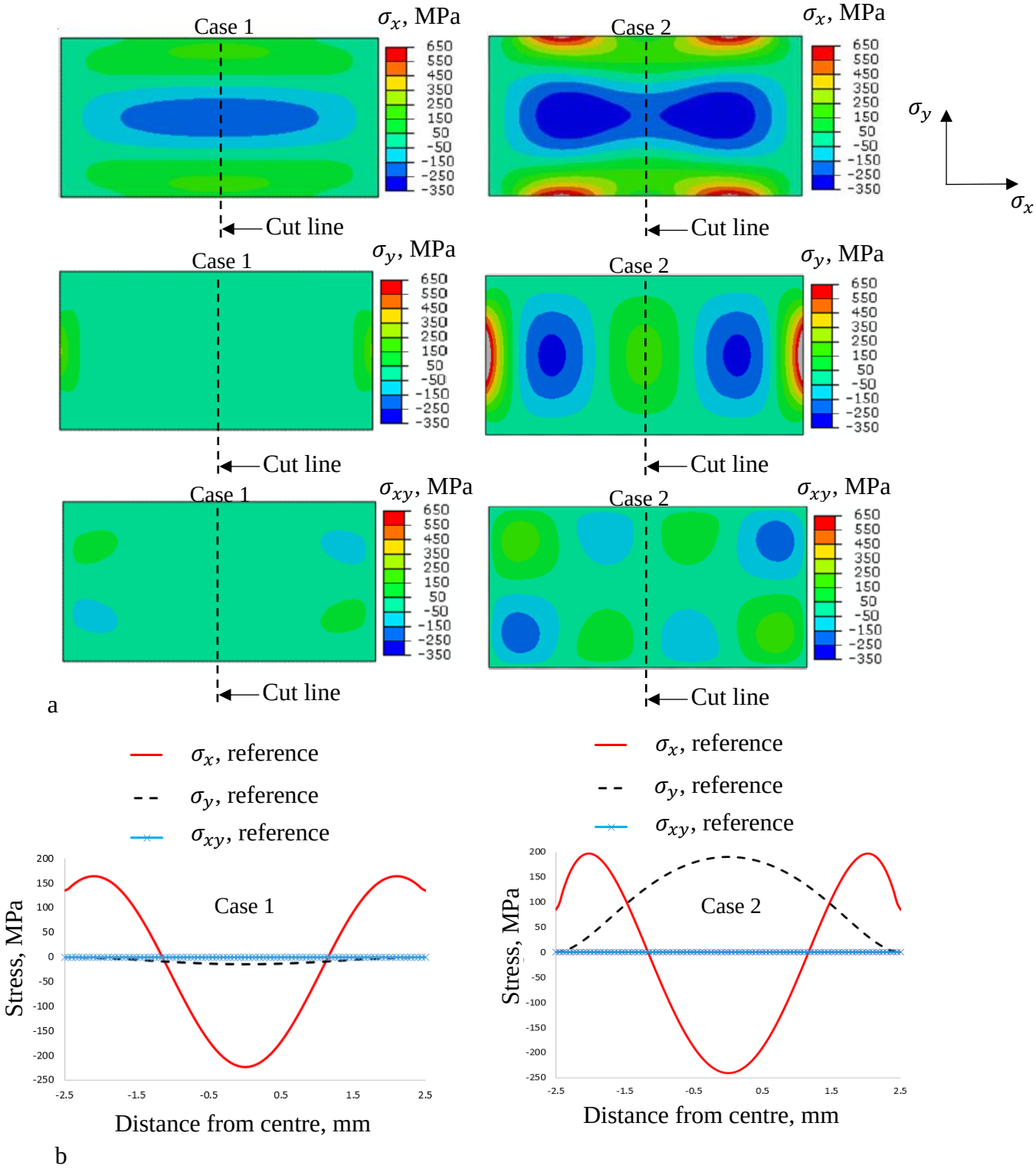

Figure 4-19 (a) 2D maps of residual stress in one sample 'Case 1' where out of plane, in-plane and no shear stress are acting along the cut line and another sample 'Case 2' where only out-of-plane stress is acting and (b) line profile distribution along cut line.

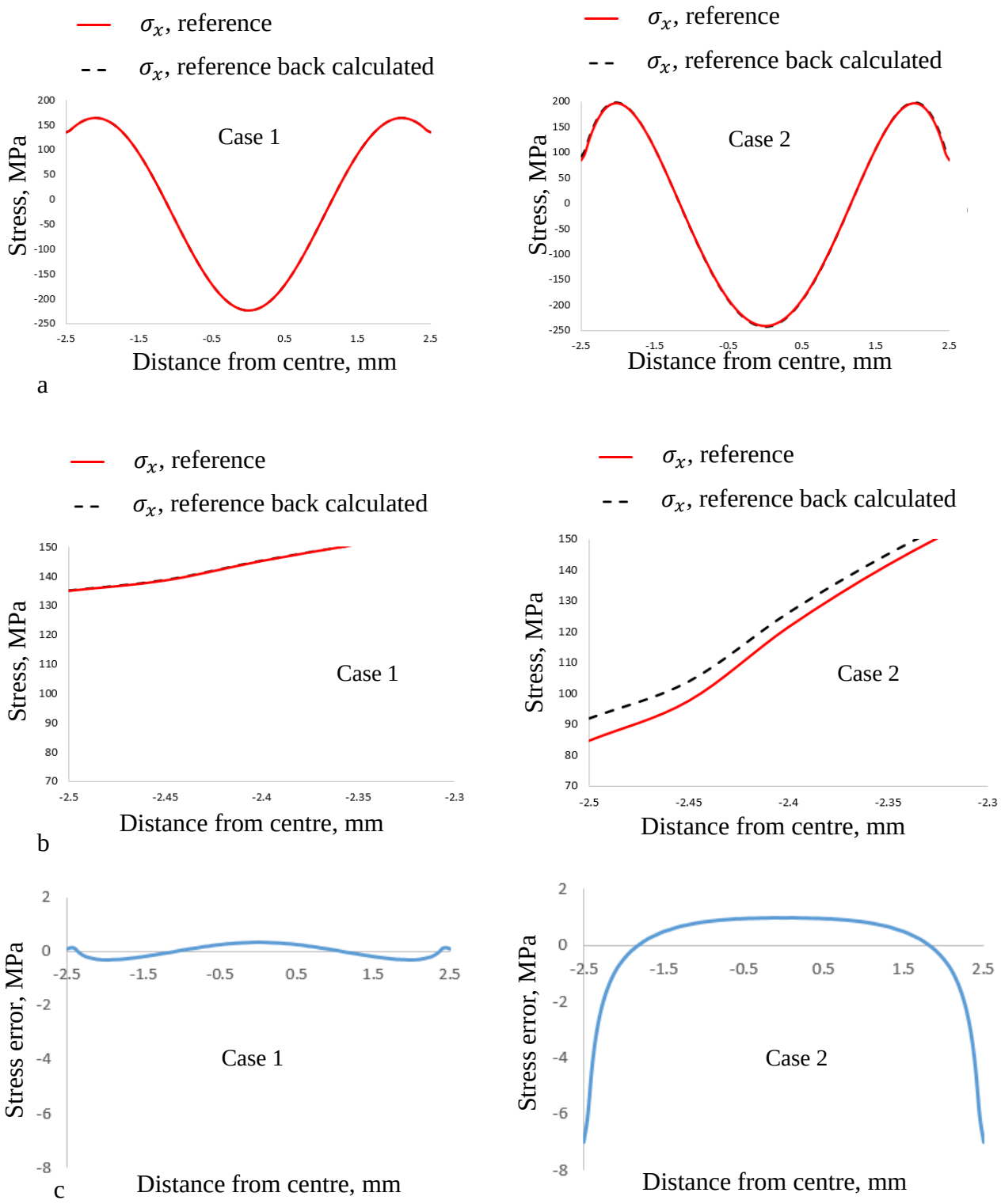

Figure 4-20 (a) Comparison of reference and back-calculated stresses using the conventional contour method in one sample 'Case 1' where out of plane, in-plane and no shear stress are acting along the cut line and another sample 'Case 2' where only out-of-plane stress is acting, (b) zoom view and (c) line profiles of the errors along the cut lines.

4.5 Conclusion

A 3D contour method residual stress measurement simulation for the NeT TG6 welded benchmark test specimen has been undertaken using an asymmetric cut. But the error in simulated measured stress was higher than expected with clear differences evident between the original and back-calculated stress. These results contrast with the 2D asymmetric benchmark simulations presented in chapter 3 where negligible errors were found. The error in the 3D model cannot be attributed to plasticity, because an instantaneous cut was modelled with elastic material properties. Various approaches were investigated to explore potential contributing factors leading to the observed error.

The relaxation displacements of the cut surfaces due to the release of shear stress are anti-symmetric in nature relative to the cut plane. A back calculation sensitivity study was performed where corresponding nodes on the mating cut surfaces were tied together to move in the opposite direction relative to each other but this led to a greater discrepancy between the simulated measurement and the original stress field. Hooke's law for a 2D case was explored to investigate the effect of in-plane displacement gradients on the back-calculated stresses but this confirmed the findings of chapter 3 for 2D asymmetric cut cases. However, when both the in-plane and out-of-plane displacements were used to back-calculate residual stress for an asymmetric cut the error between the original and back-calculated stresses was negligible. Whilst this approach can be implemented for in a numerical study, only the out of plane displacements can be measured accurately at present in practical contour method measurements.

Wide ranging studies were conducted to investigate reasons for the error in the 3D case. It is conjectured that the level of in-plane stresses present in body may influence the out of plane displacement, and this could cause the observed error. Several FE studies conducted by the author (but not detailed here) suggest that this might be the case. But if true this would undermine the validity of the contour method.

The significance of in-plane stress in measurement area needs to be further assessed. The conjecture about the effect of in-plane stress in measurement area for the contour method was a result of early observations and were evidenced in a pilot study. However, theoretical considerations and experimental protocols need to be defined to validate the proposed conjecture. A main challenge would be to generate a residual stress field suitable for each case study. For example, in order to isolate the effect of in-plane stress two case studies can be defined. In one case, only out of plane stress would be acting along the measurement plane,

while in the other case, both in-plane and out of plane stress would be acting along the measurement plane. Also, in both cases no shear stress should be acting along the measurement plane. Moreover, the pilot study was done using 2D finite element models for simplicity reasons. However, 3D models would capture better the effect of the in-plane stress in measurement area for the contour method. In fact, in a 3D case more stress components can potentially contribute to the effect of in-plane stress in the contour method. This is a topic for future work as discussed at the end of chapter 6.

Chapter 5: the incremental contour method for residual stress measurement

5.1 Introduction

Development of plasticity during a contour cut can introduce residual stress measurement error that limits the application and reliability of the technique as detailed in the Literature review (chapter 2). A new approach aimed at mitigating plastic deformation in such measurements is proposed in this chapter. This novel approach aims to relax incrementally and elastically the residual stress at a location of interest until the stress magnitude is lower than a target threshold such that plastic deformation will not occur during the contour cut, thereby avoiding introduction of plasticity error in the measured stress results. The incremental relaxation is done by using successive asymmetric cuts and applying the principle of superposition to determine the residual stress at the plane of interest prior to cutting. Hence the new approach, termed the 'incremental Contour Method' (iCM), relies on using the asymmetric contour cut data analysis approach presented in chapter 3, but may be limited by the observations noted in chapter 4.

In this chapter, theoretical considerations related to the iCM are first explored. Then numerical simulation of the iCM is conducted to demonstrate the accuracy of the approach. Finally, iCM simulations are compared with iCM measurements conducted on a benchmark test specimen on which neutron diffraction residual stress measurements were performed prior to contour cutting.

5.2 Theoretical considerations

The proposed incremental contour method involves conducting three main steps. Each step is detailed below following the overview set out in this paragraph. First, the die-away length of the self-equilibrated residual stress field acting normal to the plane of interest in the component needs to be estimated. This stress die-away length can then be used to estimate the reduction of stress in the body at potential incremental cut locations. A series of incremental cuts may have to be undertaken to ensure that no plasticity is introduced during each cut. The proposed approach for dealing with asymmetric contour cut data must be performed to assess the 2D map of stresses at the location of each cut. Finally, the multiple cut approach is used to take into account the relaxation caused by each cut on the location of the following cut and on the final location of interest.

5.2.1 Estimation of the stress die away length scale

Consider an idealized sinusoidal stress profile on a body that has a characteristic wave length I_y (see $\sigma_z^{orig}(y)$ in Figure 5-1a). The stress field will redistribute after extracting a block of dimensions y_0 and z_0. The remaining stress in the block can be estimated by applying the negative of the idealized sinusoidal stress profile at the edge of a stress free body having the same dimensions y_0 and z_0 as the extracted block [15]. The stress will die away from the edge toward the inside of the block (see $\sigma_z^{appl}(y,z)$ in Figure 5-1b). Hence the die away length of the sinusoidal stress can be estimated by calculating the distance over which the stress decays to zero. The decay profile for the stress field can be estimated from the following equation for a 2D case.

$$\sigma_z(z) = \left[1 - \left(\frac{2\pi z}{l_y} + 1\right) e^{\frac{-2\pi z}{l_y}}\right] A \cos\frac{2\pi x}{l_y} \qquad \text{Equation 5-1}$$

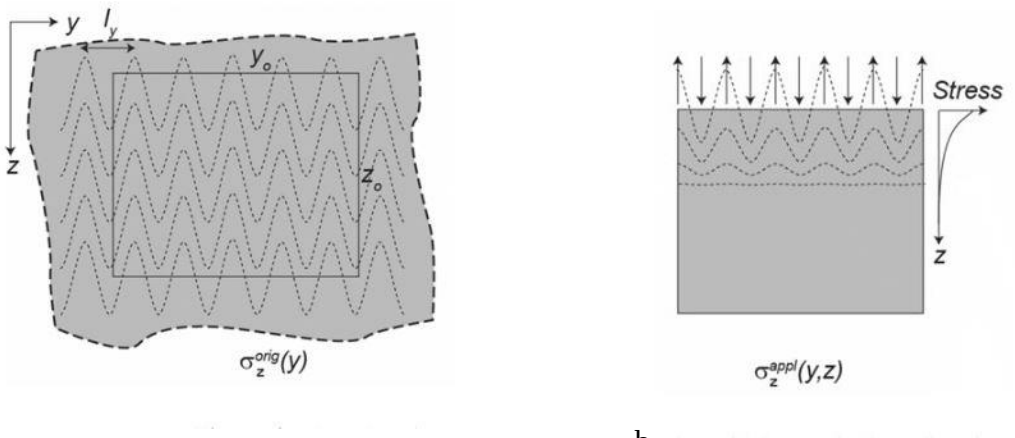

a b

Figure 5-1 Large body containing an idealized sinusoidal distribution σ_z^{orig}, from which a block of dimensions $y_0 \times z_0$ is extracted. The residual stress die-away length scale can be estimated by solving for a negative σ_z^{appl} traction applied to the edge of a stress free block of the same dimensions and the residual stress profile in the extracted block determined by adding the edge loaded block stress field to large body stress field. Adapted from [15].

The analytical solution can be reproduced for the idealised case using FE analysis and applied to more general cases (see Figure 5-2). However, it requires pre-knowledge of the original residual stress field. The original residual stress profile for which the die away length needs to be determined can be estimated in different ways. It can be extracted from an FE simulation of the residual stress field in the body for example. When the residual stress field is unknown and cannot be accurately predicted, the yield strength of the material can be used to estimate a self-balanced residual stress profile along the location of interest. Then the negative of the original stress profile can be applied to the edge of a stress free FE model having the same dimensions as the section where the die away stress profile needs to be determined. Hence the die away length can be estimated and when the decay profile is added to the original profile along the line of interest within the body, the stress drop as a function of distance from the line of interest can be estimated.

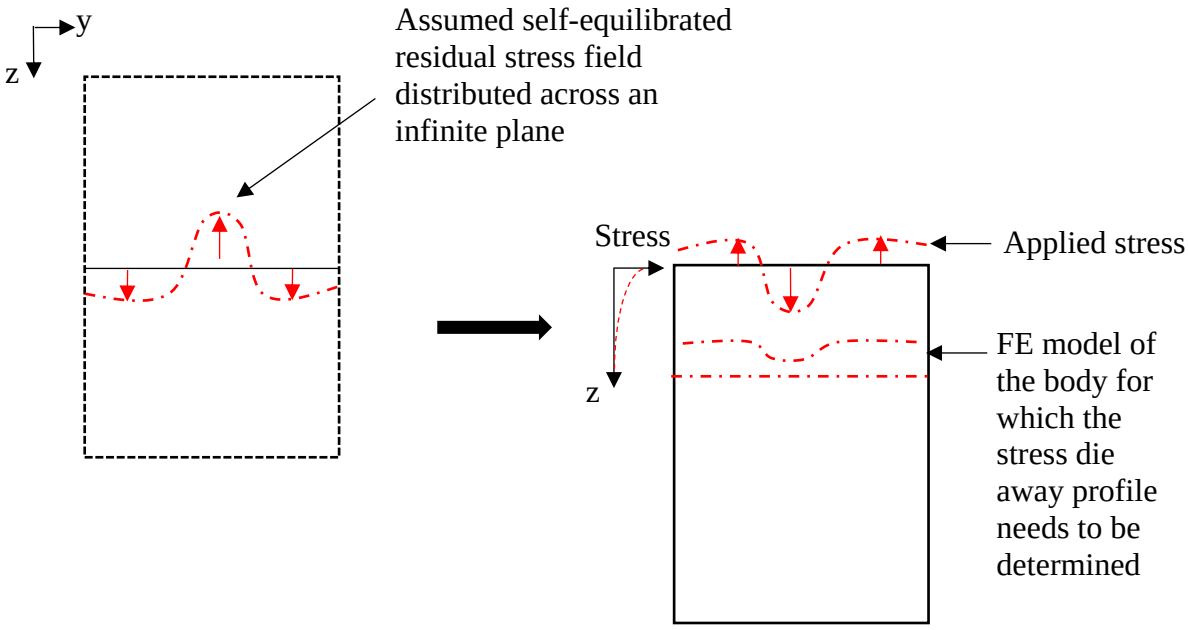

Figure 5-2 Generalisation of the approach to estimate the residual stress die away length and decay profile. An idealized residual stress profile of material yield strength magnitude is assumed to be present throughout an infinite body. Then the negative of the stress profile is applied at the edge of a stress-free FE model of the body where the stress die away length scale and decay profile needs to be determined. This is then superposed on the infinite body stress field to determine the residual stress decay profile approaching the free edge.

5.2.2 Contour cut for the incremental contour method

Once the die away length scale of residual stress at the location of interest is estimated then the number and locations of the incremental cuts can be assessed. The incremental cuts aim to partially relax the residual stress at the location of interest as discussed in the introduction section of this chapter. The threshold of the stress magnitude value to prevent plasticity error in the contour results can be, for example, 50% of the yield strength of the material. The incremental contour method can involve a series of successive cuts that incrementally relax the stresses elastically at the location of the main cut. Using the die away decay profile the distance from the location of interest over which the stress magnitude drops by 50% or (or other percentage) can be estimated. This distance gives the location of the next contour cut. This process can be repeated increasing the number of incremental cuts until the remaining stress magnitude on the location of the main contour cut is lower than the target threshold ensuring elastic relaxation of stress for a contour method measurement at the chosen location of interest.

Once the locations and number of incremental contour cut are defined, the contour cuts can be done. Incremental cuts can sequentially be done until the main cut as shown in Figure 5-3.

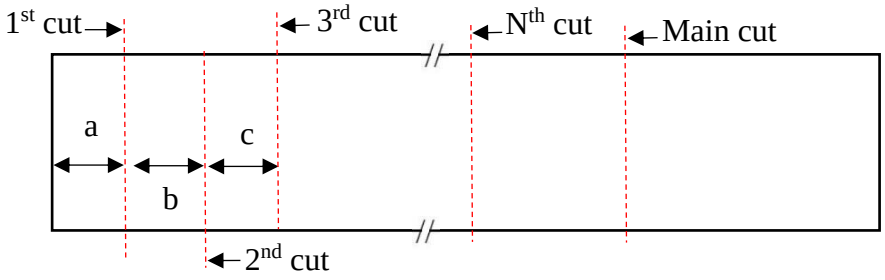

Figure 5-3 Illustration of the incremental contour method where a sequence of intermediate cuts is done before the main cut.

It is worth noting that only the back-calculated stress for the first cut gives the original stress distribution directly. The measured stresses for the second cut and beyond give the remaining stresses following the previous cuts. Hence the effect of stress relaxation due to each cut should be taken into account by implementing the multiple cut approach [93].

5.3 Simulation of the conventional contour for TG6

The conventional contour method has been previously applied to simulate the measurement of longitudinal residual stresses at the mid-length plane of the TG6 plate in chapter 4 section 4.2, that is using a geometric symmetric cut (see Figure 5-4a). Following the approach discussed in chapter 4 (section 4.1) the predicted residual stress field for the TG6 model of Muransky [46] was mapped onto a new FE model where the mesh was refined along the intended incremental cut planes. The aim here was to have the exact same mesh for both a conventional and an incremental contour method measurement simulation. During the mapping step the displacements were constrained in xyz and z direction on the bottom corners of the face of the plate (see Figure 5-4b) and the xz directions at one top corner of the same face (see Figure 5-4b).

The cut was simulated by incrementally removing lines of elements through thickness along the cut path. The cut width modelled was 0.3 mm and elastic-plastic material properties [112] were used.

During the last increment of the cut simulation, additional boundary conditions were applied by mirroring the constraints of the front corners to corners of the opposite face to prevent rigid body motion.

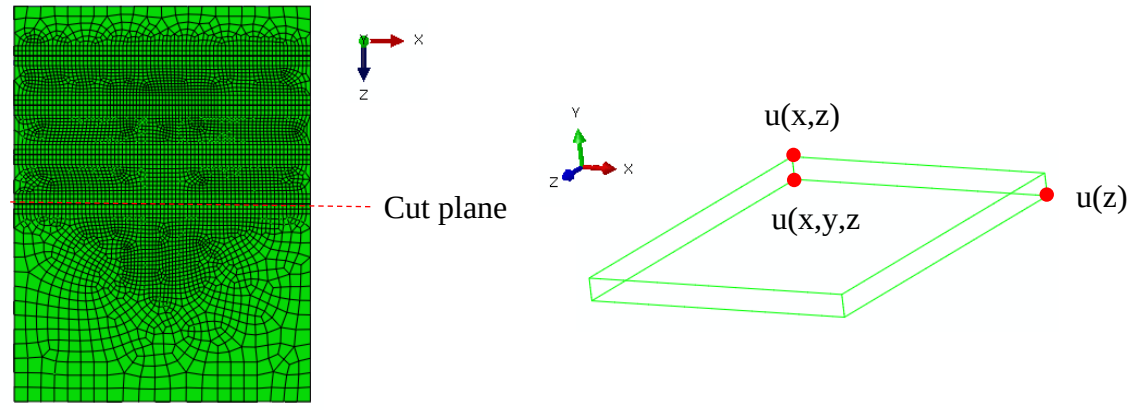

(a) (b)

Figure 5-4 (a) The FE model of the TG6 benchmark plate used for the conventional contour method measurement simulation showing the location of the contour cut, (b) isometric view of the 3D model showing the boundary conditions used during the simulation.

The equivalent plastic strain after the equilibrium step and prior to cutting was subtracted from the PEEQ after the cut was completed in order to subtract the welding induced plasticity. The plasticity on the top surface of the plate generated during the cutting step is shown in Figure 5-5.

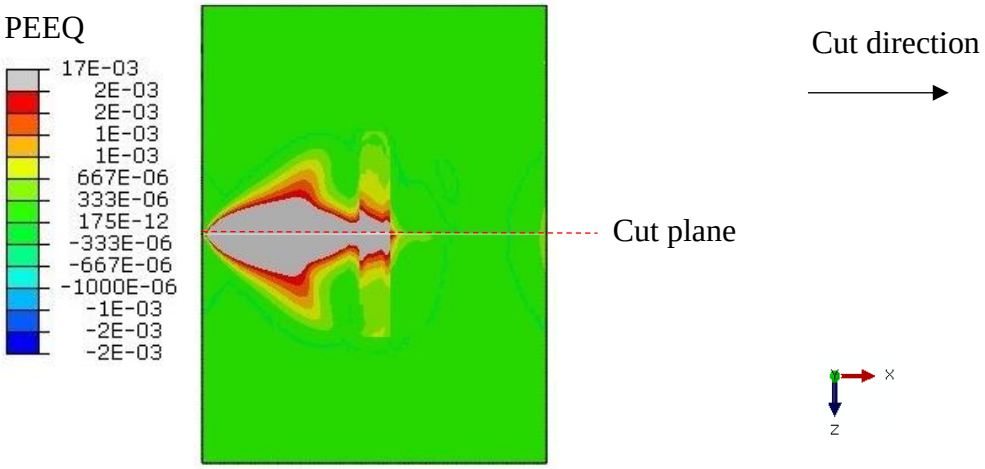

Figure 5-5 View of the equivalent plastic strain generated by the simulation of a contour cut at mid-length of the TG6 plate.

The reference (prior to cut) and back-calculated stress maps are shown in Figure 5-6. The difference between both stress maps is believed to be due mainly to plasticity effect.

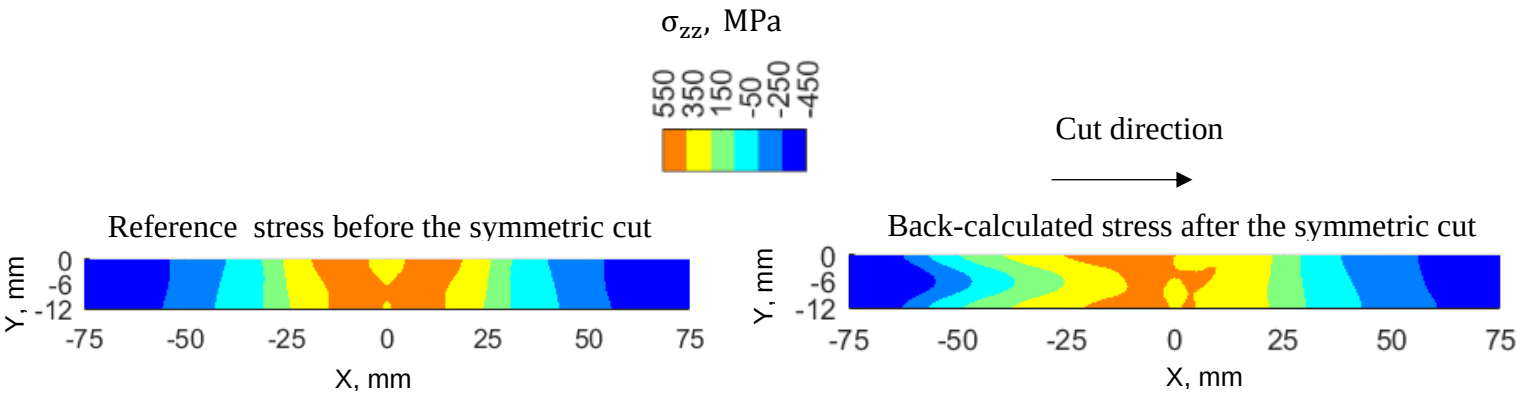

Figure 5-6 Comparison between the 2D maps of the reference and back-calculated stresses on a section at mid-length of the TG6 specimen using the conventional contour method.

The cutting induced plasticity on the cut surface is shown in Figure 5-7.

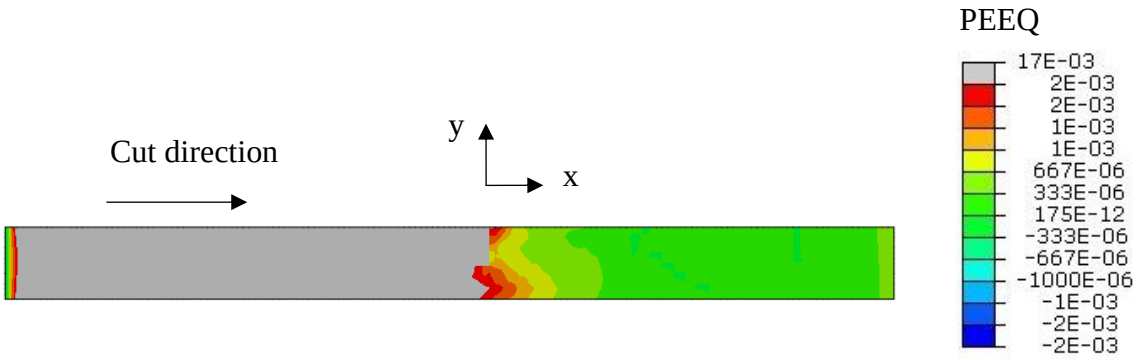

Figure 5-7 View of the equivalent plastic strain (PEEQ) on the cut surface.

The maximum equivalent plastic strain (PEEQ) was found to be 1.7%. However plasticity was observed through all the thickness of the cut surface as shown in Figure 5-7. Moreover, the RMS error between the reference and original stress field maps across the cut surface was 353 MPa, and the normalized (using the range of the reference stress) RMS error was 36.4 %. The error is large and considered to be due to the high plasticity generated during cutting. This simulation implies that no meaningful residual stress measurement can be made for this benchmark component using the conventional contour method. The question remains as to whether the incremental contour method can be implemented to mitigate plasticity errors and thereby improve the accuracy of the residual stress measurement results.

5.4 Incremental contour method simulation on TG6 sample

The TG6 benchmark specimen, presented in chapter 4, was used to evaluate application of the incremental contour method using the residual stress simulation results of Muransky [46].

5.4.1 Estimation of the cut locations

The cut planes were chosen at locations where predicted stress magnitudes were lower than the yield stress of the material, thereby reducing the risk of plasticity induced error [67]. The die

away length scale was used to estimate the amount of relaxed stress and identify the candidate location of interest for the next cut. A compromise was made between the number of cuts, amount of relaxed stress at the location of interest after each cut and the minimum width of each cut part to ensure that secure clamping during cutting could be achieved. A total of three asymmetric cuts were finally chosen prior to the 4^{th} cut at the plane of interest (i.e. mid-length of the welded plate).

The contour method simulations for each asymmetric cut are detailed below. Also, the superposition of the back calculated stress and the relaxed stress from previous cuts is shown for each intermediate measurement plane during the incremental contour method simulation.

5.4.2 Contour method simulation using asymmetric cuts

The non-linear contour simulations on the TG6 plate were done using the same approach and material properties as detailed in chapter 4. Blunt cuts were simulated by removing 0.3 mm width elements along the cut lines (see Figure 5-8a). 36085 8-node linear bricks with reduced integration and hourglass control (C3D8R in Abaqus) elements were used for meshing, and the size was refined to 2 mm along the cut planes in the cut direction. 7 elements were used through the thickness of the plate which was 12 mm.

The boundary conditions were used only to stop rigid body motion. For each cut, the displacements were constrained at three corners of the top edge of the plate in z, xz and xyz directions as shown in Figure 5-8b. Moreover, when cutting the last ligament for each cut plane, the boundary conditions were mirrored to the opposite edge to prevent rigid body motion when the two cut parts are separated.

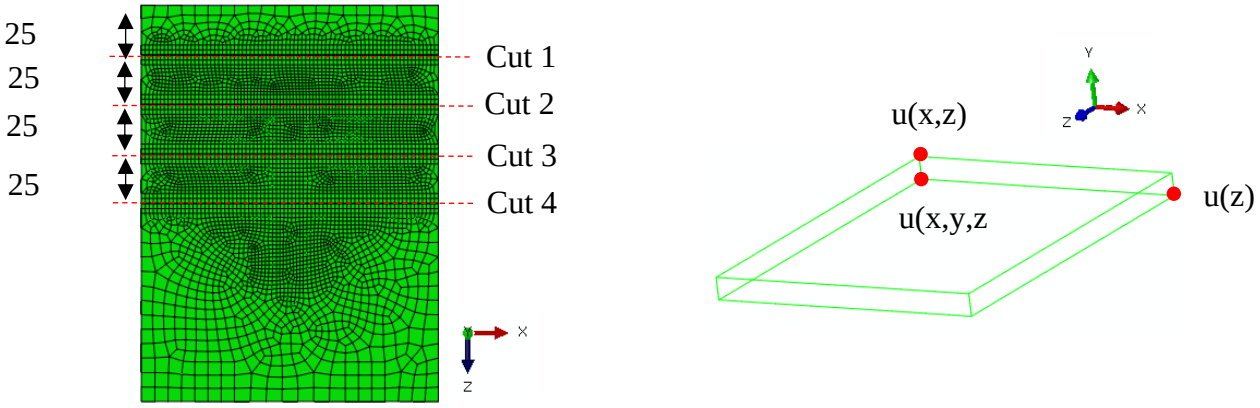

(a) (b)

Figure 5-8 (a) XZ view of the FE model of the TG6 used for the simulation of the iCM showing the mesh and location of contour cuts, (b) isometric view of the 3D model showing the BC used during the iCM simulation.

The map of initial state of residual stress predicted due to welding is shown in Figure 5-9.

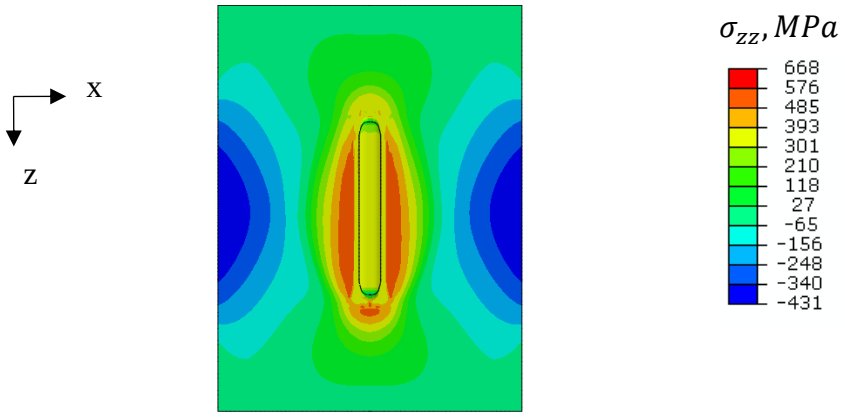

Figure 5-9 Map of initial state of residual stress predicted due to welding on the TG6 plate [114].

The plastic strain (PEEQ in Abaqus) accumulated as a result of the cutting process for each cut (see Figure 5-10) was calculated by subtracting the plastic strain from the welding process before the cut from the plastic strain after each cut. The maximum plastic strain was found for the cut 2 and was equal to 1.5%. However, the plastic strain was observed in an area smaller than the one for the symmetric cut presented in section 5.3. Therefore, the plastic strain level was deemed acceptable. A material yield strength equal to 437 MPa [112] was used.

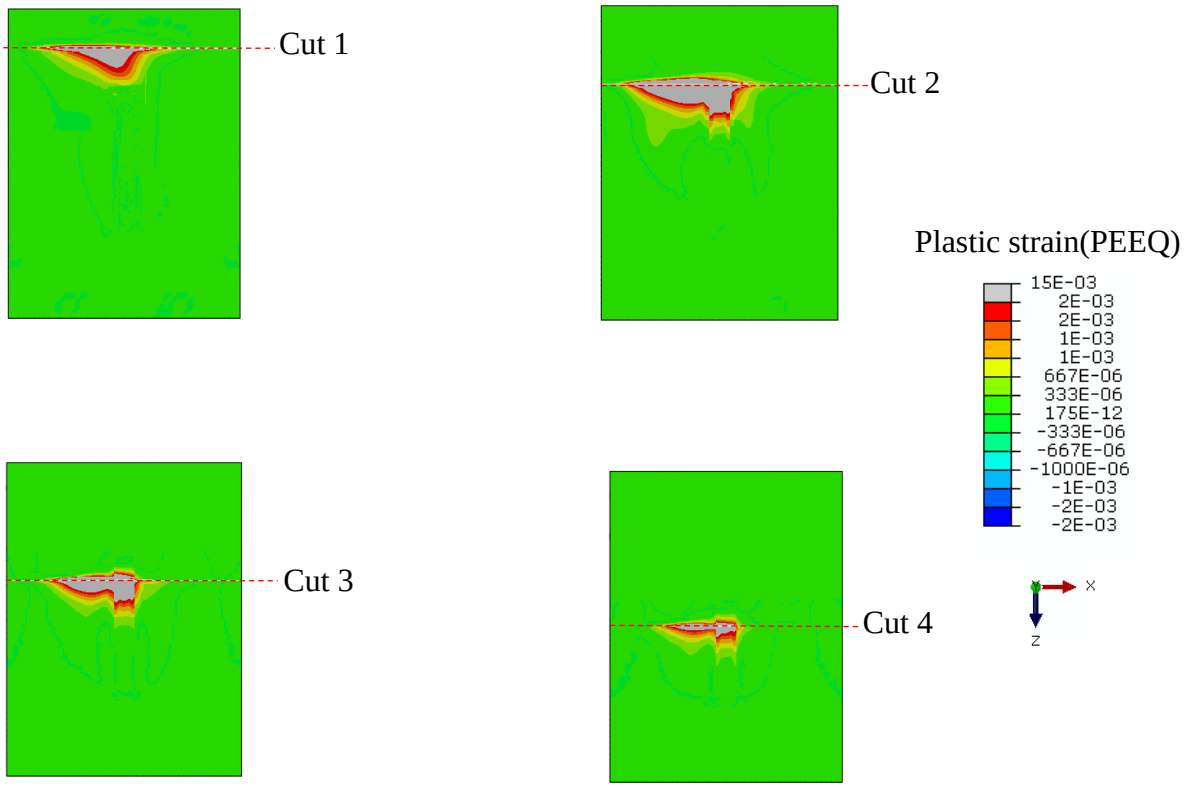

Figure 5-10 Map of the plastic strain (PEEQ) accumulated during the cutting process for each iCM cut of the TG6 sample.

Prior to the multiple cut superposition analysis for each incremental contour cut, the new data analysis approach for asymmetric cuts was applied. The back-calculated stresses for each contour cut are compared with the corresponding predicted stresses. For cut 1 it is actually the reference stresses but for cut 2 the back-calculated stresses are compared with the remaining stresses predicted at the location of cut 2 after cut 1 is completed. The same procedure was repeated for the following cuts. For cut 3 the back-calculated stresses are compared with the remaining stresses predicted at the location of cut 3 after cut 2 is completed. For cut 4 the back-calculated stresses are compared with the remaining stresses predicted at the location of cut 4 after cut 3 is completed.

The predicted reference and back-calculated stress maps for the first asymmetric contour cut are shown in Figure 5-11.

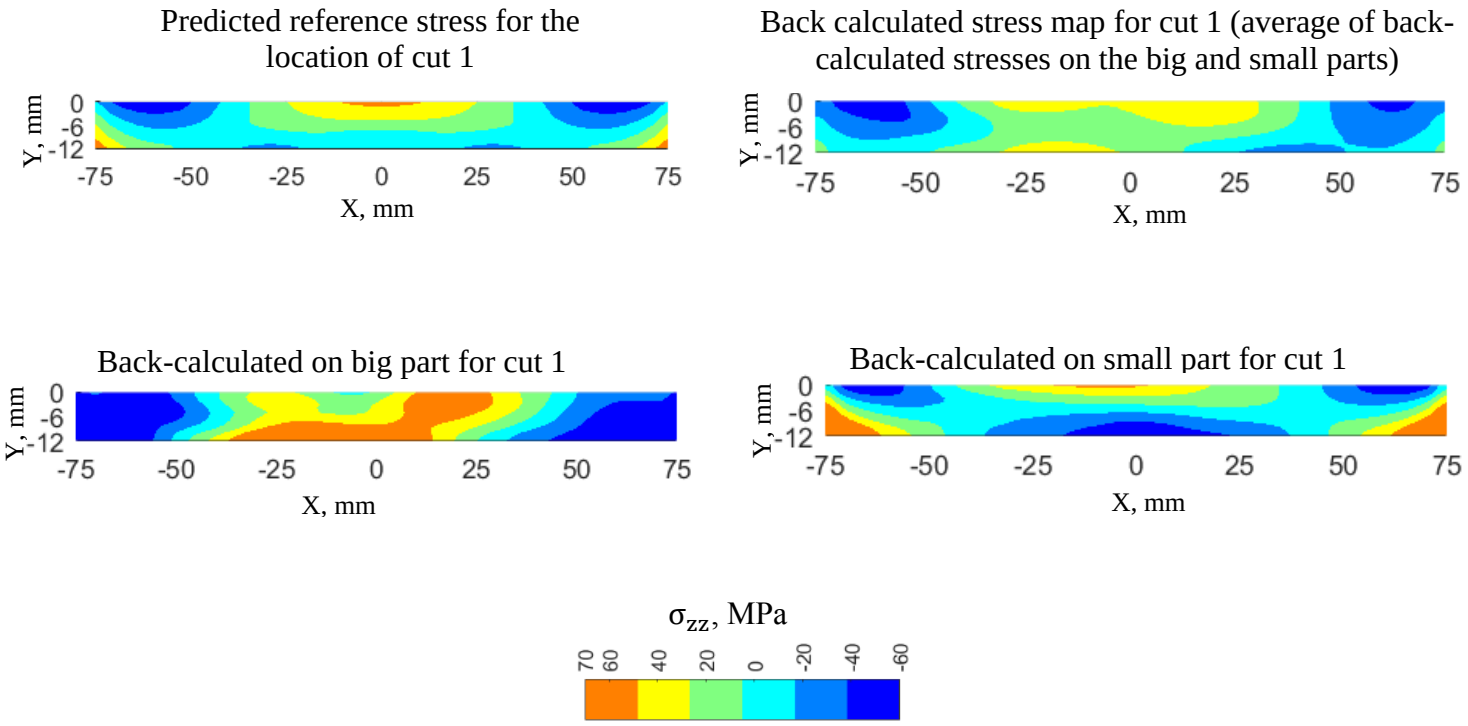

Figure 5-11 Predicted reference and back-calculated stress maps for the asymmetric contour cut 1 using contour method simulation for the TG6 benchmark sample.

The predicted remaining stress map on the location of cut 2 after cut 1 is performed and the back-calculated stress maps for the second asymmetric contour cut are shown in Figure 5-12.

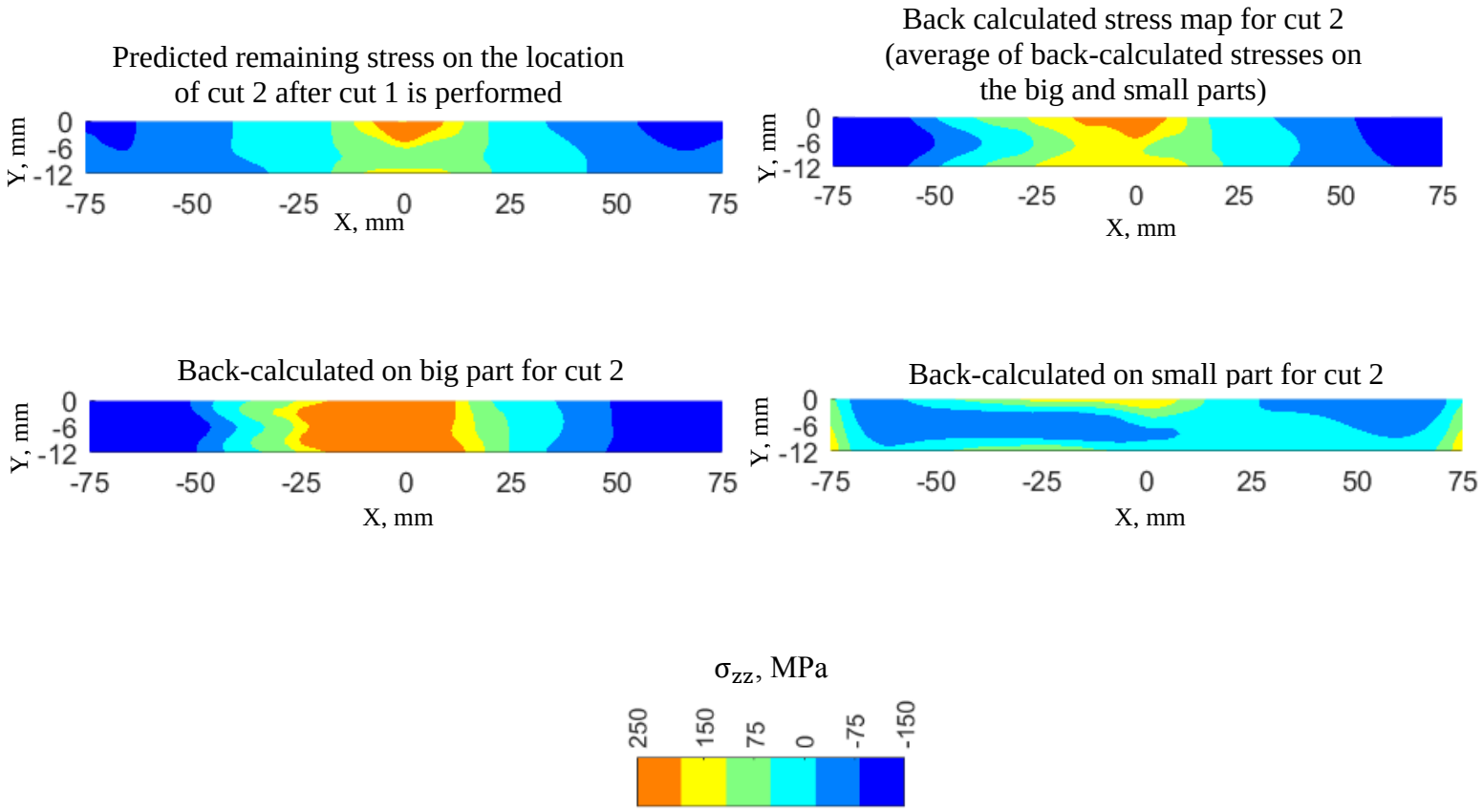

Figure 5-12 Predicted remaining and back-calculated stress maps for the second asymmetric contour cut using contour method simulation on TG6 sample.

The predicted remaining stress map on the location of cut 3 after cut 2 is performed and the back-calculated stress maps for the third asymmetric contour cut are shown in Figure 5-13.

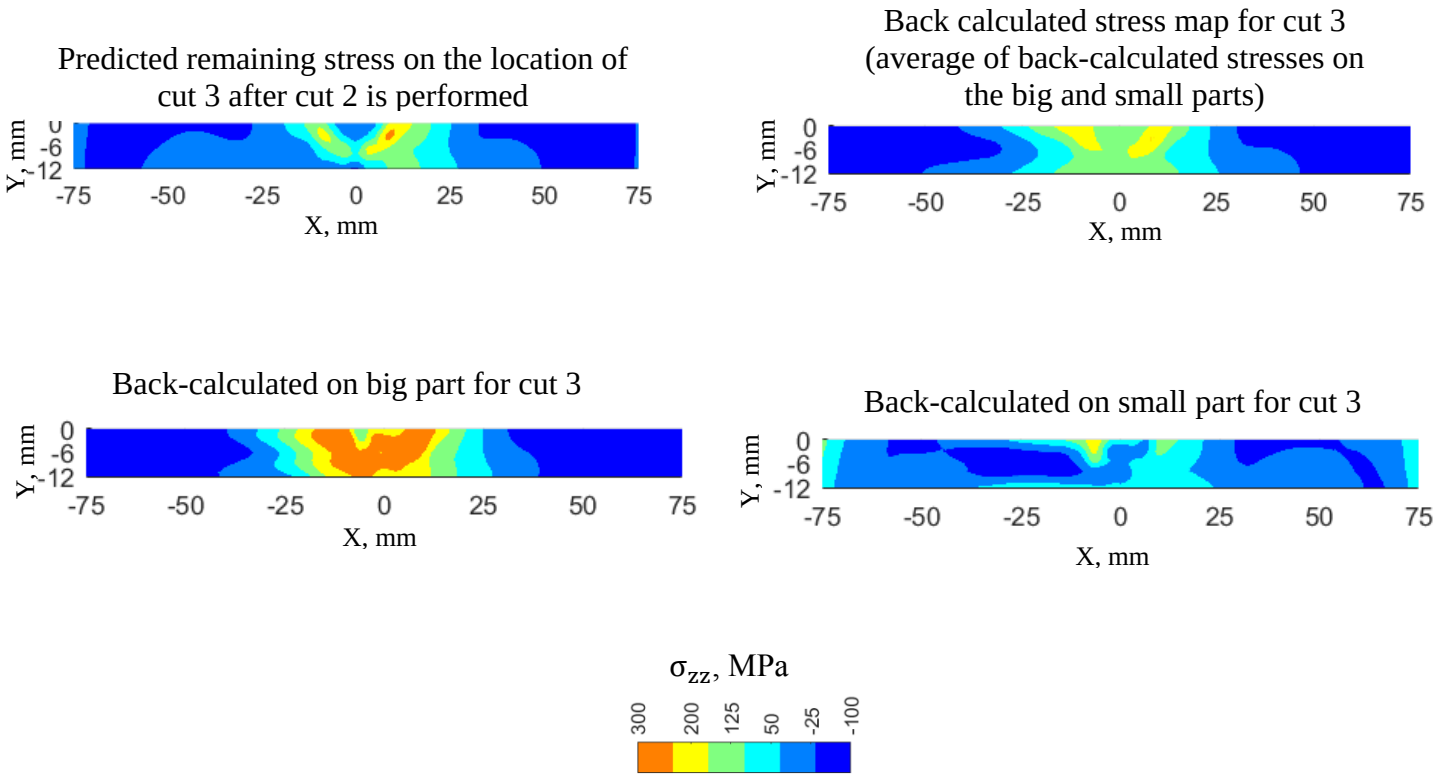

Figure 5-13 Predicted remaining and back-calculated stress maps for the third asymmetric contour cut using contour method simulation on TG6 sample.

The predicted remaining stress map on the location of cut 4 after cut 3 is performed and the back-calculated stress maps for the fourth asymmetric contour cut are shown in Figure 5-14.

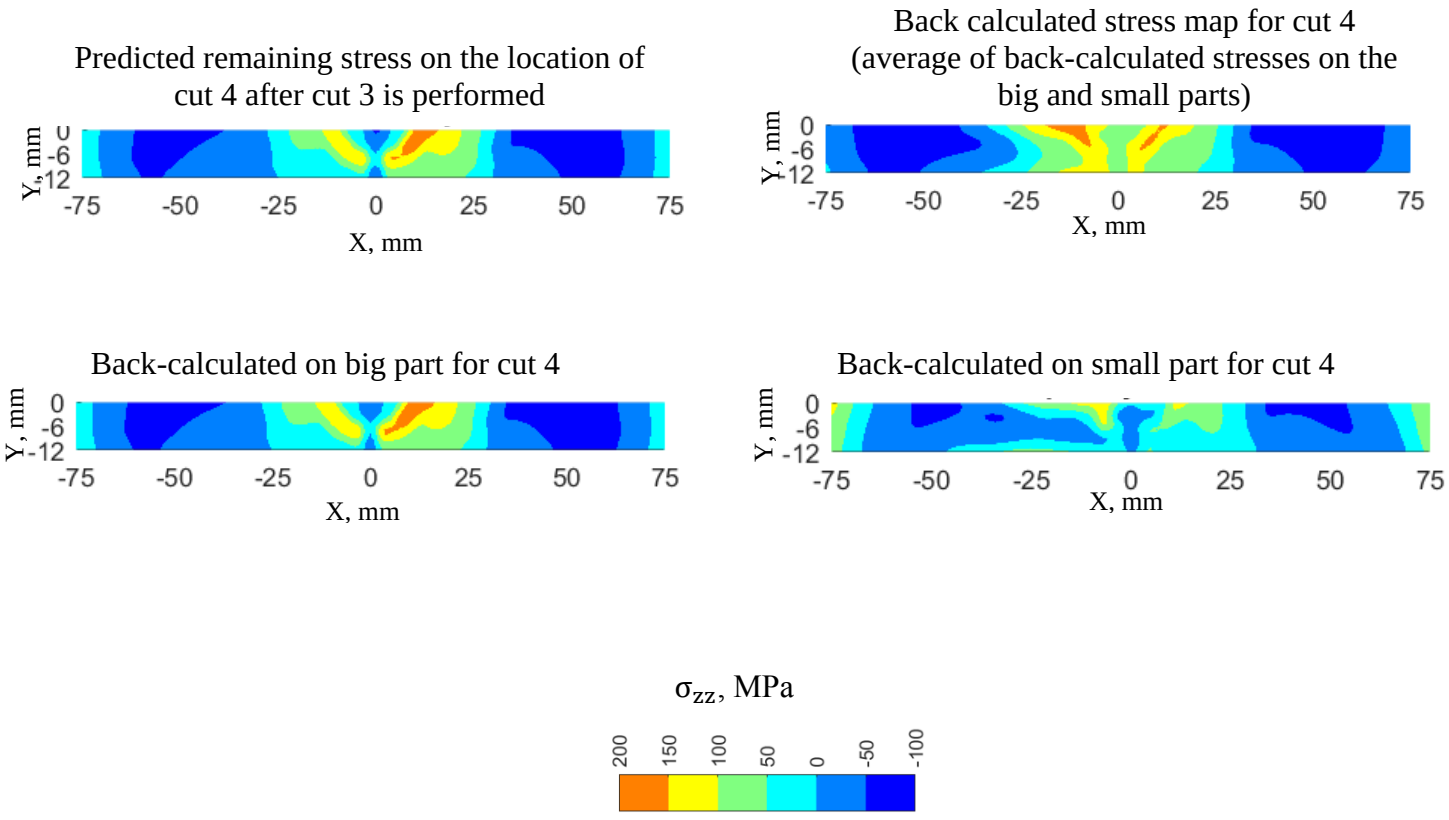

Figure 5-14 Predicted remaining and back-calculated stress maps for the fourth asymmetric contour cut using contour method simulation on TG6 sample.

5.4.3 Superposition of back calculated and relaxed stress

The results from the back-calculation step after asymmetric contour cut 2 were superposed with the relaxed stress from cut 1 along cut plane 2. This gives the back-calculated residual stresses along the cut plane 2 that were retained in the TG6 plate before any cut was done on it. Similarly, the results from the back-calculation step after the asymmetric contour cut 3 were superposed with the relaxed stress from cut 1 and 2 along the cut plane 3. This gives the back-calculated residual stresses along cut plane 3 that were present on the TG6 plate before any cut was made. Also the results from the back-calculation step after asymmetric contour cut 4 were superposed with the relaxed stresses from cuts 1, 2 and 3 along the cut plane 4. This gives the reconstructed residual stresses along the cut plane 4 that were retained in the TG6 plate before any contour cuts.

The reference and back-calculated stresses using the superposition principle for the location of all contour cuts are shown in Figure 5-15. The results for cut 1 are repeated here in Figure 5-14 for comparison.

The back-calculated stresses presented in section 5.4.2 do not give the reference stresses because stresses relax after each cut in the plate. Hence the relaxed stresses must be taken into account. Thus, the superposition principle using the multiple cut approach has been implemented.

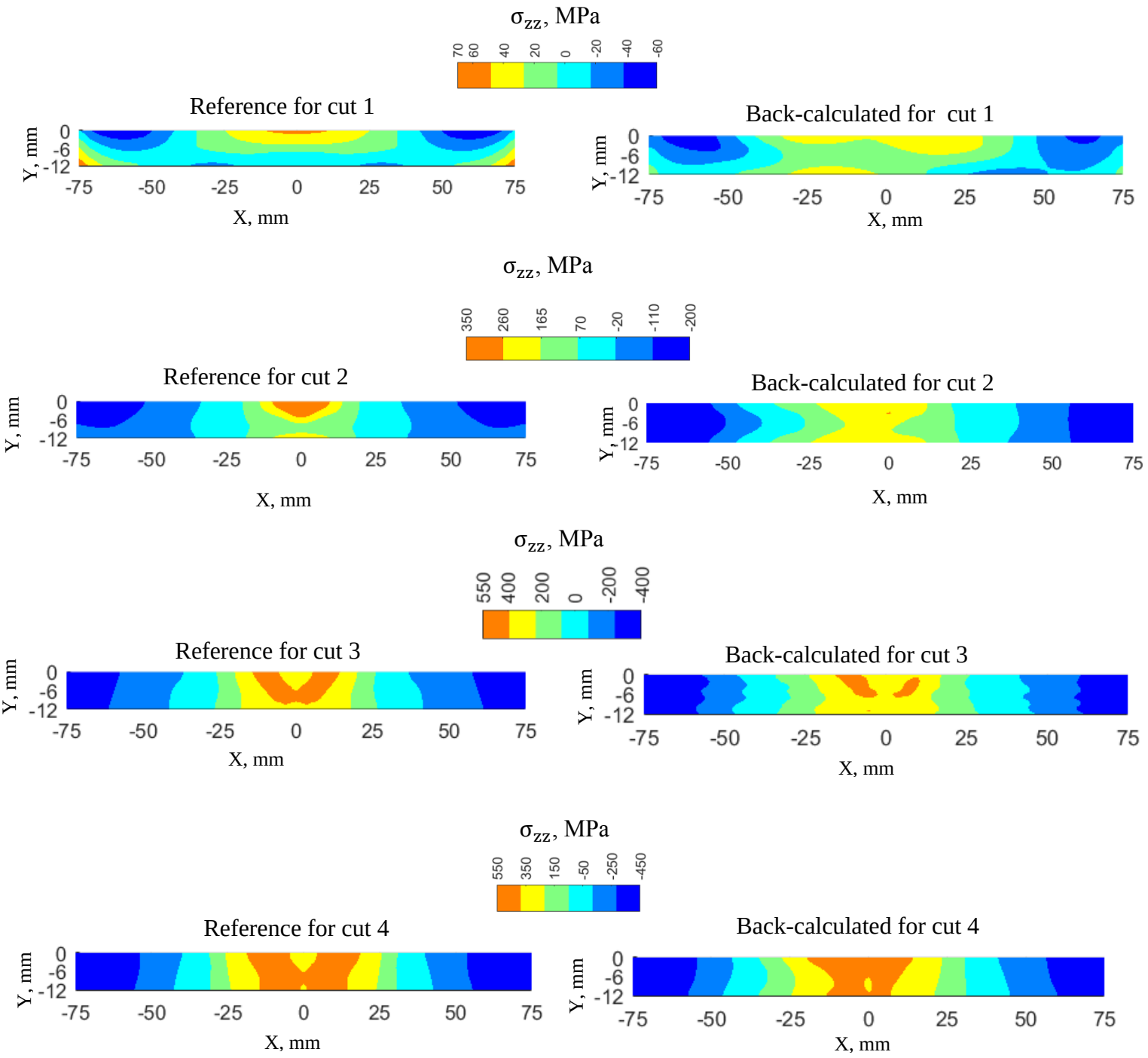

Figure 5-15 Predicted reference and back-calculated stress maps for the incremental contour method simulation on TG6 sample.

The averaged error through the cut plane between the back-calculated and references stresses for each cut was calculated using the RMS approach given by Equation 4-1. Also the error was normalized using the range of the reference stress equal to the absolute difference between the maximum and minimum stress values as shown in Equation 4-2.

The normalised averaged RMS error for each asymmetric cut and the reconstructed stress using superposition for each cut is shown in Figure 5-16a and Figure 5-16b, respectively.

The total error using the incremental contour method was found to be lower than 4.3%.

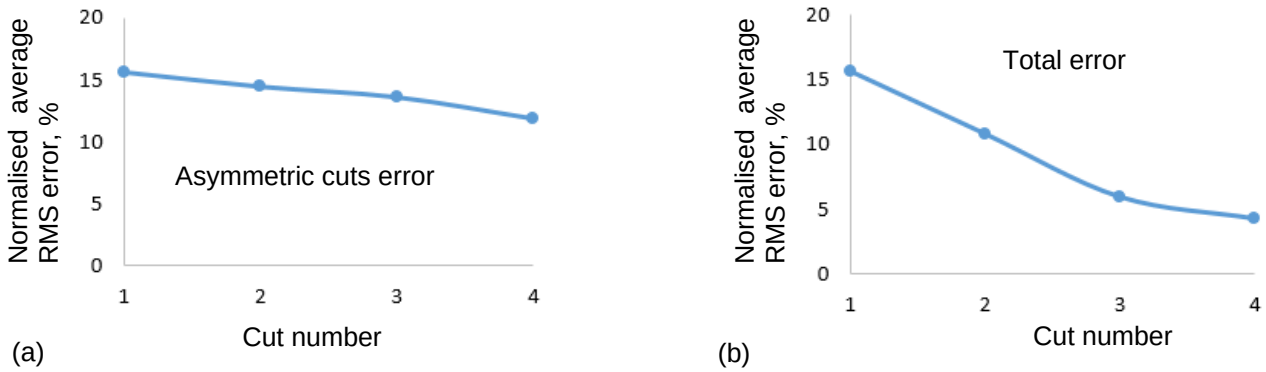

Figure 5-16 The normalized averaged RMS error (a) for back-calculated stresses for each asymmetric cut and (b) back-calculated stresses for each cut after the superposition principle and multiple-cut approach is implemented.

A comparison between 2D maps of predicted residual stress prior to cutting, back calculated residual stress using the incremental contour method (iCM), and back calculated residual stress using the conventional contour method is shown in Figure 5- 17.

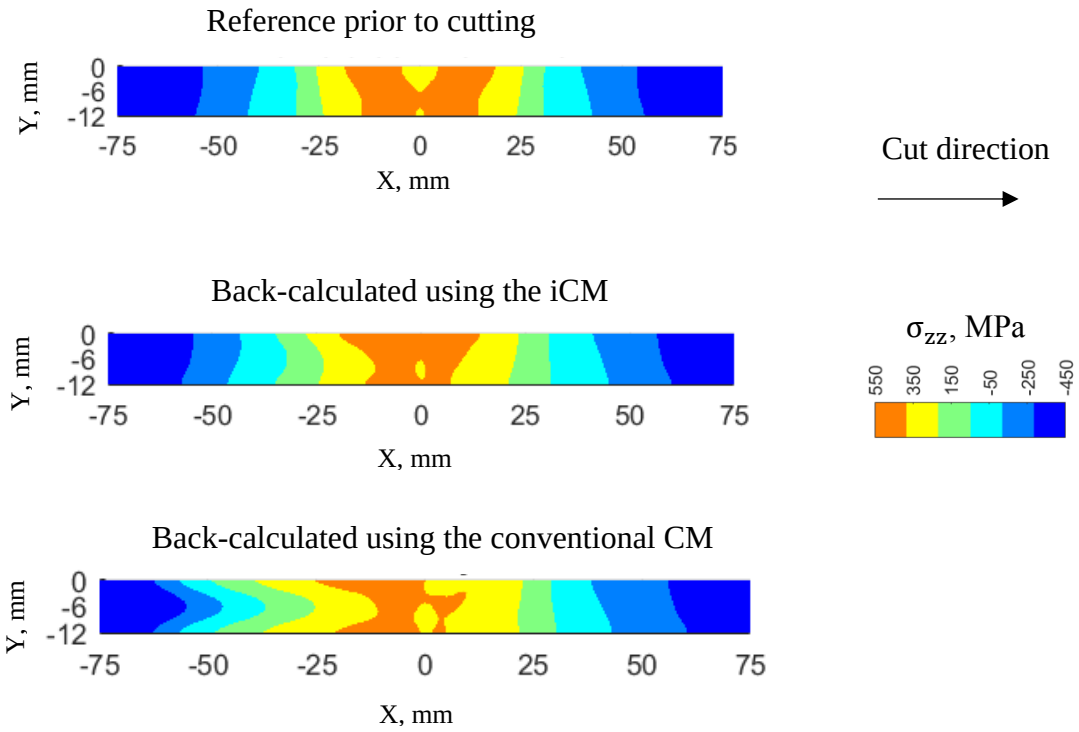

Figure 5- 17 Comparison between 2D maps of predicted residual stress prior to cutting, back calculated residual stress using the incremental contour method (iCM), and back calculated residual stress using the conventional contour method.

A comparison of stress line profiles extracted from reference and back-calculated stress maps using the conventional and incremental contour methods, along a cut plane at the centre of the TG6 plate is shown in Figure 5-18. The stress line profiles were extracted for line y = 0, y = -12, y = -6, and x = 0.

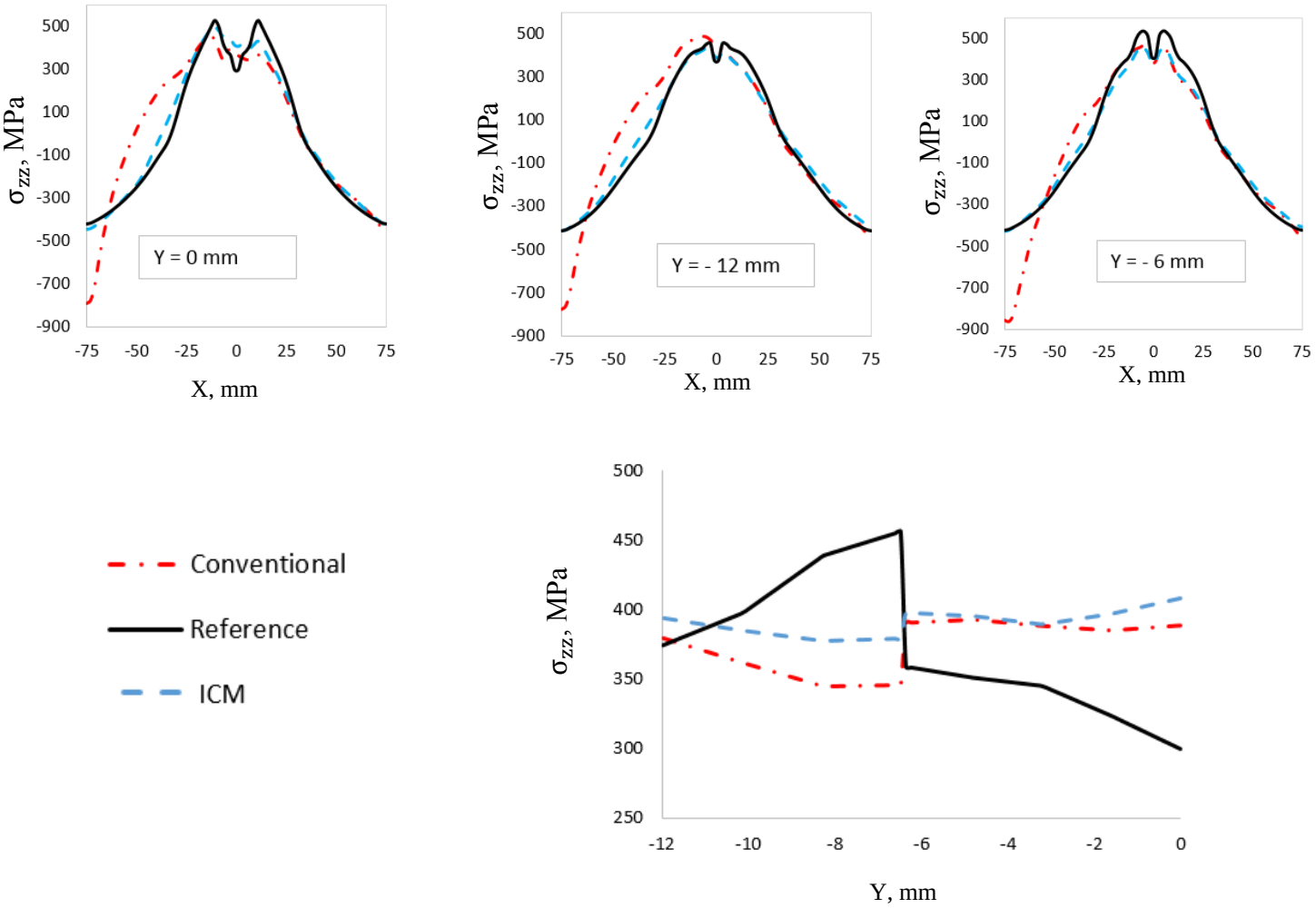

Figure 5-18 Comparison of the reference stress on TG6 with stresses obtained from simulation of the conventional contour method and iCM for line profiles y = 0, y = -12, y = -6 and x = 0.

A good correlation was obtained between the reference and the back calculated stresses using the incremental contour method. However the stress line profiles through thickness did not perfectly match and this may be because of the very detailed stress pattern shown in Figure 5-12 and because of the material discontinuity through thickness.

5.5 Neutron diffraction measurement on TG6 sample

Residual stresses were measured by the author using neutron diffraction along 6 line profiles on the TG6 plate (see Figure 5-19 and Figure 5-20). The line L75B2 was measured at 25 mm from the top edge and 2 mm below the top surface in the parent material. The lines 50B2 and 50B10 were measured at 50 mm from the top edge, 2 mm and 10 mm below the top surface in the parent material, respectively. The line 25B2 was measured at 75 mm from the top edge at 2 mm below the top surface in the weld material. The lines 25B7.5 and 25B10 were measured at 75 mm from the top edge at 7.5 mm and 10 mm below the top surface in the parent material, respectively. Stress free lattice parameter (d0) measurements were done in a 3.5 mm diameter cylinder as detailed in the TG6 protocol [112]. An average of all d0 values measured in each zone including the parent, heat affected zone (HAZ) and weld was used for the strain and stress calculations for the corresponding zones. The results were compared to the predictions of Muransky.

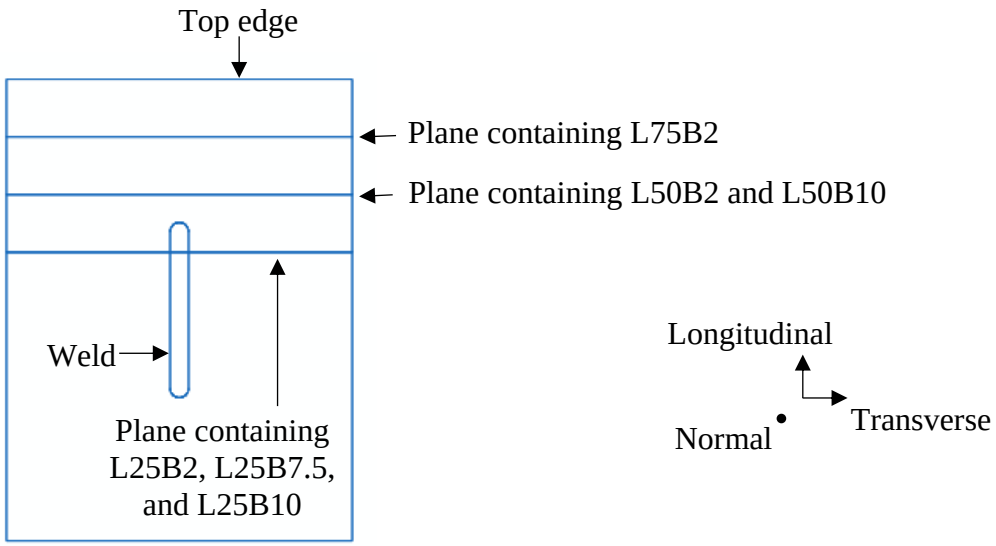

Figure 5-19 Schematic view showing the measurement planes locations on the TG6 plate.

The ND experiment was done in two parts. During the first part, the 3 strain components along the line L25B2 were measured, but only 2 principal strain components were measured along the lines 25B10, 50B2, 50B10 and 25B7.5. In fact, the neutron beam went down and the

experiment had to be interrupted. The experiment resumed 2 months later, and the remaining principal stain components, in the longitudinal direction, were measured. Also, during the second part of the experiment the 3 strain components along the line 75B2 were measured. The lattice free parameters, d0, were measured during both parts of the ND experiment. However, only the d0 values measured during the first part of the experiment were used for the strain calculations along all the measured lines. This choice was made using a self-balance criterion for the residual stress line profiles. For the 6 residual stress line profiles measured using ND, the normal stress components are reasonably close to 0 MPa, as expected. Overall, the agreement between ND and FE results was judged to be acceptable.

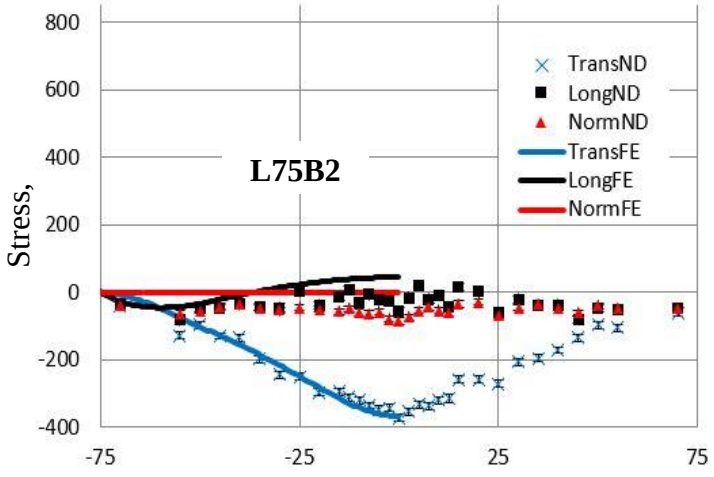

Distance from centre along transverse direction, mm

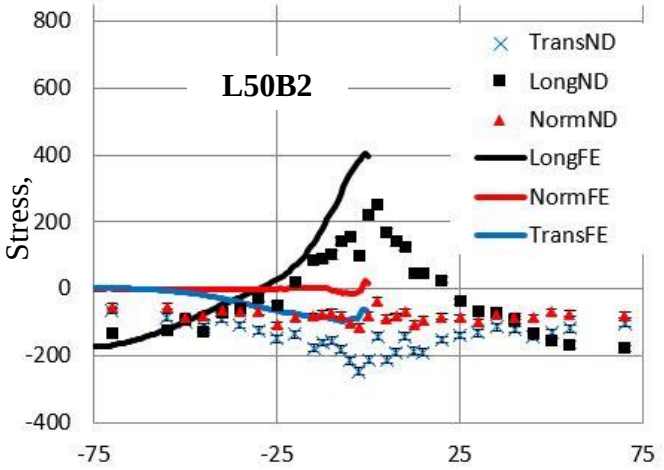

Distance from centre along transverse direction, mm

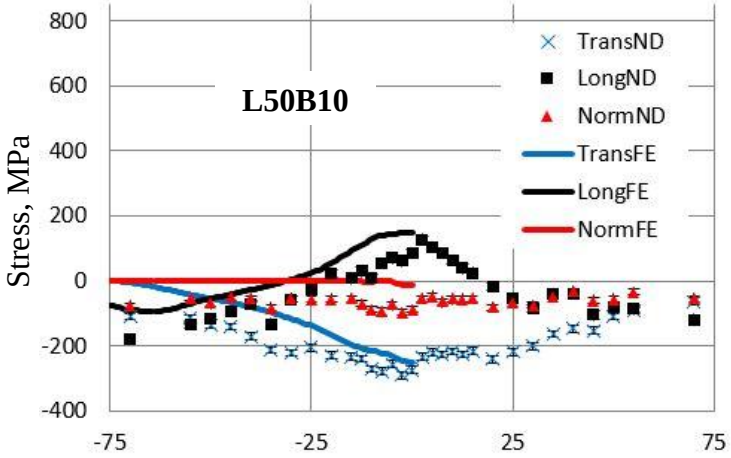

Distance from centre along transverse direction, mm

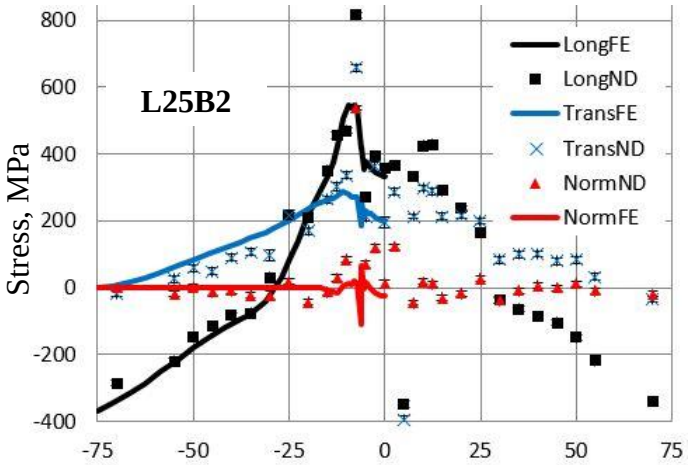

Distance from centre along transverse direction, mm

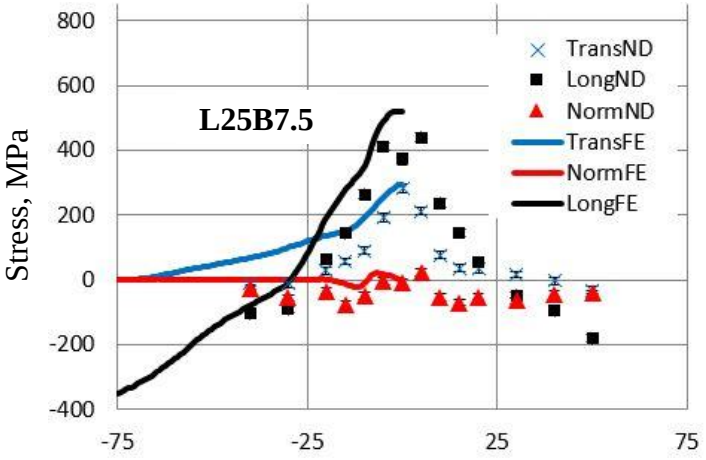

Distance from centre along transverse direction, mm

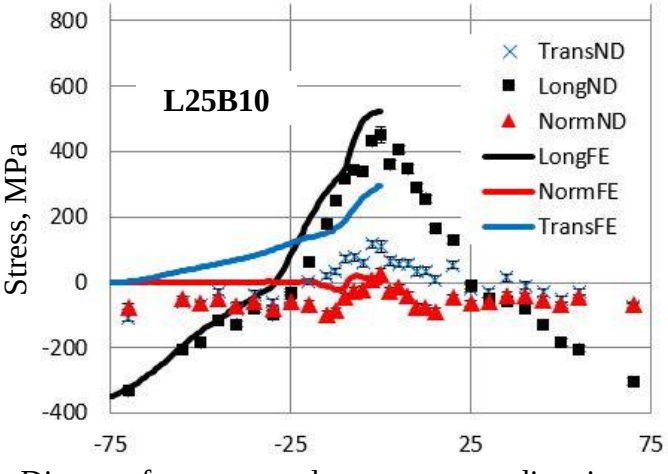

Distance from centre along transverse direction, mm

Figure 5-20 Comparison of residual stress line profiles from ND measurements and FE predictions [114].

5.6 Experimental contour measurement on TG6 sample

The incremental contour method was implemented experimentally using the approach detailed in section 5.2 Theoretical considerations. The asymmetric contour cuts were done using the same approach detailed in chapter 3. The plate was securely clamped, pilot holes at the start and end of the cut were introduced (to control the cut opening mode) and sacrificial layers were applied to the top and bottom surfaces to minimise wire EDM cutting artefacts, see Figure 5-21.

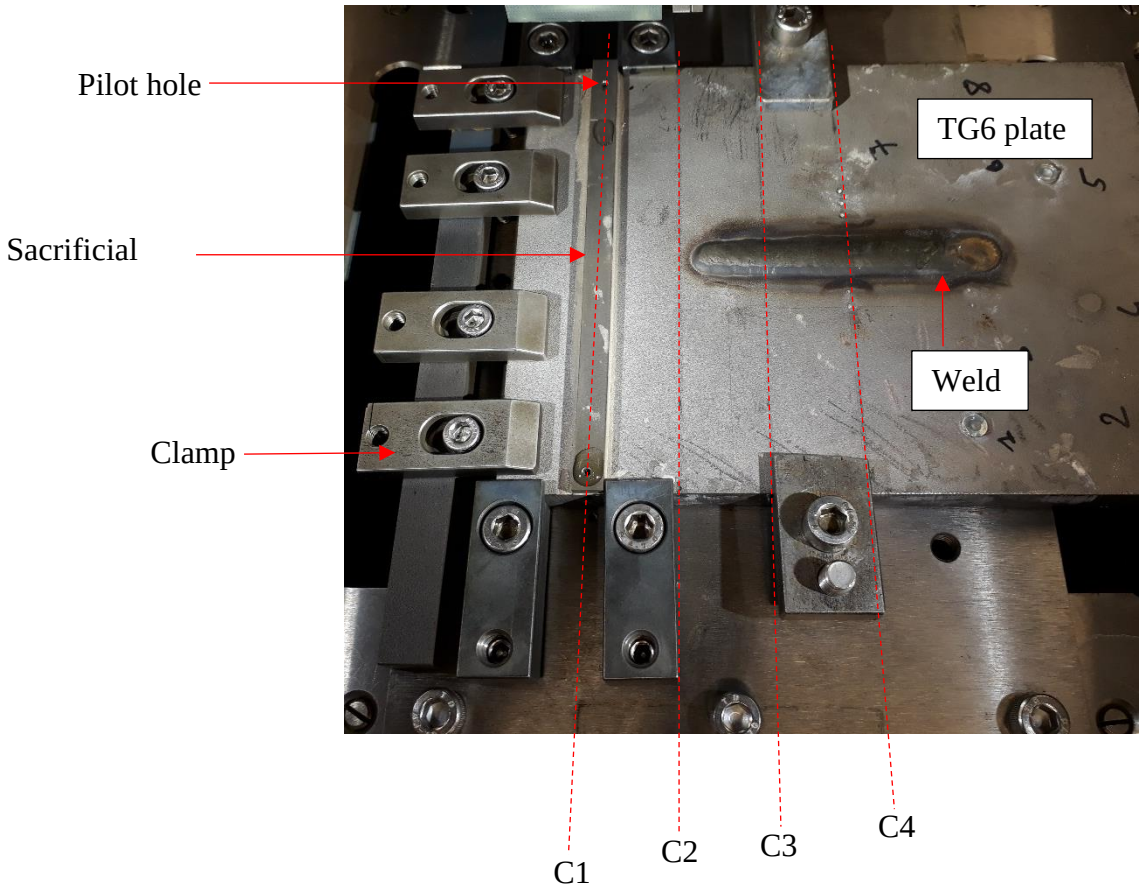

Figure 5-21 Illustration of the clamping configuration, pilot holes, sacrificial layers and cut locations on the TG6 plate during the incremental contour experiment.

The plate was cut incrementally every 25 mm from one edge (see ‘C1’, ‘C2, ‘C3’ and ‘C4’) with the main cut (C4) implemented at the location of interest at mid length of the sample.

A comparison between 2D maps of the out-of-plane stress component for each cut plane using the incremental contour method and the FE predictions is shown in Figure 5-22.

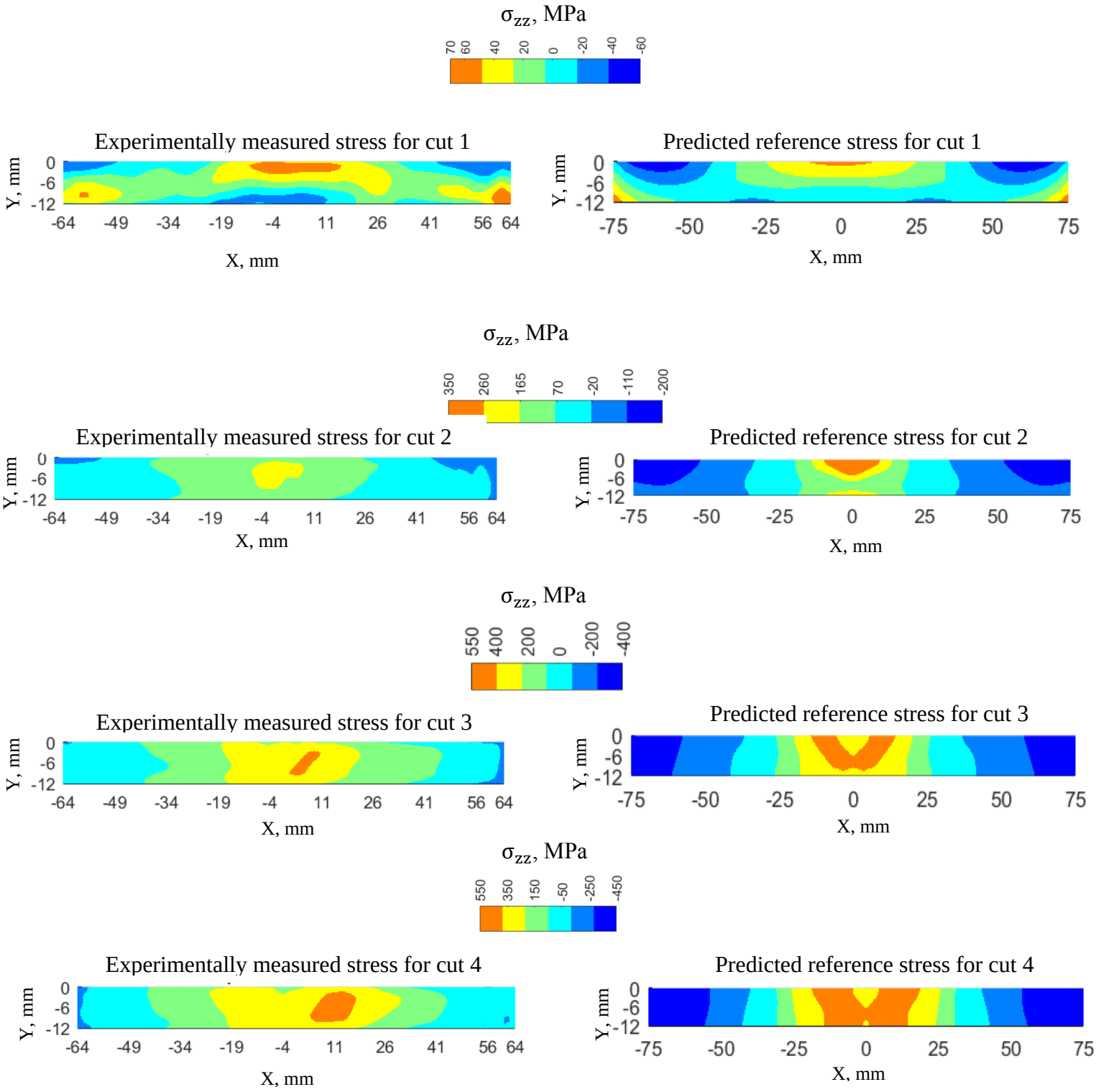

Figure 5-22 Comparison of 2D stress map results obtained using FE predictions and the incremental contour method.

Also a comparison between stress profiles 2 mm below the top surface of the plate obtained using FE predictions, neutron diffraction measurements and the incremental contour method at the location of interest ('C4' in Figure 5-21) are shown in Figure 5-23. The ND measurement shown in Figure 5-23 were provided by Beverly Stewart from The Open University. Both the Contour method and the FE predictions did not capture the tensile peak on the ND stress profile equal to 979 MPa and located at x = -7.5 mm. However, this peak on the ND stress profile might be an artefact due to the challenging microstructure of the material at the location of the measured point.

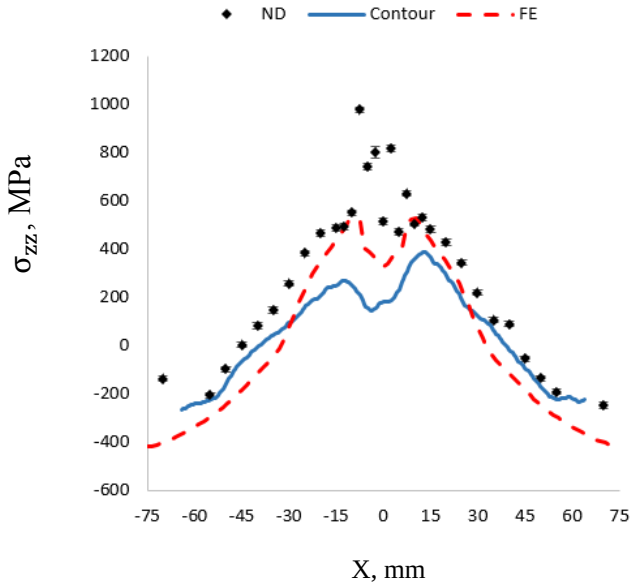

Figure 5-23 Comparison between neutron diffraction and incremental contour method results and FE predictions along a line at 2 mm below the surface of the TG6 plate.

5.7 Discussion

The conventional contour method implemented on the TG6 FE model resulted in significant error (36.4% RMS) hence the incremental contour method (iCM) was applied. The incremental contour method was implemented on the TG6 sample using the novel data analysis dealing with asymmetric cuts, and a multiple-cut approach. Four cut locations were determined by estimating the die away length scale of the stress from each location, to calculate the amount of relaxation on the following cut planes ensuring elastic relaxation of residual stress for the following cuts.

The cut location was determined by looking for planes where the stress magnitude was much lower than the material yield strength (400 MPa), to prevent plastic strain during the material relaxation due to cutting. However, plastic strain occurred for each incremental cut. Although the extent of plastic zone size for each cut was less than the one that occurred for a conventional contour method measurement, the number and location of cuts chosen was insufficient to prevent plasticity during cutting.

Numerical simulations showed that using this iCM approach the normalised averaged RMS error between the predicted residual stress prior to cutting and the back calculated stress for the final cut was lower than 5%. Similarly, when the conventional contour method was simulated the calculated error was 36.4 %, which is more than 7 times higher.

What is noteworthy from the analysis is that the presence of plasticity and consequent stress errors in the early iCM cuts did not propagate and accumulate a large error in the final cut results. The error for all of the asymmetric cuts decreased after each cut. Similarly, the accumulated error, after superposing the relaxed stress from the previous cuts with the back-calculated stress on each cut plane, decreased as well. This trend can be due to the fact that once a cut is made and stresses are partially released at the location of the next cut plane, the risk of plasticity cutting induced errors decreases (Figure 5-10). Also, it seems that the plasticity error from each incremental cut, doesn't significantly affect the overall error in the incremental contour method. This is because stress relaxation is estimated using elastic material properties only. Hence, although the plasticity error may affect the estimation of the back-calculated stress, the relaxation prediction is reasonably accurate and therefore the overall error is negligible.

The neutron diffraction measurement results match reasonably well with the finite element predictions. Hence, this gives confidence that the numerical simulations are realistic and that the efficiency of the proposed incremental contour method simulation to improve the accuracy of the results is reliable.

However, when the incremental contour method was implemented experimentally the error in the results was higher than predicted. This may have been caused by various factors. Several wire breakages occurred during the first cut, especially at mid length. These cutting artefacts introduced error in the back calculation of stress and estimated relaxation of stresses at the location of interest. Another cause can be that the geometry of the manufactured plate was irregular in the z direction. However, when estimating the relaxed stress the FE model was

made by extruding the perimeter of the cut surface hence the FE model never captured the exact (distorted) geometry of the sample prior to cutting. This can cause errors in the prediction of the relaxed stresses at the location of interest. Also errors may be accumulating through using pilot holes and then ignoring the stresses and cross-sections beyond the holes. In fact, if none negligible residual stress is retained in the ligaments beyond pilot holes discarding those stress may affect the redistribution of the back calculated stresses along the cut plane. These accumulated errors can be propagated in the incremental contour method when the superposition principle is used to reconstruct the original stresses at the location of interest.

Using a 3D scanner to have a more accurate estimation of the geometry of the cut parts could improve the back-calculation of stresses and the final results of the incremental contour method.

The agreement between the finite element predictions and the experimental measurements using the iCM can potentially be improved by increasing the accuracy of the elastic-plastic stress strain properties used for the TG6 plate, heat affect zone (HAZ) and weld metal.

5.8 Conclusion

A novel measurement approach is presented in this chapter, the incremental contour method (iCM), that is aimed at mitigating plasticity induced errors in the contour residual stress measurement method. iCM involves implementing a multiple cut strategy that progressively relieves the stresses in the component with the aim of reducing the level of stress at the section of interest to a fraction of the yield stress of the material. Numerical simulations showed that the error using an incremental contour method for the TG6 benchmark would be small. Although measurement of the benchmark TG6 sample showed evidence of plasticity using the iCM, numerical simulations showed that errors would have been several times greater for a conventional contour method measurement. Nonetheless experimental validation of the incremental contour method for benchmark TG6 produced greater stress error than expected based on the numerical simulation studies. This error may be reduced by improving the contour cut quality, increasing the accuracy of the back calculation step by taking into account the geometric irregularities of the cut part and including the stresses retained in the ligament beyond the pilot holes they are not negligible with regards to the stress range on the cut plane as mentioned earlier. However, a reasonable correlation was obtained between neutron

diffraction measurements, FE prediction and the incremental contour method results in the TG6 test specimen.

Chapter 6: General discussion, conclusions and future work

The aim of this chapter is to review the major contributions to knowledge of this PhD project. First, the new data analysis approach dealing with asymmetric cuts in the contour method for residual stress measurement is discussed. Then the application of this approach in a more general case highlighting the limitations and scope of it are reviewed. In the following section the incremental contour method used to prevent cutting induced plasticity error and improve the accuracy of the contour results is critically reviewed. Practical considerations for the implementation of both approaches are discussed in the last section.

6.1 General discussions

The new data analysis approach dealing with asymmetric cuts

The conventional contour method requires using symmetric cuts only. This limitation is due to shear stress relaxation on the cut surfaces after a contour cut is done. The out-of-plane stress and shear stresses on the created cut surfaces are fully relaxed owing to the created free surface boundary condition. The relaxation of out-of-plane stresses result in out-of-plane displacements of the cut surfaces. The release of shear stresses, however, produces in-plane as well as out-of-plane displacement of the cut surfaces. Therefore, when the created cut surfaces are measured in practice, the measured out-of-plane displacements include the contribution of shear stress relaxation.

For symmetric cuts the out-of-plane displacements owing to the relaxation of shear stresses are anti-symmetric. Hence, averaging the displacements of mating cut surfaces cancels out the effect of shear stress.

For asymmetric cuts, however, the effect of shear stresses is not cancelled out if the displacements of the cut surfaces were averaged. This is because the stiffness of the mating cut parts are different. Therefore, the contribution of shear stress in the out-of-plane displacements is not antisymmetric anymore. Applying the out-of-plane displacement of the cut surfaces to the FE model of the corresponding cut parts gives the stress state that is composed of the relaxed out-of-plane stresses as well as contribution of shear stress.

As demonstrated in chapter 3 averaging the resulting stresses should cancel out the effect of shear stresses. This proposed data analysis approach for an asymmetric cut was demonstrated numerically and experimentally in chapter 3.

However, in that chapter, the effect of relaxation of in-plane displacements owing to the contour cut on the contour results was not explored. The total out-of-plane relaxed displacements can be a mixture of three contributions including the relaxation of the out-of-plane stress, the shear stress and the in-plane stress. The only contribution of interest in the contour method is the out-of-plane displacement owing to the relaxation of the out-of-plane stress. Both other contributions, including the out-of-plane displacement caused by the relaxation of shear stress and in-plane stress, generated errors in the measurement of the out-of-plane stress prior to cutting in the contour method. In fact, during the measurement step of the contour method, the total out-of-plane displacement on the cut surface is measured and used to back-calculate the out-of-plane stress, hence the error is propagated in the results.

The next section discusses the main outcomes of chapter 4 where the new data analysis approach is applied to a more general case.

Application of the new data analysis approach dealing with asymmetric contour cuts in a more general case

The new data analysis approach was presented and demonstrated in chapter 3. However, when it was applied to simulate the contour measurement on the TG6 welded benchmark using a 3D FE residual stress model, the original and back-calculated stress didn't match perfectly. This error was investigated in chapter 4 and the potential importance of the relaxed in-plane stress along the cut plane identified.

In fact, as detailed in section 6.1 the total relaxed out-of-plane displacement is given by:

$$U_{Total} = U_{Out\ of\ plane\ stress} + U_{Shear\ stress} + U_{In-plane\ stress} \qquad \text{Equation 6-1}$$

Where $U_{Out\ of\ plane\ stress}$ is the out-of-plane displacement caused by the relaxation of the out-of-plane stress, $U_{Shear\ stress}$ is the out-of-plane displacement caused by the relaxation of shear stress and $U_{In-plane\ stress}$ is the out-of-plane displacement cause by the relaxation of the in-plane stress.

Investigating the effect of the in-plane stress on contour method results was outside the original scope of this PhD project but the out-of-plane displacements caused by the relaxation of the in-plane stress, $U_{In-plane\ stress}$, appeared to have caused errors in the back-calculated stresses as illustrated in chapter 4. This highlighted a limitation of the new data analysis approach dealing with asymmetric contour cuts presented in chapter 3. The out-of-plane displacements caused by the relaxation of shear stress, $U_{Shear\ stress}$, is cancelled by averaging the displacements from the mating cut surfaces in the conventional data analysis and it is cancelled by averaging the back calculated stresses in the new approach. However, the displacement $U_{In-plane\ stress}$ is not anti-symmetric with regards to both mating cut surfaces, and hence is not cancelled by both approaches. This limitation is common to both, the conventional contour method and the new data analysis approach dealing with asymmetric contour cuts.

The new data analysis approach was then used in the novel incremental contour method as detailed in the next section.

The incremental contour method (iCM)

Plasticity error is one of the main limitations of the contour method. In fact, a fundamental assumption in the technique is that the material unloads strictly elastically after a contour cut. However, when the deformation of the material after a cut is not elastic Hooke's law cannot be used to accurately back-calculate the residual stress prior to cutting. Therefore, errors arise in the contour method. The risk of plasticity error can be reduced by ensuring that the stress magnitude along the location of interest is low with regards to the material's yield strength. For example, a threshold value can be identified to define contour cut locations (for example where the stress magnitude is below a fraction of the material's yield strength value). The incremental contour method (iCM) aims to relax incrementally the stress at a location of interest where the stress magnitude is high with regards to the yield strength. This is done using asymmetric contour cuts and the superposition principle to reconstruct the stress at the location of interest prior to cutting. This technique was successfully demonstrated numerically and experimentally against neutron diffraction measurements. However, a main limitation of the incremental contour method is that errors such as cutting induced errors from each contour cut done before the location of interest are propagated in the final results. Moreover, the relaxation of shear stress from earlier cuts may affect the distribution of out-of-plane stress on the following cut planes and hence propagate errors in the final iCM measurement results. This shear stress effect

is not related to the new data analysis approach for asymmetric cuts but is because of the superposition principle and implementing multiple cuts approach. Therefore, a compromise needs to be made between the number and locations of the contour cuts and the target magnitude of stress to relax at the location of interest to reduce the risk of plasticity error as well as the error associated with the presence of shear stress.

Practical implementation of the asymmetric contour and the incremental contour methods

Both approaches, the asymmetric contour and the incremental contour method, have been successfully implemented numerically and experimentally. The conventional contour method involves averaging the contour displacement from both mating cut surfaces hence this cancels out error from anti-symmetric cutting induced artefacts such as crooked cuts. However, for asymmetric cuts, where the resulting stresses on both cut surfaces are averaged, the cutting induced artefacts may not produce antisymmetric features in the stress results if both cut parts have different stiffnesses. Hence cutting induced errors will not cancel out when stresses on mating cut surfaces are averaged and will propagate in the final measurement results.

6.2 Conclusions

The contour method is a powerful way of measuring a 2D map of residual stress in a body at lower cost than alternative methods such as neutron diffraction. However, two of the main limitations of the technique were that the cut needs to be done along a symmetry plane of the sample, and the contour results are prone to plasticity induced errors when measuring stresses close to the yield strength of the material.

The limitation related to symmetry of contour cuts was addressed in chapter 3. A main finding of this chapter was that the measured displacements on each cut surface can be used to back calculate stresses on the corresponding surface without averaging. Then averaging the back calculated stresses from both mating cut surfaces gives the correct stress along the cut plane prior to the cut. This new approach was successfully demonstrated numerically using finite element simulations of the whole contour method. Also, experimental contour measurements were successfully done at asymmetric locations on laser welded thin plates and the results compared very favourably with FE simulation and neutron diffraction measurements. This chapter concluded that the contour residual stress measurement method can be applied at any

random location on the specimen by using the proposed data analysis approach dealing with asymmetric contour cuts.

Chapter 4 was concerned with the case where an asymmetric cut is done on the TG6 plate that has a more general tri-axial residual stress field. Numerical simulations of the contour method on the TG6 plate were conducted and the new data analysis approach was used to back calculate the residual stress acting out of the cut plane. However, the back calculated residual stress did not perfectly match with the original stress prior to cutting. An averaged root mean square (RMS) error was calculated and normalized using the range of the original stress. This error was found equal to 4.3%. Interestingly, when the in-plane displacements extracted from the cut surfaces were used in addition to the out of plane displacements the back calculated stresses perfectly matched the original stress prior to the cut. Various potential sources of the difference between the original and back calculated stresses were explored and a conjecture highlighting the contribution of in-plane stress relaxation to error in the contour method was proposed.

The other main limitation of the contour method that is plasticity induced error when measuring stress levels comparable to the yield strength of the material was dealt with in chapter 6. The main outcome was that relaxing incrementally the residual stress at a location of interest using a series of intermediate cuts can help to mitigate plasticity induced error in the contour measurement results. This led to the development of a novel approach named the ‘incremental contour method’. Similar, to the proposed asymmetric contour method, the application of the incremental contour method was demonstrated both numerically and experimentally for a welded benchmark test specimen. A reasonable correlation was obtained between the experimental incremental contour stress measurement results, FE prediction and neutron diffraction measurements.

6.3 Ideas of future work

Like any other research, the present work could not cover all topics of interest over the course of this study and further interesting thoughts and topics arose that are worth investigating for future work.

Suggestions for future work include investigating the effects of in-plane stress, clamping, cutting induced artefacts, geometry of the FE model for stress back-calculation step and pilot holes in the contour method.

The effect of in-plane stress

The asymmetric contour method was successfully implemented on thin laser welded plates. However, when the proposed data analysis approach was conducted on a more general case, there observed some differences between the contour method results and the original residual stresses.

The presented theoretical considerations showed that the proposed data analysis approach for asymmetric contour cuts should give the correct residual stresses prior to the cut. It is believed that the differences between the contour method results and the original residual stresses may be caused mainly by the in-plane stress as detailed in chapter 4 and in the proposed conjecture in that chapter. The effect of in-plane stress could be explored analytically. Further investigation needs to be done to determine the significance of this effect on the contour method measurements.

The effect of clamping

The contour method is also sensitive to the clamping configuration of the specimen during the cutting step. Practitioners of the contour method recommend symmetric clamping of the sample during the cutting step for the conventional contour method where symmetric cuts are performed. Asymmetric clamping of the cut parts results in asymmetry features in the measured out of plane displacements on the cut parts. If the level of introduced asymmetry is significant it could cause error in the back calculated stresses. Besides symmetric and rigid clamping is recommended to help reducing the risk of plasticity cutting induced errors [61]. Exploring more closely the effect of an asymmetric clamping configuration for asymmetric contour cut seems to be an interesting idea of future work.

The effect of cutting induced artefacts

The conventional contour method requires averaging the displacements from both cut surfaces. Hence this cancels out any anti-symmetric feature such as cutting artefacts. However, this cannot be done for the case of asymmetric cuts. In fact, both cut parts have different stiffnesses and this may prevent anti-symmetric features between the cut surfaces. Investigating the effect of anti-symmetric features such a crooked cut artefact in asymmetric contour cuts can be an interesting future work.

The effect of the geometry of the FE model for stress back-calculation step of the contour method

In chapter 6, the incremental contour method was implemented on TG6 sample. TG6 was manufactured by making a slot of 11 mm wide and 76 mm long on the top face and 6 mm wide and 58 mm long at its bottom [112]. Then the slot was filled with three superimposed weld beads. Significant butterfly distortion of the sample was evident as a result of the welding process. One of the contributing factors to the differences observed between the measured contour stresses and neutron diffraction stresses was attributed to the distorted geometry of the sample. The back calculation of stresses involves creating an FE model of the cut part and performing an elastic stress analysis. The common practice is to use the measured perimeter of the cut surface and extrude the perimeter in the direction normal to the cut surface to create an FE model of the cut part. However, in welded structures, similar to the TG6 plate, the sample is distorted and the geometry of the cut part is not always uniform in the direction normal to the cut surface. Hence generating an FE model based on the perimeter of the cut surface does not create a true representation of the geometry of the actual cut part. This, depending on the distortion of the sample, could introduce errors in the contour method results.

Therefore, it is suggested for future work to investigate the effect of creating a more accurate FE model that represents the true geometry of the cut parts on the back calculated stresses. One idea is to 3D scan the cut part and use it as a STEP file to generate the FE model for the back-calculation step of the contour method.

The effect of pilot holes in the contour method

The use of pilot holes during the contour cut can introduce errors in the back-calculation step if the stresses retained within the ligaments are not negligible with regards to the range of the measured stress at the cut plane. Further investigations would help to assess the errors introduced when using pilot holes through finite element sensitivity studies.

7 References

[1] P. J. Withers and H. K. D. H. Bhadeshia, “Residual stress. Part 2 – Nature and origins,” *Mater. Sci. Technol.*, vol. 17, no. 4, pp. 366–375, 2001.

[2] G. S. Schajer *et al.*, *Practical Residual Stress Measurement Methods*. Wiley, 2013.

[3] P. J. Withers and H. K. D. H. Bhadeshia, “Residual stress. Part 1 – Measurement techniques,” *Mater. Sci. Technol.*, vol. 17, no. 4, pp. 355–365, 2001.

[4] “EDF Energy, R6 Revision 4, Assessment of the integrity of structures containing defects, with amendments to 2014,” 2014.

[5] S. Kumar *et al.*, “Residual stresses in laser welded ASTM A387 Grade 91 steel plates,” *Mater. Sci. Eng. A*, vol. 575, pp. 160–168, 2013.

[6] P. Hofer, E. Kaschnitz, and P. Schumacher, “Simulation of distortion and residual stress in high pressure die casting – modelling and experiments,” *IOP Conf. Ser. Mater. Sci. Eng.*, vol. 33, no. 1, p. 012055, 2012.

[7] M. P. Mungi, S. D. Rasane, and P. M. Dixit, “Residual stresses in cold axisymmetric forging,” *J. Mater. Process. Technol.*, vol. 142, no. 1, pp. 256–266, 2003.

[8] P. J. F. Martina, M. J. Roy, B. A. Szost, S. Terzi, P. A. Colegrove, S. W. Williams and M. H. Withers, J. Meyer, “Residual stress of as-deposited and rolled wire + arc additive manufacturing Ti – 6Al – 4V components,” *Mater. Sci. Technol.*, vol. 0836, pp. 1439–1448, 2016.

[9] N. S. Rossini, M. Dassisti, K. Y. Benyounis, and A. G. Olabi, “Methods of measuring residual stresses in components,” *Mater. Des.*, vol. 35, pp. 572–588, 2012.

[10] M. B. Prime, D. J. D. J. Hughes, and P. J. P. J. Webster, “Weld application of a new method for cross-sectional residual stress mapping,” *Soc. Engineeering Mech. Annu. Conf. Expo.*, vol. 836, pp. 1–5, 2001.

[11] L. Cardamone, A. Valentín, J. F. Eberth, and J. D. Humphrey, “Origin of axial prestretch and residual stress in arteries,” *Biomech. Model. Mechanobiol.*, vol. 8, no. 6, pp. 431–446, 2009.

[12] M. K. Rausch and E. Kuhl, “On the effect of prestrain and residual stress in thin biological membranes,” *J Mech Phys Solids*, vol. 61, no. 1, pp. 1–23, 2014.

[13] A. Valentín and J. D. Humphrey, “Modeling effects of axial extension on arterial growth and remodeling,” *Med. Biol. Eng. Comput.*, vol. 47, no. 9, pp. 979–987, 2009.

[14] J. Urevc, M. Brumen, V. Flis, and B. Stok, “Applying_thermomechanical_anal.PDF,” *J. Mech. Eng.*, vol. 61, pp. 5–23, 2015.

[15] P. J. Withers, “Residual stress and its role in failure,” *Reports Prog. Phys.*, vol. 70, no. 12, pp. 2211–2264, 2007.

[16] B. Nadri, L. Edwards, M. E. Fitzpatrick, and A. Lodini, “Analysis of residual stresses following overloading of cold expanded holes using the X-ray diffraction technique and finite element method,” *J. Neutron Res.*, vol. 12, no. 1–3, pp. 219–224, 2004.

[17] M. Asadi and J. A. Goldak, “An Integrated Computational Welding Mechanics With Direct-Search Optimization for Mitigation of Distortion in an Aluminum Bar Using Side Heating,” *J. Manuf. Sci. Eng.*, vol. 136, no. 1, p. 011007, 2013.

[18] L. S. Santos, S. K. Gupta, and H. A. Bruck, “Simulation of buckling of internal features during selective laser sintering of metals,” *Addit. Manuf.*, vol. 23, no. April, pp. 235–245, 2018.

[19] L. E. Lindgren and A. Lundbäck, “Approaches in computational welding mechanics applied to additive manufacturing: Review and outlook,” *Comptes Rendus - Mec.*, vol. 1, pp. 1–10, 2018.

[20] N. Doynov and V. G. Michailov, “Distortion analysis of heat spot straightening thin-walled welded structures: part 1: formation of the plastic deformation zone,” *Int. J. Adv. Manuf. Technol.*, vol. 94, no. 1–4, pp. 667–676, 2018.

[21] T. K. S. Aburuga, A. S. Sedmak, and Z. J. Radakovic, “Numerical aspects for efficient welding computational mechanics,” *Therm. Sci.*, vol. 18, pp. S139–S148, 2014.

[22] V. M. J. Varghese, M. R. Suresh, and D. S. Kumar, “Recent developments in modeling of heat transfer during TIG welding—a review,” *Int. J. Adv. Manuf. Technol.*, vol. 64, no. 5–8, pp. 749–754, 2013.

[23] M. C. Smith, A. C. Smith, R. Wimpory, and C. Ohms, “A review of the NeT Task Group 1 residual stress measurement and analysis round robin on a single weld bead-on-plate specimen,” *Int. J. Press. Vessel. Pip.*, vol. 120–121, no. 1, pp. 93–140, 2014.

[24] P. J. Bouchard, “The NeT bead-on-plate benchmark for weld residual stress simulation,”

Int. J. Press. Vessel. Pip., vol. 86, no. 1, pp. 31–42, 2009.

[25] M. C. Smith and A. C. Smith, "NeT bead-on-plate round robin: Comparison of transient thermal predictions and measurements," *Int. J. Press. Vessel. Pip.*, vol. 86, no. 1, pp. 96–109, 2009.

[26] M. C. Smith and A. C. Smith, "Advances in weld residual stress prediction: A review of the NeT TG4 simulation round robins part 2, mechanical analyses," *Int. J. Press. Vessel. Pip.*, vol. 164, no. March, pp. 130–165, 2018.

[27] M. C. Smith and A. C. Smith, "Advances in weld residual stress prediction: A review of the NeT TG4 simulation round robins part 2, mechanical analyses," *Int. J. Press. Vessel. Pip.*, vol. 164, no. November 2017, pp. 130–165, 2018.

[28] F. Hosseinzadeh, "Personal page." [Online]. Available: http://technology.open.ac.uk/materials/staff/Staff_fh-2.htm. [Accessed: 29-Aug-2018].

[29] M. E. Fitzpatrick, A. Fry, P. Holdway, F. a Kandil, J. Shackleton, and L. Suominen, "Measurement Good Practice Guide No. 52. Determination of Residual Stresses by X-ray Diffraction," 2005.

[30] "ISIS - ISIS Home Page." [Online]. Available: www.isis.stfc.ac.uk. [Accessed: 02-Sep-2018].

[31] E. Harati, L. Karlsson, L. E. Svensson, T. Pirling, and K. Dalaei, "Neutron diffraction evaluation of near surface residual stresses at welds in 1300 MPa yield strength steel," *Materials (Basel).*, vol. 10, no. 6, 2017.

[32] J. Lu, *Handbook of measurement of residual stresses*. Lilburn, GA: Fairmont Press, 1996.

[33] Veqter, "Residual stress measurement techniques.," 2013. [Online]. Available: http://www.veqter.co.uk/. [Accessed: 30-Aug-2018].

[34] M. Turski and L. Edwards, "Residual stress measurement of a 316l stainless steel bead-on-plate specimen utilising the contour method," *Int. J. Press. Vessel. Pip.*, vol. 86, no. 1, pp. 126–131, 2009.

[35] M. B. Prime, "Cross-Sectional Mapping of Residual Stresses by Measuring the Surface Contour After a Cut," *J. Eng. Mater. Technol.*, vol. 123, no. 2, pp. 162–168, 2001.

[36] A. Stacey, h. J. Macgillivary, g. A. Webster, p. J. Webster, and k. R. A. Ziebeck,

"Measurement of residual stresses by neutron diffraction.," *J. Strain Anal.*, vol. 20, no. 2, 1985.

[37] M. T. Hutchings, *Introduction to the characterization of residual stress by neutron diffraction*. Boca Raton, FL : CRC Press, 2005.

[38] D. F. O. R. Development and D. D. Cen, "Non-destructive testing — Standard test method for determining residual stresses by neutron diffraction," 2008.

[39] R. B. Von Dreele, J. T. Jorgensen, and C. G. Windsor, "Rietveld refinement with spallation neutron powder diffraction data," *J. Appl. Crystallogr.*, vol. 15, no. 6, pp. 581–589, 1982.

[40] G. S. Pawley, "Unit-cell refinement from powder diffraction scans," *J. Appl. Crystallogr.*, vol. 14, no. 6, pp. 357–361, 1981.

[41] Geneva Switzerland: ISO, "Polycrystalline materials - determination of residual stresses by neutron diffraction," 2002.

[42] A. D. Krawitz and R. A. Winholtz, "Use of position-dependent stress-free standards for diffraction stress measurements," *Mater. Sci. Eng. A*, vol. 185, no. 1–2, pp. 123–130, 1994.

[43] P. J. Withers, M. Preuss, A. Steuwer, and J. W. L. Pang, "Methods for obtaining the strain-free lattice parameter when using diffraction to determine residual stress," *J. Appl. Crystallogr.*, vol. 40, no. 5, pp. 891–904, 2007.

[44] L. Clapham, K. Abdullah, J. J. Jeswiet, P. M. Wild, and R. Rogge, "Neutron diffraction residual stress mapping in same gauge and differential gauge tailor-welded blanks," *J. Mater. Process. Technol.*, vol. 148, no. 2, pp. 177–185, 2004.

[45] S. P. Timoshenko and J. N. Goodier, *Theory of elasticity*, Third ed. 1984.

[46] "ANSTO." [Online]. Available: https://www.ansto.gov.au/research/facilities/australian-centre-for-neutron-scattering. [Accessed: 29-Aug-2018].

[47] "ISIS Engin-X." [Online]. Available: https://www.isis.stfc.ac.uk/Pages/engin-x.aspx. [Accessed: 29-Aug-2018].

[48] H. F. Bueckner, "The propagation of cracks and the energy of elastic deformation," *Trans. ASME*, vol. 80, pp. 1225–1230, 1958.

[49] "A rational analytic theory of fatigue - P. Paris M. Gomez W. Anderson .pdf." .

[50] G. I. BARENBLATT, “The Mathematical Theory of Equilibrium Cracks in Brittle Fracture,” *Adv. Appl. Mech.*, vol. 7, pp. 55–129, 1962.

[51] M. B. Prime and A. L. Kastengren, “The Contour Method Cutting Assumption: Error Minimization and Correction,” *Exp. Appl. Mech.*, vol. 6, pp. 233–250, 2011.

[52] M. B. Prime and A. T. DeWald, “The Contour Method,” in *Practical Residual Stress Measurement Methods*, Wiley., 2013, pp. 109–138.

[53] J. P. Nobre, M. Kornmeier, A. M. Dias, and B. Scholtes, “Use of the hole-drilling method for measuring residual stresses in highly stressed shot-peened surfaces,” *Exp. Mech.*, vol. 40, no. 3, pp. 289–297, 2000.

[54] F. Hosseinzadeh, J. Kowal, and P. J. Bouchard, “Towards good practice guidelines for the contour method of residual stress measurement,” *J. Eng.*, Jan. 2014.

[55] M. B. P. W. Cheng, I. Finnie, M. Gremaud, “Measurement of Near Surface Residual Stresses Using Eletric Discharge Wire Machining,” *J. Eng. Mater. Technol.*, vol. 116, 1994.

[56] C. C. Wang, H. M. Chow, L. D. Yang, and C. Te Lu, “Recast layer removal after electrical discharge machining via Taguchi analysis: A feasibility study,” *J. Mater. Process. Technol.*, vol. 209, no. 8, pp. 4134–4140, 2009.

[57] M. Kunieda, B. Lauwers, K. P. Rajurkar, and B. M. Schumacher, “Advancing EDM through Fundamental Insight into the Process,” *CIRP Ann.*, vol. 54, no. 2, pp. 64–87, 2005.

[58] T. A. Spedding and Z. Q. Wang, “Parametric optimization and surface characterization of wire electrical discharge machining process,” *Precis. Eng.*, vol. 20, no. 1, pp. 5–15, 1997.

[59] K. H. Ho and S. T. Newman, “State of the art electrical discharge machining (EDM),” *Int. J. Mach. Tools Manuf.*, vol. 43, no. 13, pp. 1287–1300, 2003.

[60] S. H. Shin, “FEM analysis of plasticity-induced error on measurement of welding residual stress by the contour method,” *J. Mech. Sci. Technol.*, vol. 19, no. 10, pp. 1885–1890, 2005.

[61] F. Hosseinzadeh, J. Kowal, and P. J. Bouchard, “Towards good practice guidelines for the contour method of residual stress measurement,” *J. Eng.*, pp. 1–16, 2014.

[62] R. J. Dennis, D. P. Bray, N. A. Leggatt, and M. Turski, “Assessment of the influence of plasticity and constraint on measured residual stresses using the contour method.,” in *Proceedings of PVP2008*, 2018, pp. 1–9.

[63] D. Flack, *Good Practice Guideline No. 41: CMM Measurement Strategies*, no. 2. Metalworking Production, 2011.

[64] Micro-Epsilon, “Instruction manual optoNCDT 22xx.”

[65] R. J. Hocken and P. H. Pereira, *Coordinate Measuring Machines and Systems*, 2nd ed. Chapman and Hall/CRC, 2016.

[66] S. H. R. Ali, “Probing system characteristics in coordinate metrology,” *Meas. Sci. Rev.*, vol. 10, no. 4, pp. 120–129, 2010.

[67] Y. Traore, “Controlling plasticity in the contour method of residual stress measurement.,” PhD thesis, The Open University, 2013.

[68] M. B. Prime, R. J. Sebring, J. M. Edwards, D. J. Hughes, and P. J. Webster, “Laser Surface-contouring and Spline Data-smoothing for Residual Stress Measurement,” *Exp. Mech.*, vol. 44, no. 5, pp. 541–541, 2004.

[69] Y. Traore, S. Paddea, P. J. Bouchard, W. Hall, and M. K. Mk, “Measurement of the Residual Stress Tensor in a Compact Tension Weld Specimen,” *Exp. Mech.*, pp. 605–618, 2013.

[70] A. T. DeWald, J. E. Rankin, M. R. Hill, M. J. Lee, and H.-L. Chen, “Assessment of Tensile Residual Stress Mitigation in Alloy 22 Welds Due to Laser Peening,” *J. Eng. Mater. Technol.*, vol. 126, no. 4, p. 465, 2004.

[71] F. Hosseinzadeh, M. B. Toparli, and P. J. Bouchard, “Slitting and Contour Method Residual Stress Measurements in an Edge Welded Beam,” *J. Press. Vessel Technol.*, vol. 134, no. February 2012, pp. 1–6, 2012.

[72] A. Achouri, “Improving the spatial resolution of the contour method for residual stress measurement on P91 laser welded plate.,” 2014.

[73] M. E. Kartal, “Analytical solutions for determining residual stresses in two-dimensional domains using the contour method,” in *Proceedings of the Royal Society A*, 2013, vol. 469.

[74] J. Araujo de Oliveira, M. E. Fitzpatrick, and J. Kowal, “Residual Stress Measurements

on a Metal Matrix Composite Using the Contour Method with Brittle Fracture," *Adv. Mater. Res.*, vol. 996, no. June 2015, pp. 349–354, 2014.

[75] M. B. Prime, A. T. DeWald, M. R. Hill, B. Clausen, and M. Tran, "Forensic determination of residual stresses and KIfrom fracture surface mismatch," *Eng. Fract. Mech.*, vol. 116, pp. 158–171, 2014.

[76] J. Araujo de Oliveira, J. Kowal, S. Gungor, and M. E. Fitzpatrick, "Determination of normal and shear residual stresses from fracture surface mismatch," *Mater. Des.*, vol. 83, pp. 176–184, 2015.

[77] C. Sciammarella, F. Sciammarella, C. A. Sciammarella, and and F. M. Sciammarella, "Digital Image Correlation (DIC) 20.1," in *Experimental Mechanics of Solids*, 1st ed., no. 1, I. John Wiley & Sons, Ed. 2012, pp. 607–630.

[78] N. Naveed, "Improving the spatial resolution of the contour method.," PhD thesis, The Open University, 2015.

[79] A. H. Mahmoudi, F. Hosseinzadeh, and M. Jooya, "Plasticity effect on residual stresses measurement using the contour method," *Int. J. Eng.*, vol. 26, no. 10, pp. 1203–1212, 2013.

[80] G. C. Sih, "Methods of Analysis and Solutions of Crack Problems," *Int. J. Rock Mech. Min. Sci. Geomech.*, vol. 33, no. 8, 1973.

[81] Y. Traore, P. J. Bouchard, J. A. Francis, and F. Hosseinzadeh, "A novel cutting strategy for reducing plasticity induced errors in residual stress measurements made with the contour method," in *Proceedings of the ASME 2011 Pressure Vessels & Piping Division Conference*, 2011, pp. 1–12.

[82] F. Hosseinzadeh and P. J. Bouchard, "Residual stress measurement of a ferritic bead on plate benchmark test specimen using the contour method," in *Proceedings of the ASME 2012 Pressure Vessels & Piping Division Conference*, 2012, pp. 1–9.

[83] O. Muránsky, C. J. Hamelin, F. Hosseinzadeh, and M. B. Prime, "Mitigating cutting-induced plasticity in the contour method. Part 2: Numerical analysis," *Int. J. Solids Struct.*, 2015.

[84] F. Hosseinzadeh, Y. Traore, P. J. Bouchard, and O. Muránsky, "Mitigating cutting-induced plasticity in the contour method , part 1 : Experimental," *Int. J. Solids Struct.*, vol. 94–95, pp. 247–253, 2016.

[85] F. Hosseinzadeh and P. J. Bouchard, “Mapping Multiple Components of the Residual Stress Tensor in a Large P91 Steel Pipe Girth Weld Using a Single Contour Cut,” *Exp. Mech.*, vol. 53, no. 2, pp. 171–181, 2013.

[86] F. Hosseinzadeh, P. Ledgard, and P. J. Bouchard, “Controlling the Cut in Contour Residual Stress Measurements of Electron Beam Welded Ti-6Al-4V Alloy Plates,” *Exp. Mech.*, vol. 53, no. 5, pp. 829–839, 2013.

[87] M. B. Prime, T. Gnaupel-Herold, J. A. Baumann, R. J. Lederich, D. M. Bowden, and R. J. Sebring, “Residual stress measurements in a thick, dissimilar aluminum-alloy friction stir weld,” *Acta Mater.*, vol. 54, no. 15, pp. 4013–4021, 2006.

[88] M. D. Olson, A. T. DeWald, M. B. Prime, and M. R. Hill, “Estimation of Uncertainty for Contour Method Residual Stress Measurements,” *Exp. Mech.*, vol. 55, no. 3, pp. 577–585, 2015.

[89] O. Muránsky, F. Hosseinzadeh, C. J. Hamelin, Y. Traore, and P. J. Bendeich, “Investigating optimal cutting configurations for the contour method of weld residual stress measurement,” *Int. J. Press. Vessel. Pip.*, vol. 164, pp. 55–67, 2018.

[90] M. E. Kartal, C. D. M. Liljedahl, S. Gungor, L. Edwards, and M. E. Fitzpatrick, “Determination of the profile of the complete residual stress tensor in a VPPA weld using the multi-axial contour method,” *Acta Mater.*, vol. 56, no. 16, pp. 4417–4428, 2008.

[91] A. T. DeWald and M. R. Hill, “Multi-Axial Contour Method for Mapping Residual Stresses in Continuously Processed Bodies,” *Exp. Mech.*, vol. 46, pp. 473–490, 2006.

[92] M. D. Olson and M. R. Hill, “A New Mechanical Method for Biaxial Residual Stress Mapping,” *Exp. Mech.*, vol. 55, no. 6, pp. 1139–1150, 2015.

[93] P. Pagliaro, M. B. Prime, H. Swenson, and B. Zuccarello, “Measuring multiple residual-stress components using the Contour method and multiple cuts,” *Exp. Mech.*, vol. 50, no. 2, pp. 187–194, 2010.

[94] P. Pagliaro, “Mapping multiple residual stress components using the contour method and superposition,” PhD thesis, University of Palermo, 2008.

[95] Y. Zhang, “Numerical and Experimental Exploration of the Contour Method for Residual Stress Evaluation,” PhD thesis, The Open University, 2004.

[96] A. H. Mahmoudi and A. Saei, “Influence of asymmetrical cuts in measuring residual stresses using contour method,” *Int. J. Press. Vessel. Pip.*, vol. 134, pp. 1–10, 2015.

[97] “Assessment of the integrity of structures containing defects, R6 Revision 4, Amendment 7,” *Br. Energy Gener. Ltd.*, 2009.

[98] Y. Traore, F. Hosseinzadeh, and P. J. Bouchard, “Plasticity in the Contour Method of Residual Stress Measurement,” *Adv. Mater. Res.*, vol. 996, pp. 337–342, 2014.

[99] J. Araujo de Oliveira, “Feasibility Study on Developing a Novel Complex Contour Method using Closed Circular Cuts, OU/MatsEng/109, Issue 1.”

[100] H. F. Bueckner and S. N. Y., “The Propagation of Cracks and the Energy of Elastic Deformation,” *Trans. Am. Soc. Mech. Eng.*, pp. 1225–1230, 1958.

[101] A. Inc, “ABAQUS Version 14.1 Analysis User’s Manual,” 2017.

[102] “Toolbox TE Convective Heat Transfer,” 2018. [Online]. Available: http://www.engineeringtoolbox.com/connective-heat-transfer-d_430.html. [Accessed: 27-Sep-2018].

[103] M. Prager, “MPC Material Property Database for ASME Div II Rewrite.”

[104] J. Chen, B. Young, M. Asce, and B. Uy, “Behavior of high strength structural steel at elevated temperatures,” *J. Struct. Eng.*, vol. 132, no. 12, pp. 1948–1954, 2006.

[105] S. T. Methods, “Standard Test Methods for Determining Average Grain Size 1,” pp. 1–28, 2018.

[106] ASTM, “Standard Test Methods for Tension Testing of Metallic Materials 1,” 2013.

[107] N. P. Laboratory, “A national measurement good practice guide No. 98: Elastic Modulus Measurement.”

[108] ABAQUS, “Abaqus 6.13-Analysis User’s Guide: Volume IV: Elements,” vol. IV, 2013.

[109] A. E, G. S, Y. D, W. S, and P. A, “Characterisation of residual stress state in laser welded low carbon mild steel plates produced in keyhole and conduction mode.,” *Sci. Technol. Weld. Join.*, pp. 239–243, 2010.

[110] A. C. Larson and R. B. Von Dreele, “GSAS,” 2000.

[111] V. A. and J. A. Mike C. Smith, Ondrej Muransky, “The NeT Task Group 6 Weld Residual Stress Measurement and Simulation Round Robin in Alloy 600/82,” *ASME*

2016 Press. Vessel. Pip. Conf., vol. 6B, 2016.

[112] C. Ohms, J. Bouchard, M. Smith, and A. Smith, "NeT-Task Group 6 : Three-Pass Slot Weld Specimen in Inconel Nickel / Chromium Alloy Protocol for the Destructive and Non-Destructive Determination of Residual Stress in a Three-Pass Slot Weld Specimen in Inconel Nickel / Chromium Alloy," 2015.

[113] M. Janssen, Z. J, and W. RJH, *Fracture Mechanics*, 2nd ed. Delft University Press, 2002.

[114] Ondrej Muransky, "Private communication with Ondrej Muransky at Ansto (17/11/2016)."